[illegible]

IN-46-CR

253013
111P.

Earth Resources Laboratory
Department of Earth, Atmospheric and Planetary Sciences
Massachusetts Institute of Technology
Cambridge, MA 02139

SEMI-ANNUAL REPORT TO: National Aeronautics and Space Administration
(Crustal Dynamics)

TITLE: The Interpretation of Crustal Dynamics Data in Terms of Plate Interactions and Active Tectonics of the "Anatolian Plate" and Surrounding Regions in the Middle East

NASA GRANT: NAG5-753

PRINCIPAL INVESTIGATOR: M. Nafi Toksoz, (617)253-7852, [redacted]

CO-PRINCIPAL INVESTIGATOR: Robert E. Reilinger, (617)253-7860, [redacted]

PERIOD: 15 March 1989 - 14 September 1989

Date: 15 January 1990

(NASA-CR-186200) THE INTERPRETATION OF CRUSTAL DYNAMICS DATA IN TERMS OF PLATE INTERACTIONS AND ACTIVE TECTONICS OF THE ANATOLIAN PLATE AND SURROUNDING REGIONS IN THE MIDDLE EAST Semiannual Report, 15 Mar. - G3/46

N90-18824

Unclas
0253013

SUMMARY

During the past 6 months our effort has been concentrated on the following 3 general areas:

(1) Continued development of realistic, finite element modeling of plate interactions and associated deformation in the Eastern Mediterranean,

(2) Neotectonic field investigations of seismic faulting along the active fault systems in Turkey with emphasis on identifying seismic gaps along the North Anatolian fault,

(3) Establishment of a GPS regional monitoring network in the zone of ongoing continental collision in eastern Turkey (supported in part by NSF).

A short summary is given below. More detailed descriptions of each of these aspects of our research are given in the attached Appendices.

Finite Element Modeling (Appendix 1)

The purpose of this research is to develop a simple but robust approach to modeling plate interactions using a contact problem in 2-D elastic finite element method. An individual plate is considered as a continuum, whereas an aggregate of plates is treated as a discontinuum such that plate boundaries are represented as contact surfaces. The behavior of plates at the contacts is defined by the Coulomb-Navier failure criterion, and three types of contacts are considered: sliding contact(slip), tension release(separation), and sticking contact(single-node-continuum). The first and second modes correspond to transcurrent and divergent plate boundaries respectively. Convergent motion at plate boundaries is achieved by the double-node differential displacement technique with a recursive solution. Internal deformation caused by mid-plate processes, and body forces caused by elevation changes, are also implemented. A set of typical examples are discussed to validate this approach. To demonstrate its application, preliminary modeling of the Eastern Mediterranean, where tectonic deformation is produced by the interactions of the Eurasian, Arabian and African plates, is carried out. An attempt is made to constrain the displacement and stress fields by geological observations and earthquake stress fields, respectively. We find that the deformation pattern in the Eastern Mediterranean is substantially controlled by differential motion between the African and Arabian plates and gravitational forces. Westerly escape of the Anatolian block accelerates markedly when buoyancy forces caused by elevation changes are taken into account.

Neotectonic Investigations (Appendices 2 and 3)

Analysis of historical and instrumental earthquakes as well as recent field investigations of seismic surface fault offsets conducted by our group are used to understand better the seismotectonics of the North Anatolian fault, recent rates of plate deformation, the relationship between seismic slip and fault geometry, and the potential for future gap-filling earthquakes. These analyses suggest that recurrence intervals for large earthquakes is controlled by the geometry and length of individual segments. Furthermore, the eastern part of the westward escaping Anatolian block appears to be divided into 2 wedge shaped blocks each of which moves independently. Recurrence intervals from historical earthquakes and geological data indicate a slip rate of 0.8-1 cm/yr for the eastern segment of the North Anatolian fault, suggesting about 2 m slip deficit on the 1784 rupture segment. Thus, this segment is identified as a potential seismic gap.

GPS Measurements in Eastern Turkey (Appendix 4)

During the Summer and Fall of 1989, MIT in cooperation with the Turkish Union of Geodesy and Geophysics (TUJJB), IFAG, and Durham University undertook a GPS field campaign aimed at establishing first epoch relative point positioning in the region of continental collision in Eastern Turkey. As part of this campaign, SLR sites were observed with GPS, footprints were established around each of the Turkish SLR stations, 16 regionally distributed sites were observed in Eastern Turkey, and a dense network was monitored in the Aegean Trough region of Western Turkey. Ten of the stations observed in 1989 were reobservations of sites established and observed by MIT in 1988. Our group, in cooperation with our collaborators, plans a reoccupation in Western Turkey in 1990 and in Eastern Turkey in 1991.

APPENDIX 1

Finite Element Modeling of Plate Motions and its Application to the Eastern Mediterranean

ORAL, M.B., Earth Resources Laboratory, Department of Earth, Atmospheric and Planetary Sciences, Massachusetts Institute of Technology, Cambridge, MA 02139, USA.

Abstract

Plate deformation patterns present a complex picture, and are primarily affected by the interactions of plates at their boundaries and by their internal processes. The purpose of this study is to present a simple but robust approach to modeling plate interactions using a contact problem in 2-D elastic finite element method. An individual plate is considered as a continuum, whereas an aggregate of plates is treated as a discontinuum such that plate boundaries are represented as contact surfaces. The behavior of the plates at the contacts is defined by the Coulomb-Navier failure criterion, and three types of contacts are considered: the sliding contact(slip), the tension release(separation), and the sticking contact(single-node-continuum). The first and second modes correspond to transcurrent and divergent plate boundaries, respectively. The convergent motion at the boundaries is achieved by the double-node differential displacement technique with a recursive solution. Internal deformation caused by mid-plate processes, and body forces caused by elevation changes, are also implemented. A set of typical examples are discussed to validate this approach. To demonstrate its application, a preliminary modeling of the Eastern Mediterranean, where tectonic deformation is produced by the interactions of the Eurasian, Arabian and African plates, is carried out. An attempt is made to constrain the displacement and stress fields by the geological observations and earthquake focal mechanism solutions, respectively. The deformation pattern in the Eastern Mediterranean is substantially controlled by the differential motion between the African and Arabian plates and the gravitational forces. However, the westerly escape of the Turkish block accelerates markedly when the buoyancy forces caused by elevation changes are taken into account.

Introduction

Boundary forces/displacements caused by the interaction of plates at their boundaries, as well as internal deformation at mid-plates, gravitational forces and basal tractions, create extreme deformation. The finite element methods serve as a very applicable tool in understanding deformational behavior of interacting plates. In analysis of plate deformation patterns, the geometry of the plate boundaries requires a certain attention: the creation and destruction of material, as well as relative plate motions are observed at the boundaries. Hence, this study is primarily engaged in for searching and investigating finite element models, and implementing the 2-D contact problem for moving plates, that incorporates pre-existing plate boundaries into solutions, in order to analyze deformational patterns caused by the interactions of the Eurasian, African and Arabian plates, and Turkish Block, where boundary displacements and gravitational forces are very significant.

Since the classic paper by Turner, Clough, Martin and Topp which appeared in 1956, the deformation pattern of moving plates(bodies, mechanical parts, etc.) in contact, using finite element technique, has been studied by several authors in a variety of disciplines, e.g., earth sciences, civil and mechanical engineering, aerodynamics and geomechanics. Efforts in modeling are also diversified in their approaches to the problem as well as their solution techniques: strong emphasis on the rheological behavior of the plates, concern for the behavior and formulation of the contact surfaces of the plates, and derivation of the governing mathematical relationships and their solution techniques.

England and McKenzie(1982, 1983) suggested a thin viscous sheet model for continental deformation which led to a number of studies (England, Houseman and Sonder, 1985; England and Houseman, 1986; Houseman and England, 1986; Sonder, England and Houseman, 1986) examining the deformational pattern of collision. They regarded the aggregate of plates as a continuum, which obeys a Newtonian or a power-law rheology. This approach ignored faulting/failure between the plates. Papers following this approach continued to define the medium as a continuum, and motions along the boundaries(e.g. faults), alternatively at the contacts of plates, are regarded as accommodating the strain rate field.

The crustal deformation in southern California, modeled as a creeping flow in a non-linear continuum(Bird and Piper, 1980) formed the basis of a discontinuity approach(Bird and Baumgardner, 1984). Both studies utilized the finite element method for solving their governing equations. The former study assumed that the aggregate of plates is in a state of membrane stress subjected to plate-tectonics boundary conditions. The flow law of this membrane contained a rigid-plastic term to represent frictional faulting in the upper crust and a power-law term to represent the dislocation creep in the lower crust. The continuum approximation to the region in which the strain-rate is fixed precludes the prediction of slip-rates on faults(contact surfaces). In the latter paper, the zones of contact(faults) are modeled by "special" elements to account for slip rates.

In the engineering disciplines, emphasis on the behavior at contact first occurred in development of the joint element(1968-Element) of Goodman et al.(1968). For the analysis of foundations and joint systems, Wilson(1976) employed an interface element. The analysis of jointed rocks(Goodman, 1976) was further refined to account for several modes of behavior at the contacts(Goodman, 1975; Goodman and St. John, 1976). Wang and Voight(1969) alternatively utilized a contact algorithm to account for the behavior of the moving plates in contact. Goodman's joint element method, using parabolic failure, defines the following modes at a contact: closing, opening, rotation, sliding with/without dilatancy/contractancy.

In the finite element contact algorithm, used by Wang and Voight(1969) obeying the Coulomb-Navier failure criterion, which accounts for the behavior of the moving plates, three modes of behavior at a contact are defined: slip, separation and single-node-continuum. The state of stress and stability in underground openings is investigated using this contact algorithm. This approach is then applied to the progressive failure of rocks subjected to shear deformation(Kasapoglu, 1973), to the analysis of contact surface traction due to glacial arcuate abrasion cracks(Johnson, 1975), and to the collision of the Arabian and Eurasian plates(Kasapoglu and Toksoz, 1983). Further developments of contact algorithms are applications to 3-D static and dynamic analyses (Bathe and Chaudhry, 1985; Chaudhry and Bathe, 1986; Bathe and Mijailovich, 1987). They define the following modes of behavior at a contact: sticking and sliding contacts, and tension release. In a broad sense, the results of joint element and contact algorithm are equivalent (Bathe, 1989; pers. comm.). A hybrid finite element formulation of the contact problem is achieved by Kumobora(1979) to investigate microscopic, moderate and extensive sliding.

Following Wang and Voigt(1969), the contact problem is developed to explain all types of plate motions and to include gravitational forces and internal deformation. Also, a potential energy derivation of the governing finite element equations for this problem is introduced(see Appendix: Finite Element Formulation). Major emphasis is given to verifying the localization of failure zones, viz., slip-rates on the transcurrent plate boundaries(contacts). To avoid rheological complexities and disputes, and eliminate complicated mathematical treatise, a linear stress-strain relation for elastic media is assumed throughout the study. The following types of plate boundaries and behavioral modes on the contact surfaces are considered:

1. For continent-continent collision, the contact surface is in sticking contact mode(single-node-continuum);
2. For divergent boundaries, the contact surface is in tension release mode(separation);
3. For transcurrent boundaries, the contact surface is in sliding contact mode;
4. For subduction, the contact surface is in sliding contact(slip).

Ideally, modeling of plate motions requires a 3-D analysis which is very voluminous and time consuming. However, introducing some a priori assumptions about the dip angle of the contact surfaces may pave the way for 2-D analyses. Assume that the boundary has a 90^o dip for the first three cases and a 0^o dip for the last one. Also, assume that material properties throughout the elastic plate are constant. Thus, dependency of the geometry in z-axis is removable. This consequently leads to 2-D analysis (Fig.1). To account for the sliding contact behavior along the subduction surface, a fourth mode(overlap mode) is defined. The calculations are carried out for plane-strain case, using 4-node quadrilateral serendipidity elements with bilinear shape functions(see Appendix). Throughout the study, the term "displacement" is equivalent to instantaneous plate velocity.

The input data, which consists of nodal point coordinates and element connectivity, is generated by a pre-processor developed for this study. The results are displayed using a postprocessor(see Appendix). In the solutions of finite element equations, a versatile program, which includes the contact algorithm, is written.

The next section gives a finite element treatise on continuum vs discontinuum approach. (Extensive treatise on the derivation of governing finite element equations are presented in Appendix.) After introducing contact algorithm and applying to a set of examples, the finite element models of present-day tectonics of the Eastern Mediterranean are discussed.

Finite Element Models: Continuum and Discontinuum

The continuum is defined as follows :

Consider an aggregate of plates with various conditions imposed interacting at their boundaries. If the pre-existing boundaries are not included in computations(no a priori boundaries), but inferred from the displacement/strain/stress pattern changes, which are spread over a region rather than being localized, then this aggregate is considered as an individual plate which deforms under the combined effects of various conditions posed on each member.

To demonstrate this, interactions of two plates are considered. Their total area is 700 km x 500 km. Their boundary which makes an azimuth with the north. In Fig.2, the deformation pattern for the simulation of a transcurrent boundary is given. Only northward edge displacements (instantaneous plate velocities), 1 cm and 3 cm relative to a reference plate, are applied to the lower boundary of plates A and B, respectively (Fig.2a). To avoid any structural instability, rollers are applied to prohibit any east-west motion. This also accounts for the sideways continuity of the plates. The expected transcurrent plate boundary is denoted by dashed lines and meshed with smaller elements. Note that a definition of two distinct plates is made by a sudden change in boundary conditions. The occurrence of slip along the boundary so that one plate slips past the other is anticipated. The deformed structure plot (Fig.2b) shows the motion of the plate(s). However, a close look at the displacement vector configuration(Fig.2c), shows that the anticipated failure is distributed over a wide range in the east-west direction rather than being localized and that there is no localization. It is obvious that the differential displacement(slip) is *linearly* distributed between the terminal ends of the plates. Though the structure is bounded on its lateral sides and compressed on the lower side, tensional features develop. There is no observable stress difference (drop) in the vicinity of the boundary. The maximum shear stress fade out is almost identical on both sides. NE-SW expansion and NW-SE contraction is observed. The strain around the boundary is markedly large and it decays with distance.

Fig.3 simulates of a divergent plate boundary. Using the mesh for the previous model, pulls of -1 cm and 1 cm are applied to east and west boundaries of the plates A and B, respectively. The deformed structure plot and displacement pattern, shows no opening, but stretching in the E-W direction and a small amount of shortening in N-S direction. Stress and strain patterns give no clue for the possible location of failure.

Next, these two cases of deformation are treated as a contact problem and solved in discontinuum with the contact algorithm (Figs.3 and 4). Details of the contact problem will be discussed in the following section. The discontinuum is defined as follows :

When an aggregate of plates with various conditions imposed on them interact at their boundaries such that the pre-existing boundaries are included in computations using dual nodes (not split nodes),and their behavior at the contacts is determined by a frictional law, this aggregate establishes the discontinuum, and the individual plates are considered as a continuum deforming under the conditions prescribed.

The boundary conditions for the example in Fig.2 are used for a similar mesh in which the boundary between two plates is shown by a solid line and the deformation field is solved as a contact problem. In Fig.6c (cf. Fig.2) there is a marked slip ($\simeq 2cm$), which is the difference between the motions of the two plates along the pre-defined plate boundary (Fig.6a). This illustrates sliding-contact behavior. There is a remarkable shear stress drop (Fig.6e) across the fault. Because no motion is allowed in the E-W direction, compression develops perpendicular to the fault. The NW-SE compression implies that the differential motion is translated across the boundary because the slower plate has nowhere to go but north. As a result, principle major and minor stresses in plate $\mathcal{A}$, in comparison to plate $\mathcal{B}$ increase and decrease, respectively. The slower plate ($\mathcal{A}$) stretches almost sub-parallel to the boundary while it shortens perpendicular to it. Note that the stress and strain patterns change with the length scale of the plates in the E-W direction which are controlled by the strike of the boundary.

For a comparison, the divergent plate boundary case is treated in discontinuum as a contact problem.In Figs.5b and c (cf. Fig.3) the opening between the plates is 2cm which is equal to the differential motion between the plates. This demonstrates the tension-release-contact behavior. Strain for both of the plates is zero as is the stress field, since the displacement field is constant.

The magnitudes of strain and stress will be discussed before other finite element models are analyzed.

Contact Problem

The problem of pressure distribution between two bodies was first solved by Hertz(1881). In the Hertz elastic theory of contact (Timoshenko, 1934), the contact surfaces are frictionless and do not transmit tangential surface tractions across their boundary. However, Cater(1926) showed the inevitable occurrence of sliding within the area of contact. This study uses frictional law defined by the Coulomb-Navier criterion.(Its incorporation into contact problem will be defined later.) A *contact* happens when two or more bodies meet each other at a contact surface (Fig.6) is created. *Impact* is generated when a dynamic contact occurs (Johnson, 1976).

The forces which develop at the contact surface determine the behavioral mode. Unless there is a tensional release, the forces acting at the contact must be equal and opposite in sign, otherwise they are zero. Moreover, the relation between tangential and normal forces acting on the contact surface must satisfy certain conditions determined by the Coulomb-Navier criterion (Jaeger and Cook, 1979). Accordingly, failure occurs when the shear stress exceeds a threshold defined by normal stress scaled by a, factor and cohesion of the material :

$$\| \tau \| = S_o + \mu \, \sigma, \tag{1}$$

where τ, σ, S_o and μ are the shear and normal stresses, shear strength(cohesion) and friction coefficient (Fig.7). Therefore, slip will occur when

$$\| \tau \| - \mu \sigma = S_o, \tag{2}$$

and tensional release will take place when

$$\sigma \geq T_o, \tag{3}$$

where T_o is tensile strength and as defined positive.

The contact forces developed on the contact surface can be related to σ and τ by averaging them over the distance $\mathcal{L}$ half-way in either direction from the contacting node which lies on the contacting segments(Fig.8):

$$\frac{P_n}{\mathcal{L}} = \sigma, \tag{4}$$

and

$$\frac{P_t}{\mathcal{L}} = \| \tau \|, \tag{5}$$

where P_n and P_t are normal and tangential contact forces and their relation to P_x and P_y is:

$$\begin{aligned} P_n = &\quad P_x \, cos\alpha + P_y \, sin\alpha \\ P_t = &\quad -P_x \, sin\alpha + P_y \, cos\alpha, \end{aligned} \tag{6}$$

where α is the angle between the normal to the contact surface and the x-axis (Fig.8). In finite element mesh and computations, the boundary(contact surface) of contacting plates is represented by dual nodes, and the forces which develop on this surface are taken into consideration when judging the behavioral mode at the contact. If the contact forces are totally ignored, dual nodes become split nodes. This is a violation of compatibility in finite element. Four modes are defined: sticking contact, sliding contact, tension release and overlap. Mode IV is introduced to account for subduction and will be discussed later. Analyses of the first three modes are given below.

Mode I : Sticking Contact(single-node-continuum)

When contact stresses are insufficient to activate any motion along the contact surface such that

$$\begin{aligned} P_n &\leq T_o\, \mathcal{L}\,, \\ P_t &< S_o\, \mathcal{L} - \mu\, P_n\,, \end{aligned} \tag{7}$$

then the components of contact forces satisfy

$$\begin{aligned} P_x^A + P_x^B &= 0\,, \\ P_y^A + P_y^B &= 0\,, \end{aligned} \tag{8}$$

where superscripts denote the plate at the contact surface. Hence, the displacements are

$$\begin{aligned} q_x^A &= q_x^B\,, \\ q_y^A &= q_y^B\,, \end{aligned} \tag{9}$$

so that the contacting plates in discontinuum behave as if they are in continuum.

Mode II : Sliding Contact(slip)

The plates in contact exhibit a sliding behavior when tangential stresses exceed the linearly defined Mohr envelope, provided that the normal contact forces are less then the tensile strength:

$$\begin{aligned} P_n &\leq T_o\, \mathcal{L}\,, \\ P_t &> S_o\, \mathcal{L} - \mu\, P_n\,. \end{aligned} \tag{10}$$

The amount of slip is determined by the frictional coefficient, and shear and tensile strength. From the continuity of the stresses across the element, the components of the contact forces are:

$$\begin{aligned} P_x^A + P_x^B &= 0\,, \\ P_y^A + P_y^B &= 0\,, \end{aligned} \tag{11}$$

with additional constraints by the frictional law:

$$\begin{aligned} \| P_t^A \| - S_o\, \mathcal{L} + \mu\, P_n^A &= 0\,, \\ \| P_t^B \| - S_o\, \mathcal{L} - \mu\, P_n^B &= 0\,. \end{aligned} \tag{12}$$

This states that the displacements perpendicular to the contact surface are equal:

$$q_x^A + q_x^B = tan\alpha\, [q_y^A + q_y^B]\,, \tag{13}$$

implying that

$$\begin{aligned} q_x^A &= q_x^B, \qquad for \quad \alpha = 0^o\,, \\ q_y^A &= q_y^B, \qquad for \quad \alpha = 90^o\,. \end{aligned} \tag{14}$$

Mode III : Tension Release(separation)

The plates diverge when the normal stress exceeds the tensile strength:

$$P_n \;\leq T_o\, \mathcal{L}\,, \tag{15}$$

in which the components of the contact forces are

$$\begin{aligned} P_x^A &= 0\,, \\ P_y^A &= 0\,, \\ P_x^B &= 0\,, \\ P_y^B &= 0\,. \end{aligned} \tag{16}$$

Note that (a) the displacements(at the nodes and contacts-dual nodes) are unknown, (b) the contact forces determine the behavioral mode at the contact, (c) *the contact forces also are unknown.* To settle the dust, recall Eqn.A14 and rewrite as

$$Kq - Q = -P, \tag{17}$$

where P contains P_x and P_y unprescribed contact nodes. The contact forces P can be calculated and used to determine the behavioral mode, provided that the nodal displacements are known. This requires another iterative scheme in which an interrogation procedure (Wang and Voight, 1969) for behavioral modes is constructed. It is clear that $P = 0$ when no contact is defined and the displacements can be calculated from Eqn.A42 in conjunction with Eqn.A41.

Calculation of Displacements at Contact Surfaces: A Contact Algorithm

To achieve a good convergence, the initial displacement vectors have to be close to those of the final solution. A first approximation can be drawn from a sticking contact solution, where discontinuum becomes asymptotic to the continuum. For the first part of iterative solution of the displacements at dual nodes, the following equations prevail(see Appendix):

$$\begin{aligned} q_i^l &= q_i^{l-1} - \omega \, \{\varphi_i^l + \varphi_{i+1}^l\}/\{K_{i,i} + K_{i+1,i+1}\} \, , \\ q_{i+1}^l &= q_i^l \, . \end{aligned} \tag{18}$$

Displacements at the other nodes are obtained from Eqn.A42.

In the rest of the iterative solution, the contact algorithm is applied. To decide on the behavioral mode, the displacements at one of the dual nodes have to be calculated from the relation:

$$\begin{bmatrix} K_{i,i} + K_{i+2,i+2} & K_{i,i+1} + K_{i+2,i+3} \\ K_{i+1,i} + K_{i+3,i+2} & K_{i+1,i+1} + K_{i+3,i+3} \end{bmatrix} \begin{bmatrix} q_i^l \\ q_{i+1}^l \end{bmatrix} = \begin{bmatrix} -(\varphi_i^l + \varphi_{i+2}^l) \\ -(\varphi_{i+1}^l + \varphi_{i+3}^l) \end{bmatrix} , \tag{19}$$

where q_i and q_{i+1} are x- and y-parallel displacements at dual node k on plate A. In $l - th$ iteration, the contact forces equal the residual defined by Eqn.A41:

$$\begin{aligned} P_n^l = & \ \ \varphi_x^l \, cos\alpha + \varphi_y^l \, sin\alpha \, , \\ P_t^l = & \ -\varphi_x^l \, sin\alpha + \varphi_y^l \, cos\alpha \, , \end{aligned} \tag{20}$$

For the contact algorithm, the angle between the contact and its normal α, the distance that the nodal contact forces uniformly distributed $\mathcal{L}$, and the trigonometric relationships are:

$$\begin{aligned}\mathcal{L} &= \sqrt{(-x_k + x_{k+1})^2 + (y_k - y_{k+1})^2}\ , \\ tan\alpha &= \tfrac{-x_k+x_{k+1}}{y_k-y_{k+1}}\ , \\ sin\alpha &= \tfrac{-x_k+x_{k+1}}{\mathcal{L}}\ , \\ cos\alpha &= \tfrac{-y_k+y_{k+1}}{\mathcal{L}}\ ,\end{aligned} \tag{21}$$

where x and y are the coordinates of the $k-th$ dual node. Dual nodes, A and B may or may not share the same location. For the purposes of this study, they have identical coordinates.

For mode I, no further calculations are necessary, and the displacements on either side of the contact are equal:

$$\begin{aligned} q^l_{i+2} &= q^l_i \\ q^l_{i+3} &= q^l_{i+1}, \end{aligned} \tag{22}$$

where q_{i+2} and q_{i+3} are x- and y-parallel displacements at dual node k on plate B.

Mode II calculations require rotations of diagonal elements of the stiffness matrix in the direction normal and parallel to the contact surface, to account for the tangential and normal stresses(see Eqn.12b). Define

$$\begin{aligned} xa = &\ -sin\alpha \pm (-\mu)\ cos\alpha\ , \\ ya = &\ \ cos\alpha \pm (-\mu)\ sin\alpha\ , \end{aligned} \tag{23}$$

where xa and ya are rotation coefficients. If $P_t > 0$ "$-$" is used. To solve for q_i, q_{i+1}, q_{i+2} and q_{i+3}, first set them to zero(which removes the force contribution at these nodes, recall Eqn.A41) and then solve :

$$\begin{bmatrix} K_{i,i}xa + K_{i+1,i}ya & K_{i+1,i+1}ya + K_{i,i+1}xa & 0 & 0 \\ K_{i,i} & K_{i,i+1} & K_{i+2,i+2} & K_{i+2,i+3} \\ K_{i+1,i} & K_{i+1,i+1} & K_{i+3,i+2} & K_{i+3,i+3} \\ 1 & tan\alpha & -1 & tan\alpha \end{bmatrix} \begin{bmatrix} q^l_i \\ q^l_{i+1} \\ q^l_{i+2} \\ q^l_{i+3} \end{bmatrix}$$

$$= \begin{bmatrix} -(\varphi^l_i xa + \varphi^l_{i+1} ya - S_o\mathcal{L}) \\ -(\varphi^l_i + \varphi^l_{i+2}) \\ -(\varphi^l_{i+1} + \varphi^l_{i+3}) \\ 0 \end{bmatrix}. \tag{24}$$

For mode III, there is no bonding between the dual nodes lying on the contact surface, and the displacements for each plate follows a different linear system solution. To solve for q_i and q_{i+1}; first set them to zero and solve:

$$\begin{bmatrix} K_{i,i} & K_{i,i+1} \\ K_{i+1,i} & K_{i+1,i+1} \end{bmatrix} \begin{bmatrix} q_i^l \\ q_{i+1}^l \end{bmatrix} = \begin{bmatrix} -\varphi_i^l \\ -\varphi_{i+1}^l \end{bmatrix}. \tag{25}$$

And to solve for q_{i+2} and q_{i+3}; first set them to zero and solve:

$$\begin{bmatrix} K_{i+2,i+2} & K_{i+2,i+3} \\ K_{i+3,i+2} & K_{i+3,i+3} \end{bmatrix} \begin{bmatrix} q_{i+2}^l \\ q_{i+3}^l \end{bmatrix} = \begin{bmatrix} -\varphi_{i+2}^l \\ -\varphi_{i+3}^l \end{bmatrix}. \tag{26}$$

The calculation of displacements for the rest of the nodes is carried out by Eqns.A42 and A41. Convergence in the first stage of iterative solution is monitored by Eqn.A41. In the next stage,

$$C = \sum_i^n \| \varphi_i^l \|, \qquad \{ \forall i \mid i \notin \mathcal{M} \}, \tag{27}$$

where $\mathcal{M}$ is the set of degrees of freedom involved contact. C is the measure of convergence and must decrease as more iterations are performed.

On the Magnitudes of Strain and Stress, and the Strength and Coefficient of Friction

The average strain per year is at the order of 10^{-7} (Turcotte and Schubert, 1982). Lithostatic stress for a 35 km thick plate is 1000 Mpa (Turcotte and Schubert, 1982). The compressive stresses caused by elevation changes(Molnar and Lyon-Caen, 1988), and the stresses induced by ridge-push and slab-pull (Richardson, 1972), range from 60 to 33-200 MPa, while thermal and membrane stresses are 400-600 Mpa. Bott(1982) reports an average of 100 Mpa.

Using the instantaneous plate velocities, the magnitudes of the strain(rate), found in this study, are at the order of 3 x 10^{-7} coheres with the reported values. Stress magnitudes are, however, at the order of 3000 Pa($=$ 12 GPa x $3x10^{-7}$). Compared to the magnitudes given above, there is a scaling factor of $10^3 - 10^4$ which arises because (a) instantaneous plate velocities are used as boundary displacements, (b) strains calculated from these displacements are strains per year(strain rate), and (c) stresses calculated from these strain rates inherit this time scaling and are stresses per year.

This "time-factor" χ also scales the contact forces which means that the magnitudes of shear and tensile strengths are also scaled corresponding $\simeq 1000 - 10000$ years(episode cycle). The calculations using zero strength do not significantly differ from those using this value, when the forces are greater than the strength of the plate. Higher strength values cause slowing in plate motions. Unless otherwise stated, all models have zero strength. For the sliding mode this implies sliding without cohesion.

The friction coefficient is another factor that reduces the motions along plate boundaries. Bird and Baumgardner (1984) point out the possibilities of a low friction coefficient ($\simeq 0.3$) for active faults. It is found that $\mu < 0.5$ produce almost the same deformation pattern. Throughout the study, a "low" friction coefficient is used.

No strength and a "low" friction coefficient are appreciable (a) when the contact surfaces have already formed and are weak,viz., have an extreme tendency to move, (b) when the instantaneous motions are modeled, assuming a certain amount motion along the boundaries per year, viz., "things change".

Examples for Plate Motions

Contact solutions of interacting two plates are demonstrated (Figs.4 and 5) and compared to those of continuum solutions. This section depicts some aspects of contact solutions for three-plate cases. At the contact of three plates, triple nodes are required to simulate the discontinuum. However, this may be avoided when the third plate boundary is translated one element away from this junction. The following models exploit this numerical treatment. Note that the goal of the study is to demonstrate the advantages of the contact problem, so a more general algorithm is not incorporated. When n-plates are in contact, instead of using contactor nodal point forces (this study; Wang and Voight, 1969), contactor segment tractions (Bathe and Chaudhry, 1985) calculations become more attractive.

In the three-plate-contact models, the following considerations are in effect: (a) a roller sub-parallel to N-S or E-W implies that there is no motion allowed in their normal directions, and this boundary corresponds to transforms; (b) a hinge means that there is no motion in either direction, which in turn serves as a reference frame; (c) there is a hypothetical reference frame for the instantaneous plate velocities (displacements) located somewhere away from the plates unless otherwise located; (d) the contact algorithm previously discussed is exploited; (e) plates are named as lower (right) plate $\mathcal{A}$, lower (left) plate $\mathcal{B}$, and upper plate $\mathcal{C}$; (f) at the end points of contacts, there is incompatibility in the deformed structure plots when either one of the components of dual nodes is constrained, or the requirement for triple node is necessary; (g) unless otherwise stated, there is no overlap, this being controlled by additional constraints(double-node differential displacements). This kind of overlap occurs due to the effects mentioned in (f) and since linear interpolation in joining two points is used, these effects are enhanced. For those nodal points, refer to displacement vector plots.

In Fig.9, the interactions of two plates with a fixed reference plate is considered. On the boundaries of right and left plate, 3 cm and 1.4 cm displacements in the N and NW directions are applied, respectively. Most of the differential motion is taken between the right and left, and between right and upper plates, as sliding contact. This type of model could be considered a Fault-Fault-Fault type triple junction. The decrease in slip along the right plate contact is mainly compensated by internal deformation as shown by the strain field (Fig.9f). The motion of the faster plate decreases toward the north for (a) there is no sideways motion allowed and (b) it meets another stable plate. This stress pattern demonstrates the sub-groupings of principal directions. Compression is dominant in the upper plate as well as in the right plate. The upper plate also has a tendency to extend sub-parallel to the contact surface with the lower right plate, due to the loading of the right plate. A striking change in maximum shear stress magnitudes marks the contacts.

For the model shown in Fig.10, the boundary conditions are identical to the previous one except that the upper plate is no more fixed, but is displaced towards N by 1 cm. These boundaries could be considered as Fault-Fault-Ridge triple junction(Fig.10b). The differential motion between left and upper plates is not enough to create the tension release mode. However, their interaction, especially the motion of upper plates, triggers divergent plate motion. Compared to Fig.9, the slip along the contact between upper and right plates decreases, whereas it remains the same along the contact between right and left plates. Due to tension release, the northerly oriented stresses in the left plate vanish while the E-W extension increases. Evidently, the change in maximum shear stress patterns occurs at plate boundaries.

The deformation pattern in Fig.11 is an example of modes I and II, sticking and sliding contacts, respectively. Boundary conditions are the same as in the previous model except that the left plate is displaced northernly by 1 cm and set free on its west end, and that the sense of upper plate motion is reversed. It may be considered as a Fault-Fault-Trench(collision) triple junction. The contact between upper and left plates is the first type of plate boundaries(continent-continent). The displacement field seems to be zero at their contact because of the opposite polarity of the plate motion. One of the dual nodes at the east end is not constrained and causes an artifact motion, and has to be ignored. The entire region is in compression. When stress and especially strain fields are considered, the left and the western of the upper plate behaves as a single plate in continuum (sticking contact). As a corollary to this observation, the maximum shear stress pattern gives no information about the existence of a contact.

The boundary conditions for the model in Fig.12 are the same as in Fig.10, except that the left plate is displaced northwesterly by 1.4 cm. To simulate Fault-Fault-Trench(subduction) triple junction, mode IV is introduced:

Overlap mode

Consider nodes q_r^A and q_s^B and let δ be the convergence amount between these plates. δ is the measure of material subducted and could be correlated to dissipation of material(displacement) over a region such that:

$$q_s^B = q_r^A + \delta \ , \tag{28}$$

where q_s^B and q_r^A are displacements on plates A and B at nodes s and r, respectively and related to each other by a constant of dissipation(rate of subduction) δ. A first solution may be obtained by ignoring convergence, and then incorporating the above relation, an additional set of prescribed degrees of freedom may be obtained. To simulate this type of plate boundary, a recursive solution could be using the additional constraints and former boundary conditions. This solution is called double-node-differential displacements with recursive solution(Overlap, Mode IVa).

A tentative solution is given in Fig.12 with boundary conditions the same as Fig.10 except that the sense of motion in the upper plate is reversed. 3 mm convergence is included across the contact of the upper and left plates. The displacement field demonstrates the success of the approach. Because of this motion, the principal stresses normal to the overlapping contact drastically decrease. The change in maximum shear stress pattern corresponds to the overlap.

An alternative solution can be obtained by considering the auxiliary contact, perpendicular to the primary contact, and then applying double-node differential displacements(Overlap, Mode IVb). This removes locking, and perfectly transmits the motions from one plate to the other. To avoid the very complicated mesh required for an auxiliary contact, the solutions for convergent motions, *at this stage*, are carried out by double-node differential displacements using primary contact.

Internal deformation caused by folding, kinking, etc., is modeled and shown in Fig.13, where the boundary conditions are the same as the previous example and exclude convergence. The elements with crosses are assigned negative initial strain corresponding to (1cm) shortening. When this region becomes softer, it takes up some of the differential motion between the plates. The displacement pattern shows that the slip along the boundary between the left and right plates decreases. This contribution boosts the stress and strain field over this region. The same result is obtainable by decreasing the Young modulus for these elements.

McKenzie(1978) discusses three possible driving forces: boundary forces which are widely used until now in the above examples; gravitational (buoyancy)forces, caused by elevation changes; and forces on the base of the lithosphere. When the area of the plates is relatively small compared to boundary and gravitational forces, basal tractions may be ignored.

Therefore, they are excluded in finite element computations. However, body forces caused by elevation changes are very significant, and included. Molnar and Lyon-Caen(1988) calculated the upper bounds these buoyancy forces.

Fig.14 shows the effect of body forces on the deformation pattern. The boundary conditions are identical to those in Fig.11 except that the east end of upper plate is free to move in the E-W direction. The left and upper plates are combined and allowed to behave as a single plate. Although this contact is locked, the upper plate escapes westwardly through the free end due to the applied body force. The exact amount of body forces is inconclusive since no lower bound is defined. In this study the first estimates are obtained from the Molnar and Lyon-Caen's calculations for horizontal driving forces. After normalizing per unit volume and per unit year, a scaling factor of 10-100 is observed.

Application to the Eastern Mediterranean

The region of interest includes the Eurasian, Arabian and African Plates, as well as the Turkish and East Anatolian Blocks. The neotectonics of the region is shaped by the second opening episode of the Red Sea during the early Pliocene (4.5 Ma). The Arabian Plate, formerly having the same velocity as the African Plate, gained acceleration and, following the closure of the Thetys Ocean, collided with the Eurasian Plate. The African Plate, on the other hand, continues its subduction under the Hellenic and Cyprean Arcs. This continuing continent-continent collision between Eurasia and Arabia creates extreme deformation in the region. Shortening in eastern Turkey was first accommodated by crustal thickening. Later, instead of excessive crustal thickening, the Turkish Block which is bounded by the North and East Anatolian Faults, wedged out towards the west under the compressive regime. Presently, the western tip of this block extends in a N-S direction, by accommodating the area of the African Plate lost by subduction(Fig.15) as westerly motion is inhibited by the Grecian Shear Zone. The major structures in this region are the Dead Sea, the East, North and Northeast Anatolian Faults, the Cyprean Arc and the Bitlis Suture. At the Maras and Karliova triple junctions the Arabian, African and Turkish, and the Arabian, Turkish and Eurasian plates meet. Fig.16 summarizes the sense of motion along the faults. Accordingly, the sense of displacement on the Dead Sea, and the East and Northeast Anatolian Faults is sinistral, whereas on the North Anatolian Fault it is dextral. Several authors calculated the rotation poles of these plates (Chase, 1978; McKenzie, 1972; Minster et al., 1978; Gordon and Jurdy, 1986). From these data, local plate velocities(Fig.17) are computed for the African and Arabian plates with respect to the Eurasian plate(Cox and Hart, 1986). Local plate velocities obtained from McKenzie(1972) are higher than the others. Mean boundary displacements(instantaneous plate velocities) for the African and Arabian Plates are northerly 5.2 mm and 22 mm, respectively. Fig.18 shows the area where finite element calculations are applied to the Eastern Mediterranean. In the west, it is bounded by the Pliny-Strabo Trench system, and excludes western Turkey. The Dead Sea, East, North, and Northeast Anatolian Faults, the Cyprean Arc and the Bitlis Suture are considered and modeled as 2-D contact surfaces.

Three finite element models of the Eastern Mediterranean are investigated. They all consider:

(a) strike-slip faulting[model 1](Fig.19),

(b) strike-slip faulting and convergence at the Cyprean Arc and Bitlis Suture[model 2](Fig.20), and

(c) strike-slip faulting and convergence at the Cyprean Arc and Bitlis Suture, internal deformation at the Palmyra Kink and gravitational forces that wedge out the Turkish and East Anatolian Blocks[model 3](Fig.21),

to be major tectonic elements in creating the deformational pattern. The first model has only historical importance and proves the need for the latter two models. At the beginning, the finite element models of the Eastern Mediterranean only accounted for strike-slip faulting and ignored convergence, especially the subduction of the African plate at the Hellenic Trench and the Cyprean Arc(Kasapoglu and Toksoz, 1983; 1988). These models, unfortunately, created skepticism about 2-D finite element calculations in a region where some plate motions, generated by the differential motion between the African and Arabian Plates, is taken up by convergence(subduction/collision). Strong emphasis on the contribution of gravitational forces also invited speculations. Other than insisting suggestions to incorporate these forces in finite element calculations, no models have appeared yet. To settle the dust, convergence and body forces, as well as internal deformation, are included into 2-D finite element computations. The contact problem previously discussed is utilized. A standard mesh is generated using a pre-processor program developed for contact problems. The boundary conditions are identical in each model. Rollers at the sides of the plates illustrate the direction in which the relevant nodes may move. Rollers west of the African and east of the Arabian Plates reflect the uniform continuity of the plate motions beyond the modeled area. The Eurasian plate is held fixed. 5.2 mm and 22 mm northerly boundary displacements(instantaneous plate velocities relative to the Eurasian Plate) are applied on the lower end of the African and Arabian Plates, respectively. The tension release mode is applied when one or both of the dual nodes at the terminal ends of plate boundaries are constrained causing incompatibility at these nodes. Therefore, the displacement/stress/strains at these nodes are ignored. In the second and third models, 3 mm convergence across the Cyprean Arc and 6 mm shortening at the Bitlis Suture is included. The third model includes 4 mm internal deformation taken up by Palmyra Kink(Barka et al., 1989) and gravitational forces. The gravitational force per unit volume is estimated from the upper bounds of the horizontal driving force(Molnar and Lyon-Caen, 1988). Assuming N-S direction components are balanced, westerly and easterly forces are applied on the elements that represent the Turkish and East Anatolian blocks, respectively(Fig.21a). A comparison of displacement fields of models 1 and 2 show that introduction of convergence at the Cyprean Arc and shortening at the Bitlis Suture, results in decrease of slip along the fault zones. Because these two features take up $\simeq 3 - 5mm$, the motions along the North, Northeast and East Anatolian faults are halved. The westerly and easterly escapes almost vanish. The slip along the Dead Sea Fault decreases northerly in both models. These data imply that the differential motion between the African and Arabian Plates are not sufficient to explain the amount of slip observed along the Anatolian transforms. Barka and Gulen(1989) argue that the slip along the North Anatolian Fault is 1 cm/yr, if the age of the fault is early-middle Pliocene(3.5-4 Ma) and has a total offset of 35 km, which decreases westerly to 5 mm/yr. The East Anatolian fault has a 5 mm/yr slip(Barka et al, 1989). Geological studies on the Dead Sea Fault show that the 10-15 mm/yr slip in the south(Gharb Segment) reduces to 5 mm in the north(Karasu segment). Given this information, finite element modeling becomes inconsistent with the observational data. "To do justice to the whole data set"(Sengor, written comm.), gravitational forces and internal deformation at Palmyra Kink, as well as convergence, are included into the computations(model 3). Fig.21 demonstrates how the Turkish and East Anatolian Blocks wedge out. The openings at the Karliova and Maras triple junctions are reflected in displacement and stress patterns. On the average, 15 mm and 5 mm slip along the Gharb and Karasu segments of the Dead Sea Fault are observed.

As some part of the differential motion is accommodated by the Palmyra Kink, build up of strain/stress occurs. The average slip rates on the North(13 mm in the east, 8 mm in the west) and Northeast Anatolian Faults(4 mm) are relatively large requiring a smaller body force magnitude. The primary conclusion is that the slip rates along the Anatolian transforms are controlled by the buoyancy forces caused by the differential stresses between higher and lower elevations. The gravitational force used for these calculations is lower than the upper bound for 2000 m elevation, but the largest for the admissable deformation patterns. When higher values are preferred, the tectonic picture changes: The transcurrent motion character along the East and North Anatolian Faults' changes to divergent and convergent type boundaries, respectively. Thus, slip rates along the North Anatolian Fault is no greater than 1 cm/yr. Major stress concentrations take place in the Turkish Block, Palmyra Kink and north of the Bitlis Suture. Compressive stresses are characteristic to the Cyprean Arc and the Bitlis Suture. Because western Turkey and the Aegean Sea are not included in the models, transition to extensional regime is not observable. However, the westerly escape of the Turkish Block is reflected as a SW-NE compression. Strain patterns suggest that the strain accumulates north of convergent zones and is at the order of 1-5 x 10^{-8}.

Conclusions and Discussions

The deformation pattern of interacting plates can be modeled using 2-D finite element method. The comparisons between continuum and discontinuum approaches demonstrate that the contact algorithm is a robust method for modeling plate motions. Derived potential energy expressions show that the contact problem is inherent in finite element equations and that implementing rheologies, other than linear elastic type, is straightforward. Application to the Eastern Mediterranean, where extreme deformation is created by the interactions of the Eurasian, African and Arabian Plates, shows that the regional tectonic picture cannot only be defined by boundary displacements(the ridge push force due to the opening of the Red Sea). Including gravitational forces is a must. These two forces control the deformational process in the region, and suggest that the differential motion between the Arabian and African Plates is responsible for the slip rate along the Dead Sea Fault, whereas the gravitational forces create the slips along the Anatolian Transforms. The models indicate that the slip rate must not exceed 1 cm/yr along the North Anatolian Fault. Accounting for the Palmyra

Kink demonstrated that mid-plate internal deformations are another source of strain accumulation. Introduction of the overlap mode shows that unless subduction and shortening are taken into account, understanding the deformational behavior of plates is incomplete, and the patterns obtained may lead to false conclusions. The overlap mode IVa illicits considerable success, however, better results can be obtained by using mode IVb. Further developments of the contact algorithm, viz., extending to the third dimension, triple-node formalism, using contactor segment tractions in calculation of contact forces instead of nodal point forces, and employing the joint element approach; and the incorporation of other rheologies into the computations will improve modeling of the deformational behavior of (micro)plates with complicated boundaries. Instead of the assumed displacement finite element approach, it is suggested that assumed strain method, for regions where strain rates are significant and hybrid finite element method for regions where prescription of both stresses and displacements are needed, be utilized. As long as the instantaneous plate velocities are used , which inevitably introduces a time scaling, the low coefficient of friction and no-strength is justifiable.

Acknowledgments

My work with Prof. E. K. Kasapoglu, writing pre- and post processors, introduced me to the realm of finite element. Long after-class discussions with Prof. T.H.H. Pian shaped this study and contributed in many aspects. Dr. A. Barka helped in understanding the regional tectonics of the Eastern Mediterranean. N. Leah Crandall, with utmost patience, edited all the drafts. This study is supported through a fellowship from the Turkish Government and partial financial support from MIT.

APPENDIX : Finite Element Formulation

Under boundary and nodal displacements, body forces, initial strain and stress and surface tractions, the deformation pattern of the plates is defined by displacement, strain and stress fields. Since instantaneous plate motions are considered in this study, they, hereinafter, will be referred to as displacements. A plane strain/stress media with linear stress-strain relation is assumed in the general derivation of governing finite element equations, including the contact problem. First, the finite element formalism using total potential energy is introduced. After finding the governing equations by variational calculus, discretization of the displacement field is discussed. Following stress calculations from strain field, numerical solutions techniques are given.

Governing Finite Element Equations

The linear relation between stress and strain for elastic materials in 2-D is given by:

$$\sigma = E\epsilon - E\epsilon_o + \sigma_o \, , \tag{1}$$

with

$$\sigma = [\ \sigma_x \ \ \sigma_y \ \ \sigma_{xy}\ ] \, , \qquad \epsilon = [\ \epsilon_x \ \ \epsilon_y \ \ \epsilon_{xy}\ ] \, , \tag{2}$$

where σ, ϵ ϵ_o and σ_o are stress, strain, initial strain and initial stress, respectively. For plane stress and strain, the material property matrices E are:

$$E = \frac{\mathcal{E}}{1-\nu^2}\begin{bmatrix} 1 & \nu & 0 \\ \nu & 1 & 0 \\ 0 & 0 & \frac{1-\nu}{2} \end{bmatrix}$$

$$E = \frac{\mathcal{E}}{(1-2\nu)(1+\nu)}\begin{bmatrix} 1-\nu & 1 & 0 \\ 0 & 1-\nu & 0 \\ 0 & 0 & \frac{1-2\nu}{2} \end{bmatrix} , \tag{3}$$

respectively, where $\mathcal{E}$ and ν are Young's modulus($\simeq$ 100GPa) and Poisson's ration ($\simeq$ 0.25) strain.

Consider a conservative system on which external and internal forces act. The internal work done(the stored energy) U_o of this system, per unit volume, is:

$$\begin{aligned} U_o &= \int \sigma d\epsilon\ , \\ &= \tfrac{1}{2}\epsilon^T E \epsilon - \epsilon^T E \epsilon + \epsilon^T \sigma_o\ , \end{aligned} \tag{4}$$

and the total strain energy U is given by:

$$U = \int_V U_o dV + q^T\ P, \tag{5}$$

Introducing the contact potential, the second term accounts for the contribution of the contact forces. The total external work done on this system is:

$$W = \int u^T\ F\ dV + \int u^T\ \phi\ dS + q^T\ R\ , \tag{6}$$

where P, $u(u(x,y), v(x,y))$, F, ϕ, q and R are internal nodal forces(discrete)[contact forces], displacement (continuous), body forces, surface tractions, displacement(discretized) and concentrated loads(nodal point forces), respectively. Then, the total potential energy functional is

$$\Pi_p = U - W\ . \tag{7}$$

The above equation indicates that the total potential energy is not simply a function of displacements and their derivatives, but also depends on their integrated effect.

For a linear elastic medium, the strain can be related to displacement by a differential operator D,

$$\epsilon = Du\ , \tag{8}$$

and the displacement field is discretized at the nodal points of an element by shape (interpolation) function matrix N,

$$u = Nq\ , \tag{9}$$

and finally, an expression for strain is:

$$\epsilon = Bq\ , \tag{10}$$

where B is the strain-displacement matrix and has κ^{-1} units when displacement q has κ units. (The explicit expressions for D, N and B will be given later.) This procedure invokes assumed-displacement finite element method where the displacements at the nodal points represent the degrees of freedom (unknowns). In this method, the essential boundary conditions are prescription of displacements, and the natural boundary conditions are prescription of stress. This implies that prescribing displacements at the boundaries alone is sufficient to solve the equations.

Substituting (4), (5) and (9) into (6), the total potential energy becomes:

$$\begin{aligned}
\Pi_p \;&= \tfrac{1}{2}q^T(\textstyle\sum\int_V B^T E B dV)q - q^T(\sum\int_V B^T E\epsilon_o dV) \\
&-q^T(\textstyle\sum\int_V N^T \sigma_o dV) - q^T(\sum\int_V N^T F_b dV) \\
&-q^T(\textstyle\sum\int_S N^T \phi dS) - q^T R + q_T\, P \\
&= \tfrac{1}{2}q^T(\textstyle\sum k)q - q^T(\gamma_{\epsilon_o} + \gamma_{\sigma_o} + \gamma_b + \gamma_s + R - P) \\
&= \tfrac{1}{2}q^T K q - q^T(Q - P)\,.
\end{aligned} \tag{11}$$

Summation has to be done over the total number of elements indicating the requirement for the assembly of element stiffness matrices and nodal forces. k is the element stiffness matrix whereas K is the assembled global stiffness matrix. Q represents the nodal forces caused by initial strain, initial stress, distributed forces and surface tractions. The stability of the equilibrium state is realized when the potential energy is minimum, i.e., when it is stationary with respect to "small variations" of displacement:

$$\Pi_p = stationary\,. \tag{12}$$

This is the principle of minimum potential energy. According to the calculus of variations, the first variation of total potential energy with respect to q must be zero:

$$\delta\Pi_p = 0\,, \tag{13}$$

such that:

$$Kq = Q - P\,. \tag{14}$$

This result is equivalent to that obtained by using the principle of virtual displacements(Zienkiewicz, 1986) and is the governing equation for contact problems. The structure stiffness matrix K relates nodal point displacements to nodal point forces. P is zero for continuum where there is no contact defined; therefore, for continuum the governing finite element equation is:

$$Kq = Q \; . \tag{15}$$

Thus, it is implied that Eqn.14 is the governing equation for discontinuum. Regardless of rheology, the finite element equations would be reduced to one of these equations, depending on what kind of medium(continuous/discontinuous) is chosen. It is, therefore, inherent in the finite element approach to solve for the deformation pattern of discontinuous media.

The j-th column of the stiffness matrix is the vector of nodal forces applied to maintain static equilibrium when j-th degree of freedom has unit displacement and others have zero displacement. The diagonal elements of the stiffness matrix are positive. A zero diagonal element would create zero reaction force Q, creating an unstable structure. It cannot be negative because this would lead to a physically unrealizable situation where displacement and force vectors lie in opposite direction. If only linear degrees of freedom are considered, the sum of each column is zero. When there is a linear relation between force and displacement, the stiffness matrix is symmetric. The stiffness matrix, however, is singular. Its rank is less than its dimensions by the number of rigid body motions. Eigenvalue analysis of the stiffness matrix determines the number of rigid body motions by the number of zero eigenvalues. In the 2-D case, there are 3 independent rigid body motions: translation in x- and y-axes and rotation.

Discretization of the Displacement Field

All the integral calculations at the element level (Fig.A1) are carried out in the isoparametric local coordinate system (ξ, η), then transformed into the global cartesian coordinate system (x, y). For a function f, this transformation is:

$$\int_v f dV = t \int_{x_a}^{x_b} \int_{y_a}^{y_b} f(x,y) dx dy = t \int_{-1}^{1} \int_{-1}^{1} f(\xi,\eta) \mid J \mid d\xi d\eta \; . \tag{16}$$

$| J |$ is the determinant of the Jacobian matrix for isoparametric transformation. t is the thickness of the elastic plate. The problem is set up as C^o and naturally considers only linear degrees of freedom (u,v). They are x-parallel and y-parallel displacements and may not be ξ-parallel and η-parallel. Plane linear isoparametric 4-node quadrilateral serendipidity elements with bilinear shape functions are used to discretize the displacement field (Fig.A2):

$$\begin{aligned} N_i &= \frac{1}{4}(1+\xi_i\xi)(1+\eta_i\eta), \\ \xi_i &= [\,-1\ \ 1\ \ 1\ \ -1\,], \\ \eta_i &= [\,-1\ \ 1\ \ 1\ \ -1], \\ i &= [\,1\ \ 2\ \ 3\ \ 4\,]. \end{aligned} \tag{17}$$

Any point in the element and its displacement can be related to the nodal point coordinates and their displacements such that:

$$\begin{bmatrix} x \\ y \\ u \\ v \end{bmatrix} = N^T \begin{bmatrix} c \\ q \end{bmatrix}, \tag{18}$$

and alternatively,

$$\begin{bmatrix} x \\ y \\ u \\ v \end{bmatrix} = \sum_{i=1}^{4} N_i \begin{bmatrix} x_i \\ y_i \\ u_i \\ v_i \end{bmatrix}, \tag{19}$$

where

$$\begin{bmatrix} N \end{bmatrix} = \begin{bmatrix} N_1 & 0 & N_2 & 0 & N_3 & 0 & N_4 & 0 \\ 0 & N_1 & 0 & N_2 & 0 & N_3 & 0 & N_4 \end{bmatrix}, \tag{20}$$

$$c = [\, x_1\ y_1\ x_2\ y_2\ x_3\ y_3\ x_4\ y_4 \,], \tag{21}$$

$$q = [\, u_1\ v_1\ u_2\ v_2\ u_3\ v_3\ u_4\ v_4 \,]. \tag{22}$$

As noted in Eqn.8, the strain field is related to the displacement field by the differential operator D,

$$D = \begin{bmatrix} \frac{\partial}{\partial x} & 0 \\ 0 & \frac{\partial}{\partial y} \\ \frac{\partial}{\partial y} & \frac{\partial}{\partial x} \end{bmatrix} . \tag{23}$$

The engineering definition for shear strain is implied; strain being:

$$\begin{bmatrix} \epsilon_x \\ \epsilon_y \\ \epsilon_{xy} \end{bmatrix} = \begin{bmatrix} 1 & 0 & 0 & 0 \\ 0 & 0 & 0 & 1 \\ 0 & 1 & 1 & 0 \end{bmatrix} \begin{bmatrix} u_{,x} \\ u_{,y} \\ v_{,x} \\ v_{,y} \end{bmatrix} . \tag{24}$$

Because the calculations are carried out in the natural(isoparametric) coordinate system, the strains have to be transformed into this coordinate system. This can be established only by transforming derivatives of the displacement vector. However, the only way to transform derivatives of displacements is by applying the chain rule. Let θ be a function of x and y, then invoking chain rule yields:

$$\begin{bmatrix} \theta_{,\xi} \\ \theta_{,\eta} \end{bmatrix} = \begin{bmatrix} x_{,\xi} & y_{,\xi} \\ x_{,\eta} & y_{,\eta} \end{bmatrix} \begin{bmatrix} \theta_{,x} \\ \theta_{,y} \end{bmatrix} , \tag{25}$$

or

$$\begin{bmatrix} \theta_{,\xi} \\ \theta_{,\eta} \end{bmatrix} = J \begin{bmatrix} \theta_{,x} \\ \theta_{,y} \end{bmatrix} . \tag{26}$$

And its the inverse relation is:

$$\begin{bmatrix} \theta_{,x} \\ \theta_{,y} \end{bmatrix} = \Gamma \begin{bmatrix} \theta_{,\xi} \\ \theta_{,\eta} \end{bmatrix} , \tag{27}$$

where

$$\Gamma = J^{-1} , \tag{28}$$

or

$$\Gamma = \frac{\begin{bmatrix} y_{,\eta} & -y_{,\xi} \\ -x_{,\eta} & x_{,\xi} \end{bmatrix}}{\mid J \mid}, \tag{29}$$

$\mid J \mid$ is the determinant of the jacobian matrix, J. Depending on the nodal point coordinates assigned, the size, shape and orientation of the element will change, and so will the elements of the Jacobian.

It is apparent that θ is either u or v. The displacements in the natural coordinate system then are related as:

$$\begin{bmatrix} u_{,x} \\ u_{,y} \\ v_{,x} \\ u_{,y} \end{bmatrix} = \begin{bmatrix} \Gamma_{11} & \Gamma_{12} & 0 & 0 \\ \Gamma_{21} & \Gamma_{22} & 0 & 0 \\ 0 & 0 & \Gamma_{21} & \Gamma_{11} \\ 0 & 0 & \Gamma_{2} & \Gamma_{12} \end{bmatrix} \begin{bmatrix} u_{,\xi} \\ u_{,\eta} \\ v_{,\xi} \\ u_{,\eta} \end{bmatrix}. \tag{30}$$

After finding the displacement function in the natural coordinate system, the nodal point displacements are found to be:

$$\begin{bmatrix} u_{,\xi} \\ u_{,\eta} \\ v_{,\xi} \\ u_{,\eta} \end{bmatrix} = \begin{bmatrix} N_{1,\xi} & 0 & N_{2,\xi} & 0 & N_{3,\xi} & 0 & N_{4,\xi} & 0 \\ N_{1,\eta} & 0 & N_{2,\eta} & 0 & N_{3,\eta} & 0 & N_{4,\eta} & 0 \\ 0 & N_{1,\xi} & 0 & N_{2,\xi} & 0 & N_{3,\xi} & 0 & N_{4,\xi} \\ 0 & N_{1,\eta} & 0 & N_{2,\eta} & 0 & N_{3,\eta} & 0 & N_{4,\eta} \end{bmatrix} \begin{bmatrix} q_1 \\ q_2 \\ q_3 \\ q_4 \\ q_5 \\ q_6 \\ q_7 \\ q_8 \end{bmatrix}. \tag{31}$$

The formulation above, recalling Eqn.10, explicitly defines the displacement-strain matrix, B,

$$\begin{bmatrix} 1 & 0 & 0 & 0 \\ 0 & 0 & 0 & 1 \\ 0 & 1 & 1 & 0 \end{bmatrix} \begin{bmatrix} \Gamma_{11} & \Gamma_{12} & 0 & 0 \\ \Gamma_{21} & \Gamma_{22} & 0 & 0 \\ 0 & 0 & \Gamma_{21} & \Gamma_{11} \\ 0 & 0 & \Gamma_{2} & \Gamma_{12} \end{bmatrix} \begin{bmatrix} N_{1,\xi} & 0 & N_{2,\xi} & 0 & N_{3,\xi} & 0 & N_{4,\xi} & 0 \\ N_{1,\eta} & 0 & N_{2,\eta} & 0 & N_{3,\eta} & 0 & N_{4,\eta} & 0 \\ 0 & N_{1,\xi} & 0 & N_{2,\xi} & 0 & N_{3,\xi} & 0 & N_{4,\xi} \\ 0 & N_{1,\eta} & 0 & N_{2,\eta} & 0 & N_{3,\eta} & 0 & N_{4,\eta} \end{bmatrix} . \tag{32}$$

Calculations of γ_{ϵ_o}, γ_{σ_o}, and γ_b are straightforward, however, x- and y-consistent forces from γ_s have to be calculated at their nodes. The present study, does not include surface tractions. For continuous media contact forces P are zero. (Note that P is another unknown as well as displacements).

The integrals in the equations are calculated by Gaussian Quadrature (Dahlquist and Björck, 1974). With this technique, a polynomial of degree $(2n - 1)$ is integrated exactly by n-point Gaussian quadrature. The Legendre polynomials are used to solve for the coefficients(referred to as Gauss-Legendre coefficients). The sampling points and weight in Gauss-Legendre integration are tabulated(for example, see Bathe, 1982). For the element described above, a 2 by 2 point integration is sufficient. However, for very distorted elements, a 3 by 3 point integration might be preferred(Bathe, 1989; pers. comm.). Once the nodal point displacements are calculated, the strains for each element are obtained from :

$$\epsilon = B\, q. \tag{33}$$

To calculate the stresses, one point integration for 4-node quadrilateral element at its center where $\xi = \eta = 0$ is sufficient and most accurate(for arguments, see, for example Cook, 1981). The stress at the center of the element, from Eqn.1 is :

$$\sigma = E\, B\, q - E\, \epsilon_o + \sigma_o\, . \tag{34}$$

From the strain and stress tensors, principal major and minor strains and stresses, and their orientation can be calculated and will be used to complement the deformation pattern. Let λ denote the tensor whose principal components (when there is no shear) and orientation is desired. Using Mohr circle representation (Johnson, 1970), the tensor rotation yields the principal components $\Lambda_{1,2}$,

$$\Lambda_{1,2} = \sqrt{\frac{1}{4}(\lambda_1 - \lambda_2)^2 \pm \lambda_3^2}\, , \tag{35}$$

the maximum shear component Λ_3,

$$\Lambda_3 = \frac{1}{2} \parallel \lambda_1 - \lambda_2 \parallel , \tag{36}$$

and their orientation Θ,

$$\Theta = \frac{1}{2} \arctan[\frac{2\,\lambda_3}{\lambda_1 - \lambda_2}] . \tag{37}$$

The deformation pattern of any structure, hence, is displayed with the following plots:

1. Undeformed structure with boundary conditions(scale in meters pointing North)
2. Deformed structure,
3. Displacement vectors(scale in meters)
4. Principal(major and minor) stress principal directions and their magnitude (scale in Pa),
5. Magnitude of Maximum shear stress (scale in Pa), and
6. Principal(major and minor) strain principal directions and their magnitude (scale has no units).

Solution of Equations

Follows a discussion of the solution of finite element equation(Eqn.15) for $P = 0$, which corresponds to continuous media. For stable solutions, at least 3 degrees of freedom must be constrained. Also, for structural stability, prescription of certain other degrees of freedom, depending on the boundary/internal conditions might be required(directly affecting q). The prescription of initial stresses (not included in the current study), body forces and initial strain also effect Q. Practically, the prescription of displacements at some nodes suppresses rigid body motion, as well as reducing the rank of the global stiffness matrix. At these nodes, the reaction forces must be calculated.

For continuous media, Eqn.15 prevails. First, the solution techniques for continuum are discussed, the deformation pattern for continuum exampled and, following the arguments favoring discontinuum approach , the solution technique and algorithms presented.

Consider Eqn.15 and partition the displacement vector q into two parts: q_a and q_b representing the unknown and prescribed displacements, respectively. The nodal force vector is partitioned in the same sense: Q_a and Q_b, where the latter represents the unknown reaction forces. A similar partitioning of the stiffness matrix is also performed. This leads to:

$$\begin{bmatrix} K_{aa} & K_{ab} \\ K_{ba} & K_{bb} \end{bmatrix} \begin{bmatrix} q_a \\ q_b \end{bmatrix} = \begin{bmatrix} Q_a \\ Q_b \end{bmatrix} . \tag{38}$$

The unknown displacements are

$$q_a = K_{aa}^{-1} \left[Q_a - K_{ab}\, q_b \right] , \tag{39}$$

and the unknown reaction forces are

$$Q_a = K_{ab}\, q_a + K_{bb}\, q_b . \tag{40}$$

This is a direct solution for the unkowns and could be solved by any linear system solvers which utilize the bandwidth of the stiffness matrix. In this study, LU decomposition technique is used (Press et al., 1986). However, when the structure gets complex, the the advantage provided by the bandwidth properties of the stiffness matrix is lost and makes direct solution techniques very costly. Therefore, an accelerated iterative solution becomes more attractive. Let φ define the residual of the $l-th$ iteration:

$$\varphi_i^l = \left[\sum_{j=1}^{n} K_{ij}\, q_j^l \right] - Q_i , \tag{41}$$

then, the ith degrees of freedom(displacement) at the lth iteration is

$$q_i^l = q_i^{l-1} - \omega\, \varphi_i^l , \qquad \{ \forall i \mid i \not\in \mathcal{N} \} , \tag{42}$$

where n is the total number of degrees of freedom, $\mathcal{N}$ is the set of prescribed degrees of freedom, and ω is the acceleration factor. This is known as the successive over-relaxation method. Later, for the contact algorithm, φ will represent the unknown contact forces developing at the contacting nodes. In calculation of φ, the sparsity of the stiffness matrix is utilized to save computational time. Any mode in a finite element mesh connects a finite number of elements and as a result, the displacement at this node is affected by the nodes of these elements. So, the multiplication amount is reduced more than 60 % by skipping the nodes which are not connected. Theoretically, the maximum number of iterations to converge and the related acceleration factor, can be calculated from the spectral radius of the relaxation operator. The large number of degrees of freedom yields $\omega \simeq 2.0$, and this causes divergence in all solutions. The number of maximum iterations will also be underestimated. These parameters are problem dependent and $\omega \simeq 1.6$ (Cook, 19781). For the problems concerned, $\omega \simeq 1.8 - 1.9$. Cost is reduced at least 5-fold and the convergence which is controlled in each iteration by(for Eqn.15):

$$\mathcal{C} = \sum_{i}^{n} \parallel \varphi_i^l \parallel . \tag{43}$$

$\mathcal{C}$ is the measure of convergence and must decrease as more iterations are performed.

References

Barka, A. A. and Gulen, L., 1989, New Constraints on Age and Total Offset of the North Anatolian Fault Zone: Implications for the Tectonics of the Eastern Mediterranean, submitted.

Barka, A. A., Gulen, L. and Toksoz, M. N., 1989, Tectonic Processes of the Continental Collision in the Vicinity of the Maras Triple Junction, Southern Turkey, submitted.

Barka, A. A. and Toksoz, M. N., 1989, Segmentation, Tectonics and Seismic Gaps of the North Anatolian Fault Zone in the Marmara and North Aegean Regions, submitted.

Bathe, K-J., 1982, Finite Element Procedures in Engineering Analysis, Prentice-Hall, Inc., New Jersey, 735 pp.

Bathe, K-J. and Chaudhry, A., 1985, A Solution Method for Axisymmetric Contact Problems, Int. J. Num., Meth. Eng., 21, 65-88.

Bathe, K-J. and Mijailovich, S., 1987, Finite Element Analysis of Frictional Contact Problems, J. De Mechanique Theorique et Applique, 375-389.

Bird, P. and Baumgardner, J., 1984, Fault Friction, Regional Stress, and Crust-Mantle Coupling in Southern California from Finite Element Models, J. Geophys. R., 89, 1932-1944.

Bird, P. and Piper, K., 1980, Plane-Stress Finite Element Models of Tectonic Flow in Southern California, Phys. Earth P. Int., 21, 158-175.

Bott, M. H. P., 1982, The Interior of the Earth, Edward Arnold Ltd., London, 403 pp.

Cater, F. W., 1926, On the Action of a Locomotive Driving Wheel,Procedings of the Royal Society, Series A, 112, 151-157.

Chaudhry, A. and Bathe, K-J., 1986, A Solution Method for Static and Dynamic Analysis of Three-Dimensional Contact Problems with Friction, Comp. Struct.,24, 885-873.

Cook, R. D., 1981, Concepts and Applications of Finite Element Analysis, John Wiley and Sons, New York, 537 pp.

Cox, A. and Hart, R. B., 1986, Plate Tectonics, Blackwell Scientific Publ., Inc., Boston, 392 pp.

Dahlquist and Björck, 1974, Numerical Methods, Prentice-Hall, Inc., New Jersey, 573 pp.

England, P. and Houseman G., 1986, Finite Srain Calculations of Continental Deformation 2. Comparison with the India-Asia Collison Zone, J. Geophys. R., 91, 3664-3676.

England, P. and McKenzie, D., 1982, A thin Viscous Sheet Model for continental deformation, Geophys. J. R. astr. Soc., 70, 295-231.

England, P. and McKenzie, D., 1983, Correction to : A thin Viscous Sheet Model for continental deformation, Geophys. J. R. astr. Soc., 73, 523-532.

England, P., Houseman G. and Sonder, L., 1985, Length Scales for Continental Deformation in

Convergent, Divergent, and Strike-Slip Environments: Analytical and Approximate solutions for a Thin Viscous Sheet Model, J. Geophys. R., 90, 3551-3557.

Goodman, R. E. and St. John, C., 1976, inite Element Analysis for Discontinous Rocks, , 149-175.

Goodman, R. E., 1975, Methods of Geological Engineering in Discontinous Rock, West Publishing Company, St. Paul, Minn.

Goodman, R. E., Taylor, R. L. and Brekke, T.R., 1968, A Model for the Mechanics of Jointed Rock, J. Soil Mechanics and Foundations Division, Proceedings of the American Society of Civil Engineers, 94, 637-659.

Hertz. H., 1881, On the Contact of Elastic Bodies, Jour. Math., 92.

Houseman G. and England, P., 1986, Finite Srain Calculations of Continental Deformation 1. Method and General Results for Convergent Zones, J. Geophys. R., 91, 3651-3663.

Johnson, A., 1970, Physical Processes in Geology, Freeman, Cooper and Co., California, 300 pp.

Johnson, C. B., 1975, Characteristics and Mechanics of Formation of Glacial Arcuate Abrasion Cracks, Ph. D. Thesis, The Pennsylvania State University, 253 pp.

Johnson, G. R., 1976, Analysis of Elastic-Plastic Impact Involving Severe Distorions, Trans. ASME Ser. E (USA),43,439-444.

Jaeger, J. C., Cook, N. G. W., 1979, Fundamentals of Rock Mechanics, Chapman and Hall, London, 593 pp.

Kasapoglu, E. K., 1973, Progressive Failure in Discontinous Rock Masses Subjected to Shear Deformation, Ph. D. Thesis, The Pensylvania State University, 165 pp.

Kasapoglu, E. K. and Toksoz, M. N., 1983, Tectonic Consequnces of the Collision of the Arabian and Eurasian Plates: Finite Element Models, Tectonophys., 100, 71-95.

Kasapoglu, E. K. and Toksoz, M. N., 1989, Plate-Motion Induced Deformations in the Eastern Mediterranean, Tectonophys., submitted.

Kumbora, K., 1979, Solutions of the Contact Problems by the Assumed Stress Hybrid Model, Ph. D. Thesis, Massachusetts Institute of Technology, 144 pp.

McKenzie, D., 1978, Active Tectonics of the Alpine-Himalyan Belt: the Aegean Sea and Surrounding Regions, Geophys. J. R. astr. Soc., 55, 217-254.

Molnar, P. and Lyon-Caen, H., 1988, Some Physical Aspects of the Support, Structure, and the Evolution of Mountain Belts, Geol. Soc. Am., Special Paper 128, 179- 207.

Press, W. H., Flanerry, B. P., Teukolsky, S. A., and Vetterling T. W., 1986, Numerical Recipes: The Art of Scientific Computing, Cambridge University Press, Cambridge, 818 p.

Richardson, R. D., 1972, Intraplalte Stress and the Driving Mechanism for Plate Tectonics, Ph. D. Thesis, M.I.T., 372 pp.

Sonder, L.,England, P. and Houseman G., 1986, Continuum Calculations of Continental Deformation in Transcurrent Environments, J. Geophys. R., 91, 3664-3676.

Timoshenko, S., 1934, Theory of Elasticity, McGraw-Hill Book Co., New York, 416 pp.

Turcotte, D. L. and Schubert, 1982, Geodynamics, Application of Continuum Physics to Geological Problems, John Wiley and Sons, New York, 450 pp.

Turner, M. J., Clough, R. W., Martin, H. C. and Topp, L. J ., 1956, Stiffness and Deflection Analysis of Complex Structures, JAeros, 23(9), 805-823.

Wang, Y. J., and Voight, B., 1969, A Discrete Element Stress Analysis Model for Discontinous Materials, Proceedings of the International Symposium of Large Permanent Underground Openings, 112-115.

Wilson, E. L., , Finite Elements for Foundations, Joints and Fluids, , 319-350.

Zienkiewicz, O. C. and Cheung, Y.K., 1967, The Finite Element Method in Structural and Continuum Mechanics., McGraw-Hill, London.

Zienkiewicz, O. C. 1986, The Finite Element Method, McGraw-Hill, London, 787 pp.

Figure Captions

Fig. 1: (a) The type of plate interactions at their boundaries in x-y-z space. (b) 2-D finite element approximation of plate boundaries when the dip of their boundary is 90° for divergent and trancurrent, and continent-continent collison boundaries , and 0° for continent-ocean collison boundary [x-z plane]. (c) The behavior of plates at their boundaries in the x-y plane. Tension release(seperation), sliding contact(slip), sticking contact(single-node-continuum) and overlap modes corresponding to divergence, strike-slip faulting, continent-ocean collision and continent-continent collision, respectively.

Fig. 2: The deformation pattern of a continuum model simulating transcurrent plate boundary.

Fig. 3: The deformation pattern of a continuum model simulating divergent plate boundary.

Fig. 4: The deformation pattern of a discontinuum model simulating transcurrent plate boundary: contact problem.

Fig. 5: The deformation pattern of a discontinuum model simulating divergent plate boundary: contact problem.

Fig. 6: Schematic representation of contact problem, after Bathe and Chaudry, (1985).

Fig. 7: Coulomb Navier Criterion, after Wang and Voight(1969).

Fig. 8: Nodal configuration at the contact surface

Fig. 9: Deformation pattern of third type plate boundary: contact problem mode II.

Fig.10 : Deformation pattern of second and third types plate boundaries: contact problem modes II and III.

Fig.11 : Deformation pattern of first type plate boundary: contact problem mode I.

Fig.12 : Deformation pattern of fourth type plate boundary: contact problem mode IV.

Fig.13 : Deformation pattern of fourth type plate boundary: contact problem mode II with internal deformation.

Fig.14 : Deformation pattern of third type plate boundary: contact problem mode II with body forces caused by elevation changes.

Fig.15 : Present-day tectonics of Eastern Mediterranean. After Hempton, 1985.

Fig.16 : Focal Mechanism Solutions. After McKenzie(1978)

Fig.17 : Local relative plate velocities.

Fig.18 : Index map of the region where the finite element contact problem is applied.

Fig.19 : Deformation pattern of the eastern Mediterranean[Model 1]: Contact. Driving force: boundary displacements.

Fig.20 : Deformation pattern of the eastern Mediterranean[Model 2]: Contact. Driving force: boundary displacements. The convergence at the Cyprean arc and shortening at the Bitlis Suture are included.

Fig.21 : Deformation pattern of the eastern Mediterranean[Model 3]: Contact. Driving forces: boundary displacements and gravitational forces. The convergence at the Cyprean arc and shortening at the Bitlis Suture, internal deformation at the Palmyra Kink are included.

Fig.A1: Global and isoparametric(natural) coordinate systems and their mapping.

Fig.A2: Bilinear shape functions for 4-node quadrilateral element.

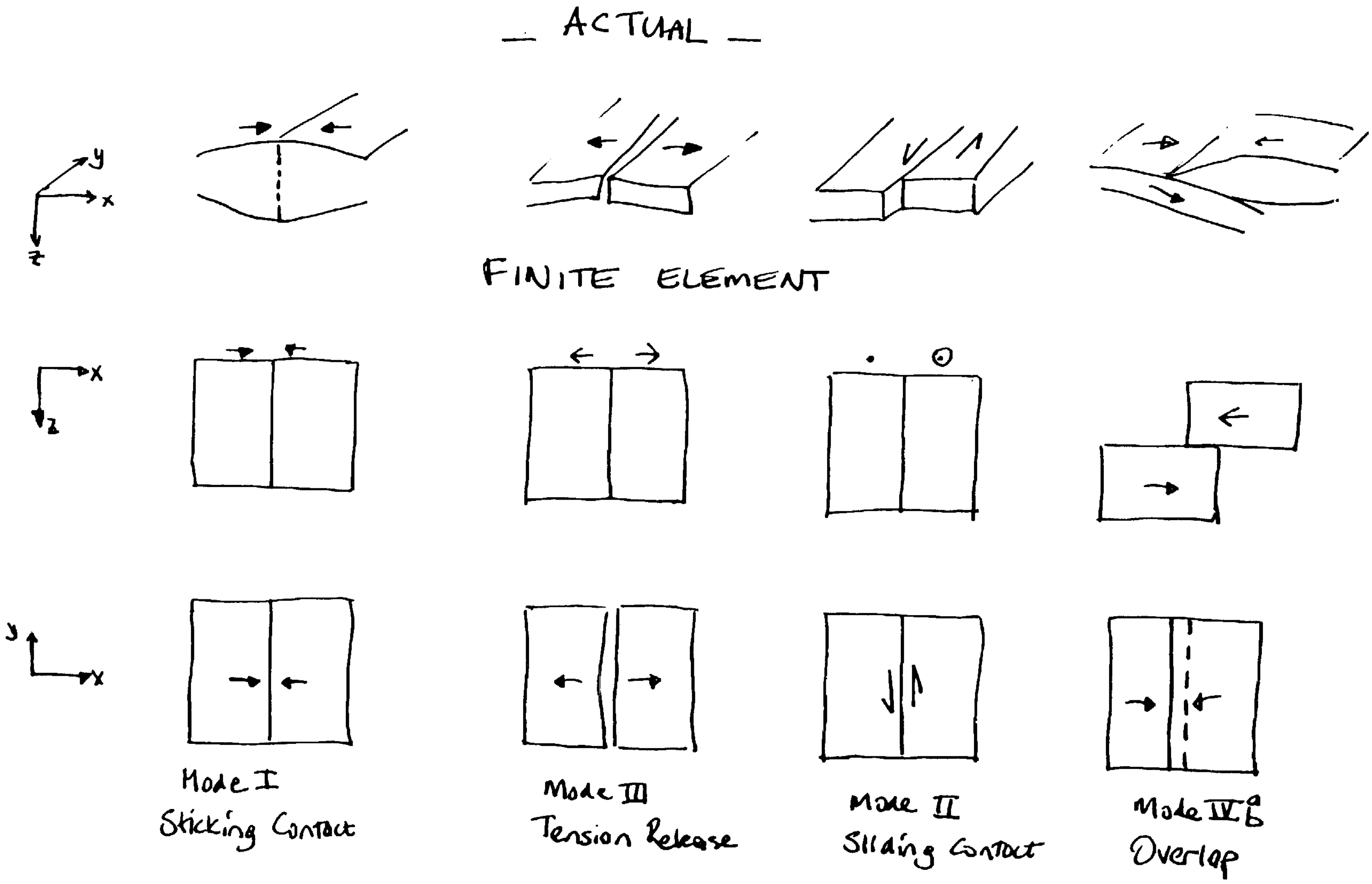

Fig. 1: (a) The type of plate interactions at their boundaries in x-y-z space. (b) 2-D finite element approximation of plate boundaries when the dip of their boundary is 90° for divergent and trancurrent, and continent-continent collison boundaries , and 0° for continent-ocean collison boundary [x-z plane]. (c) The behavior of plates at their boundaries in the x-y plane. Tension release(seperation), sliding contact(slip), sticking contact(single-node-continuum) and overlap modes corresponding to divergence, strike-slip faulting, continent-ocean collision and continent-continent collision, respectively.

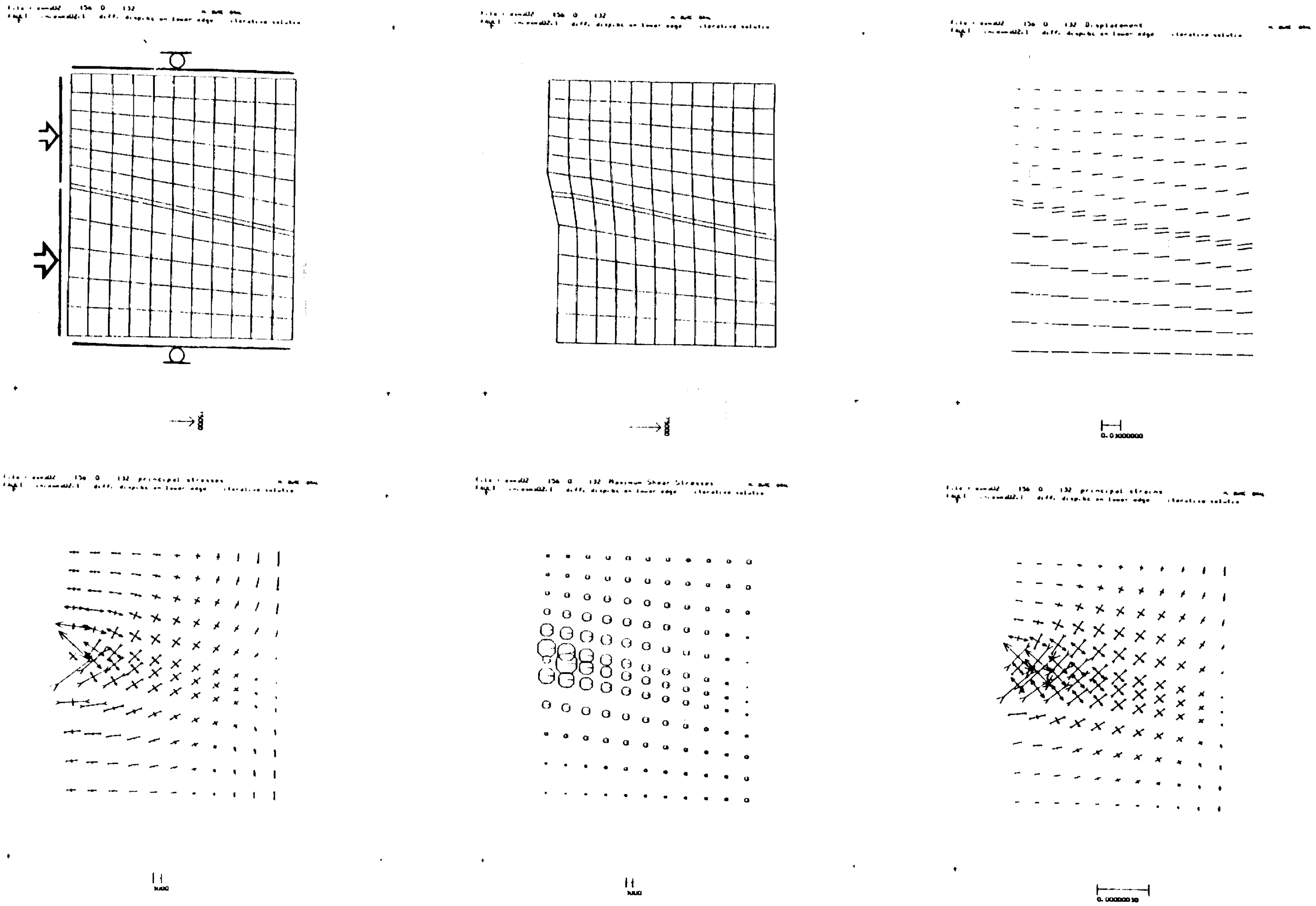

Fig. 2: The deformation pattern of a continuum model simulating transcurrent plate boundary.

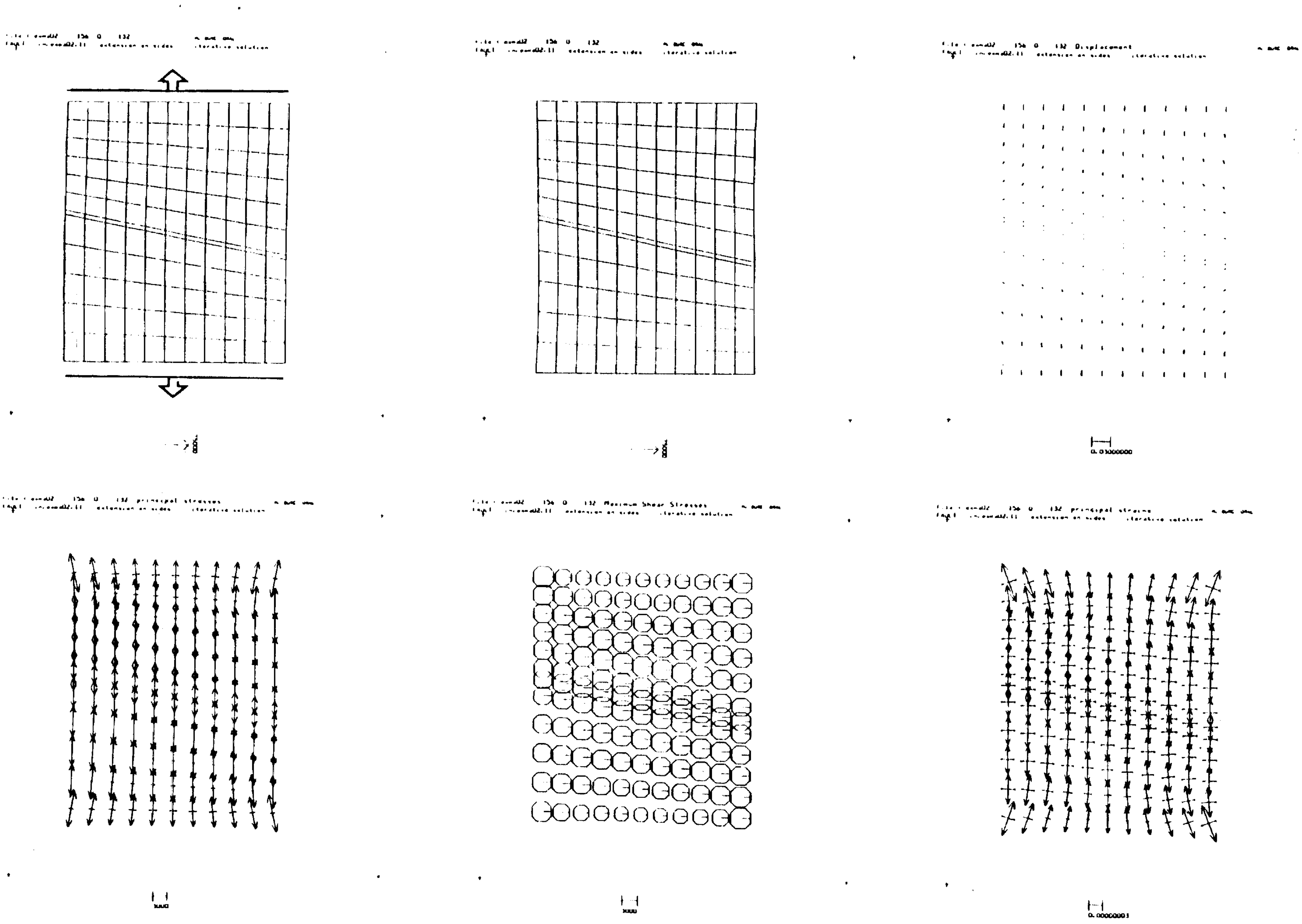

ORIGINAL PAGE IS
OF POOR QUALITY

Fig. 3: The deformation pattern of a continuum model simulating divergent plate boundary.

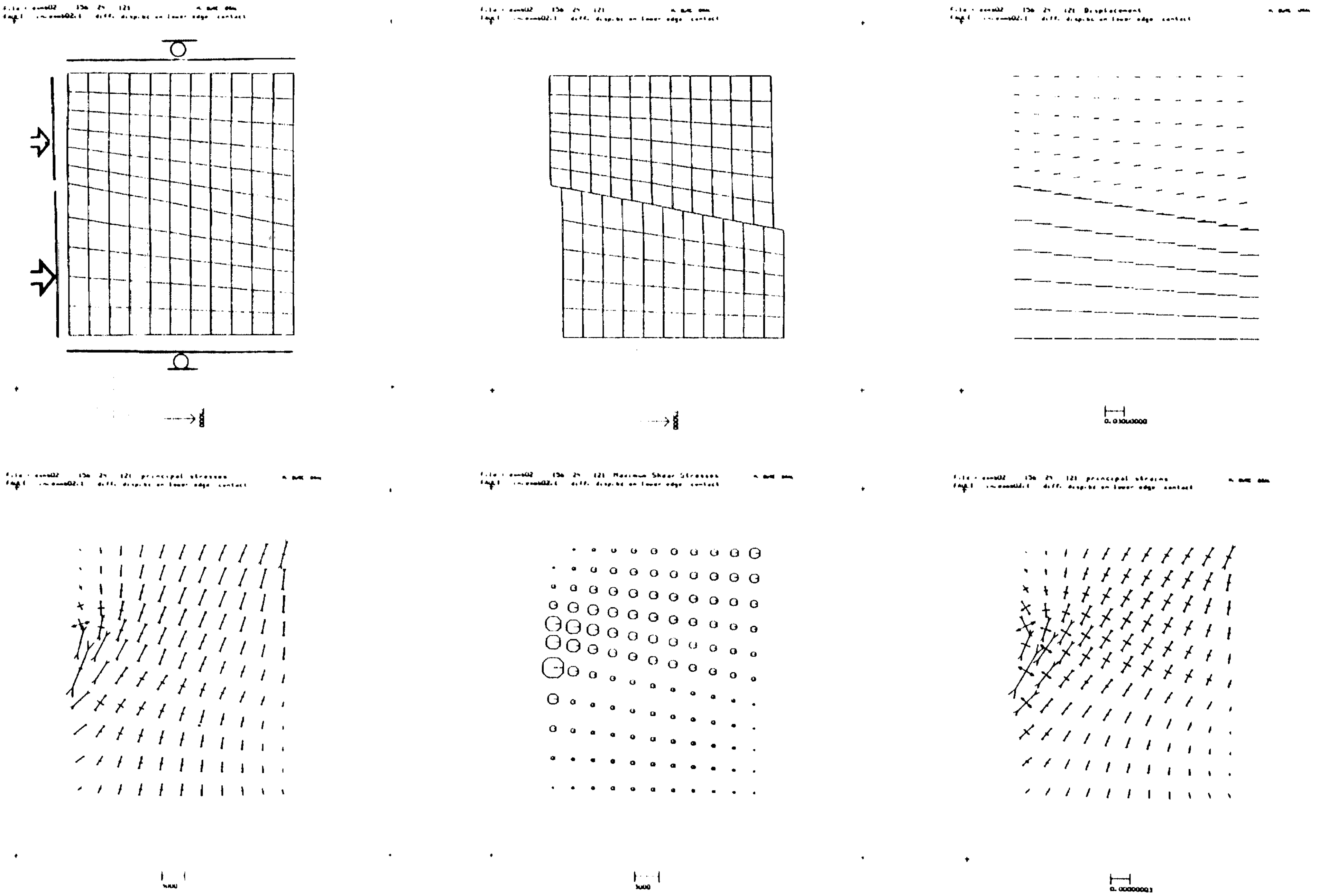

Fig. 4: The deformation pattern of a discontinuum model simulating transcurrent plate boundary: contact problem.

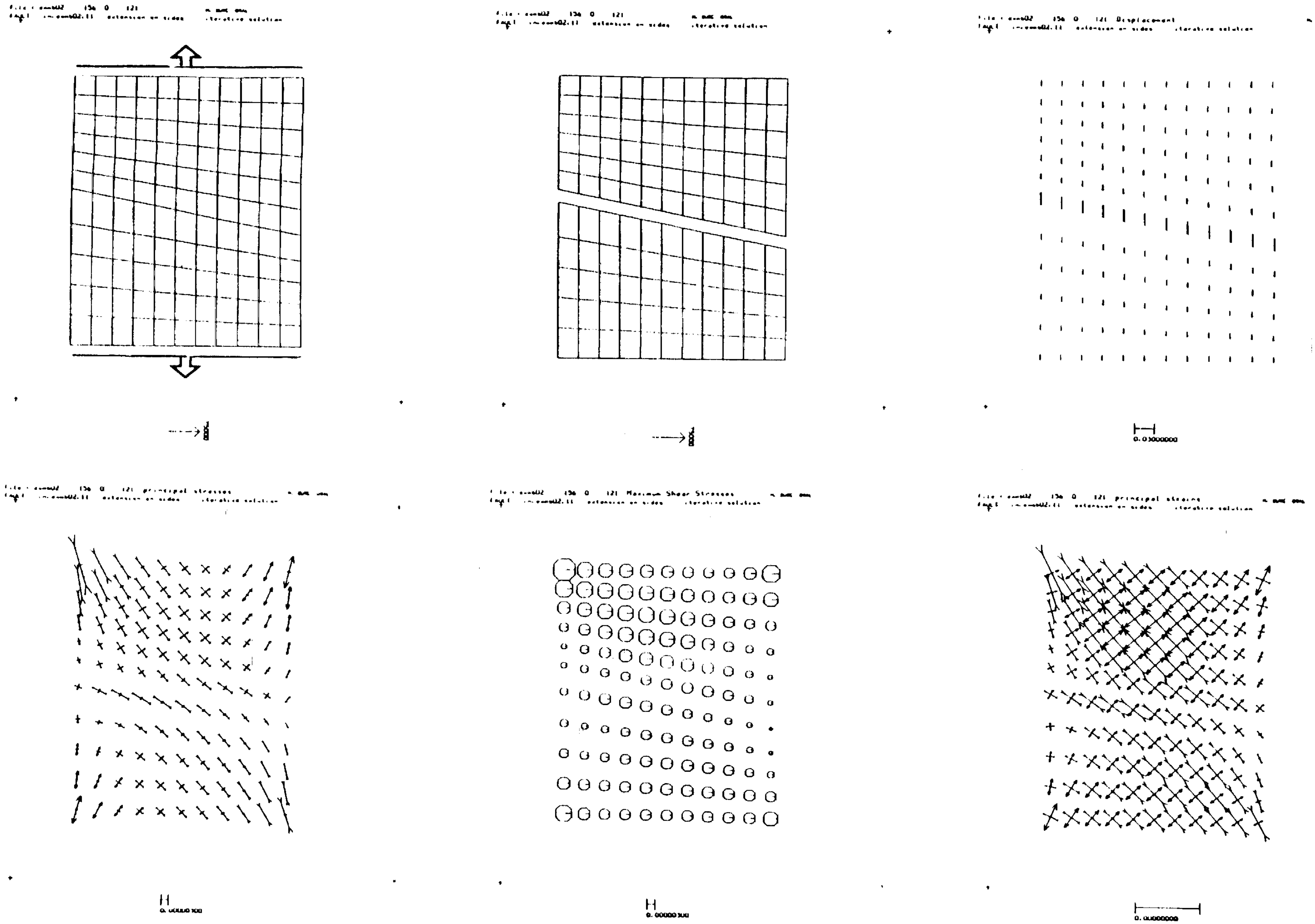

Fig. 5: The deformation pattern of a discontinuum model simulating divergent plate boundary: contact problem.

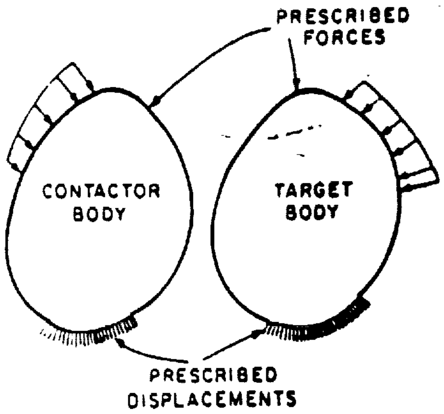

(a) Condition prior to contact

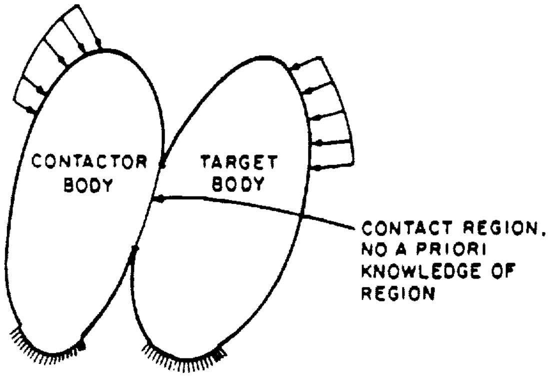

(b) Condition at contact

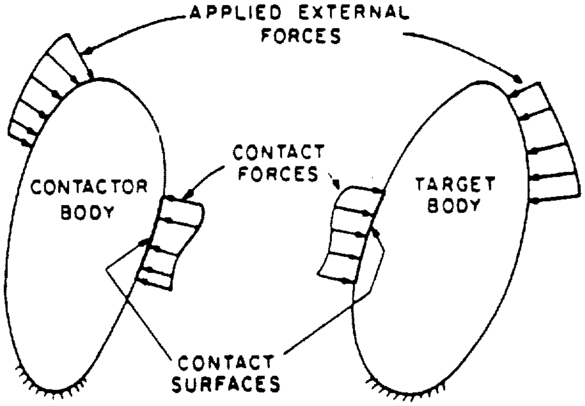

(c) Forces acting on contactor and target bodies

Figure 1. Schematic representation of problem considered

Fig. 6: Schematic representation of contact problem, after Bathe and Chaudry, (1985).

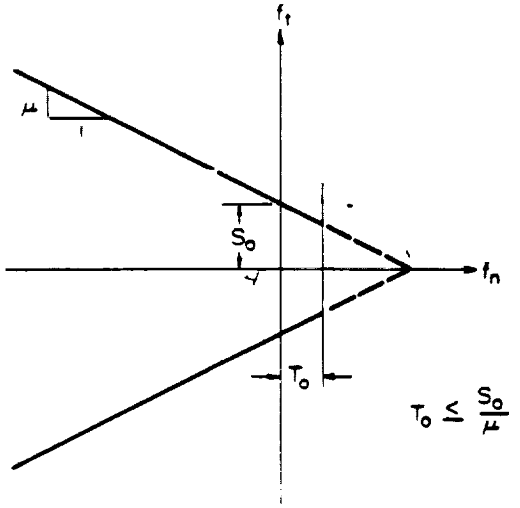

Fig. 7: Coulomb Navier Criterion, after Wang and Voight(1969).

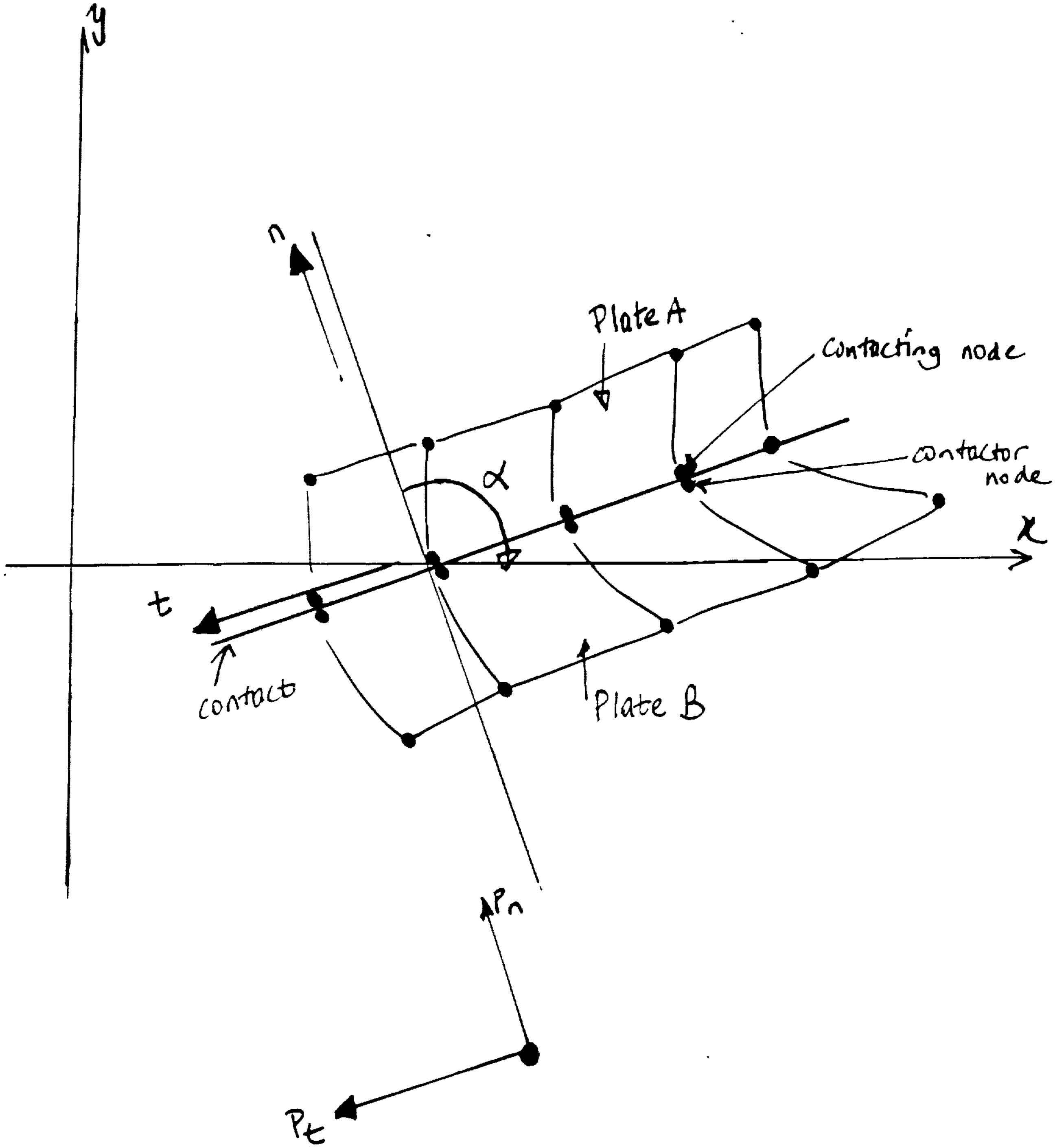

Fig. 8: Nodal configuration at the contact surface

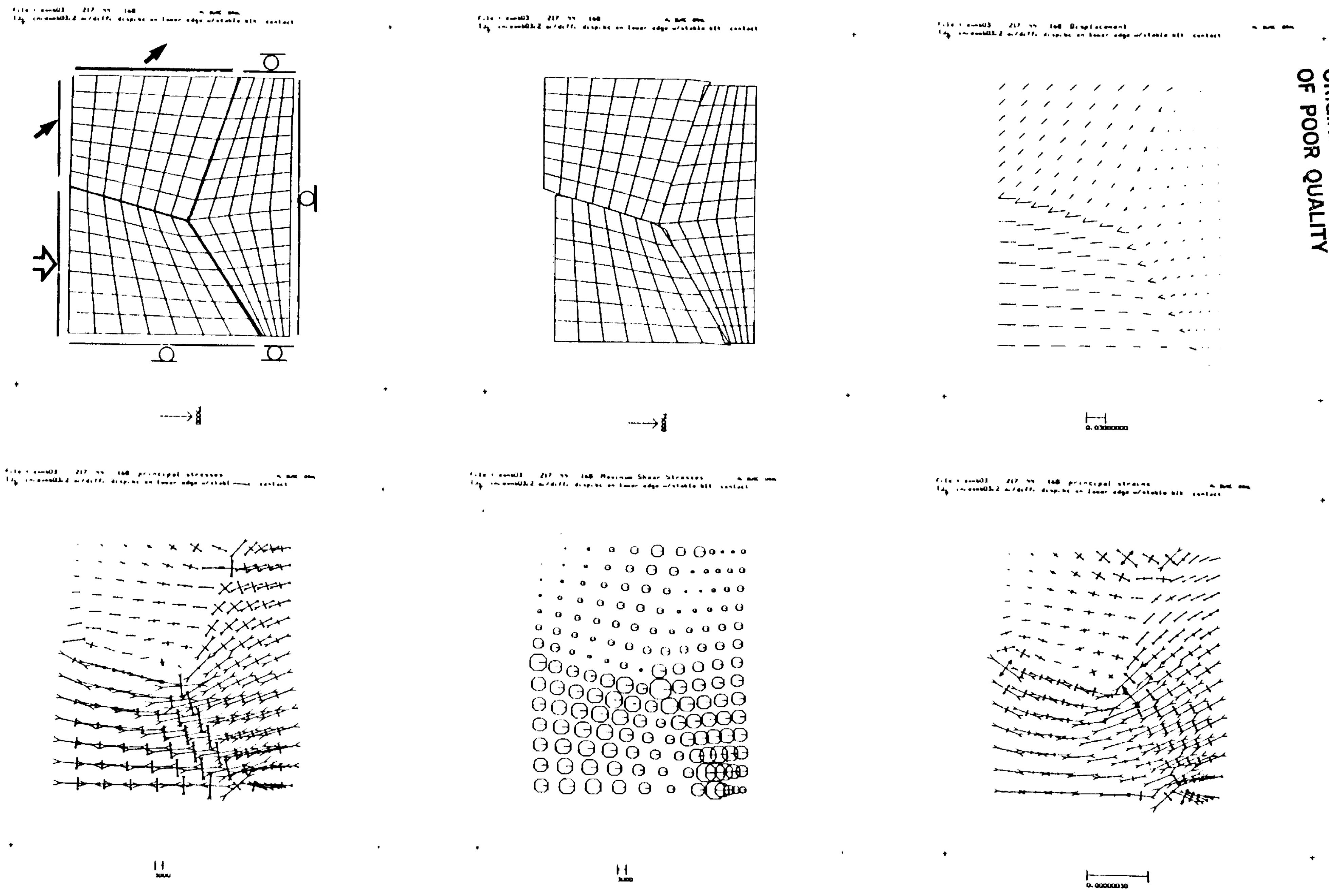

Fig. 9: Deformation pattern of third type plate boundary: contact problem mode II.

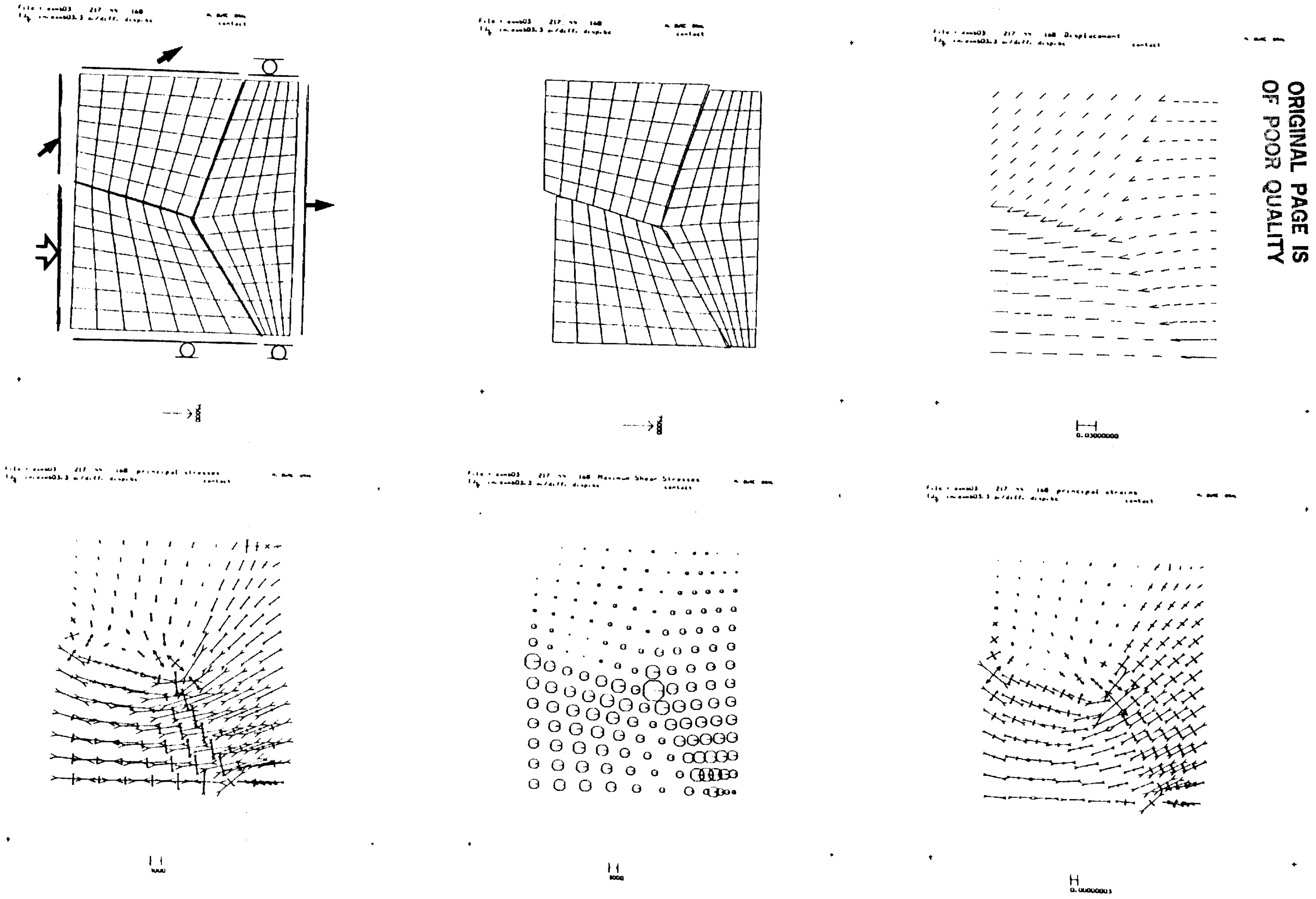

Fig.10 : Deformation pattern of second and third types plate boundaries: contact problem modes II and III.

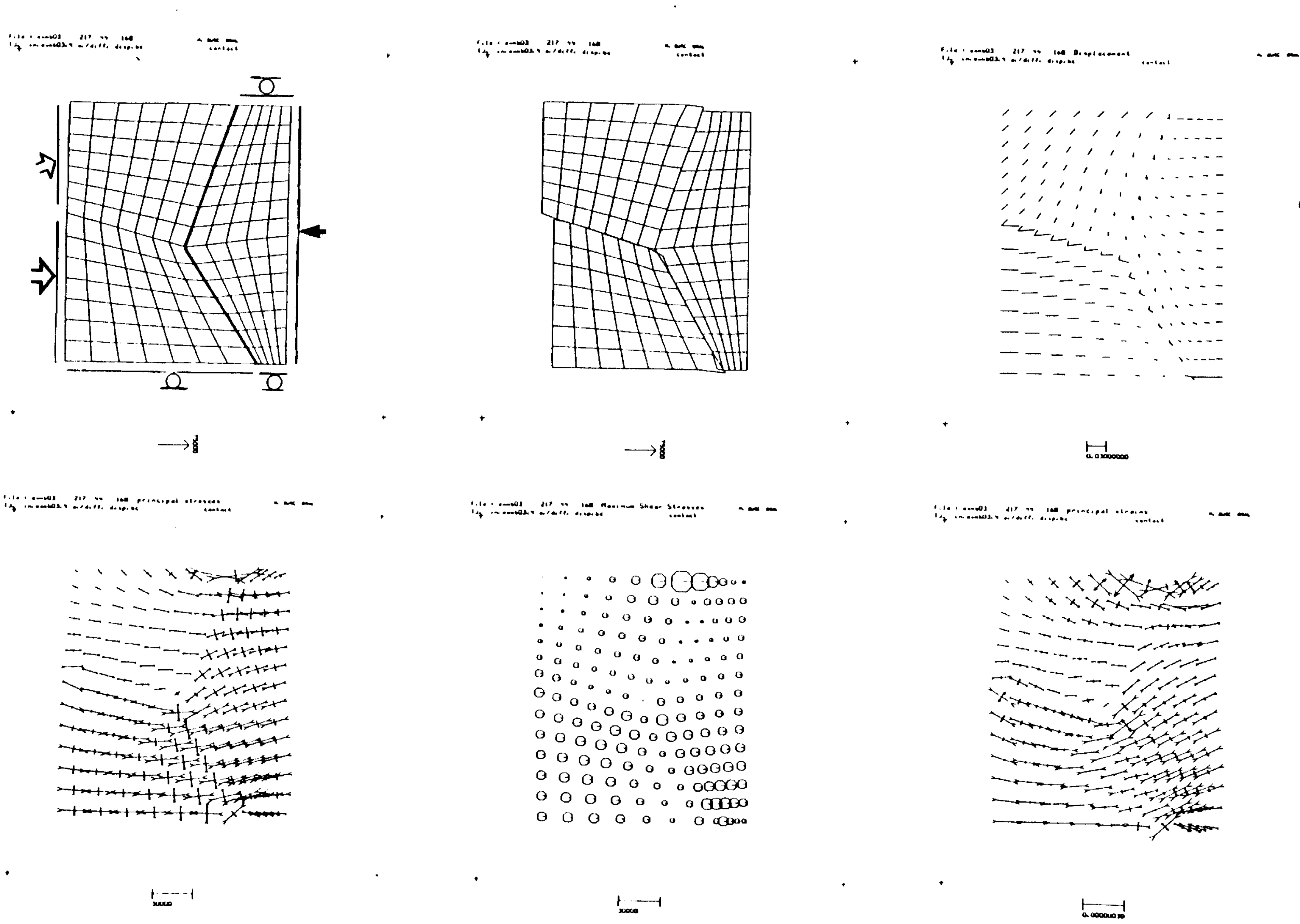

Fig.11 : Deformation pattern of first type plate boundary: contact problem mode I.

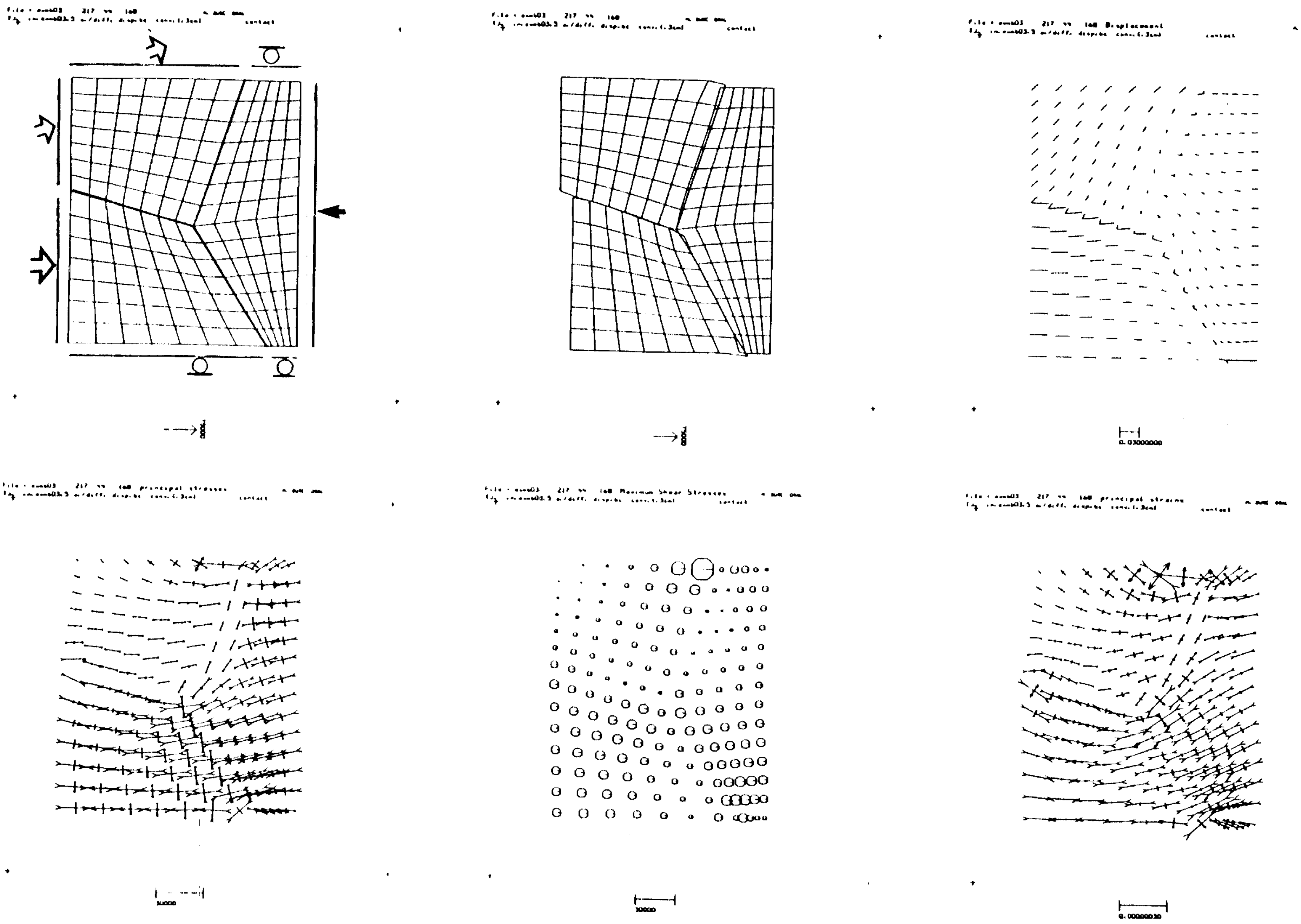

Fig.12 : Deformation pattern of fourth type plate boundary: contact problem mode IV.

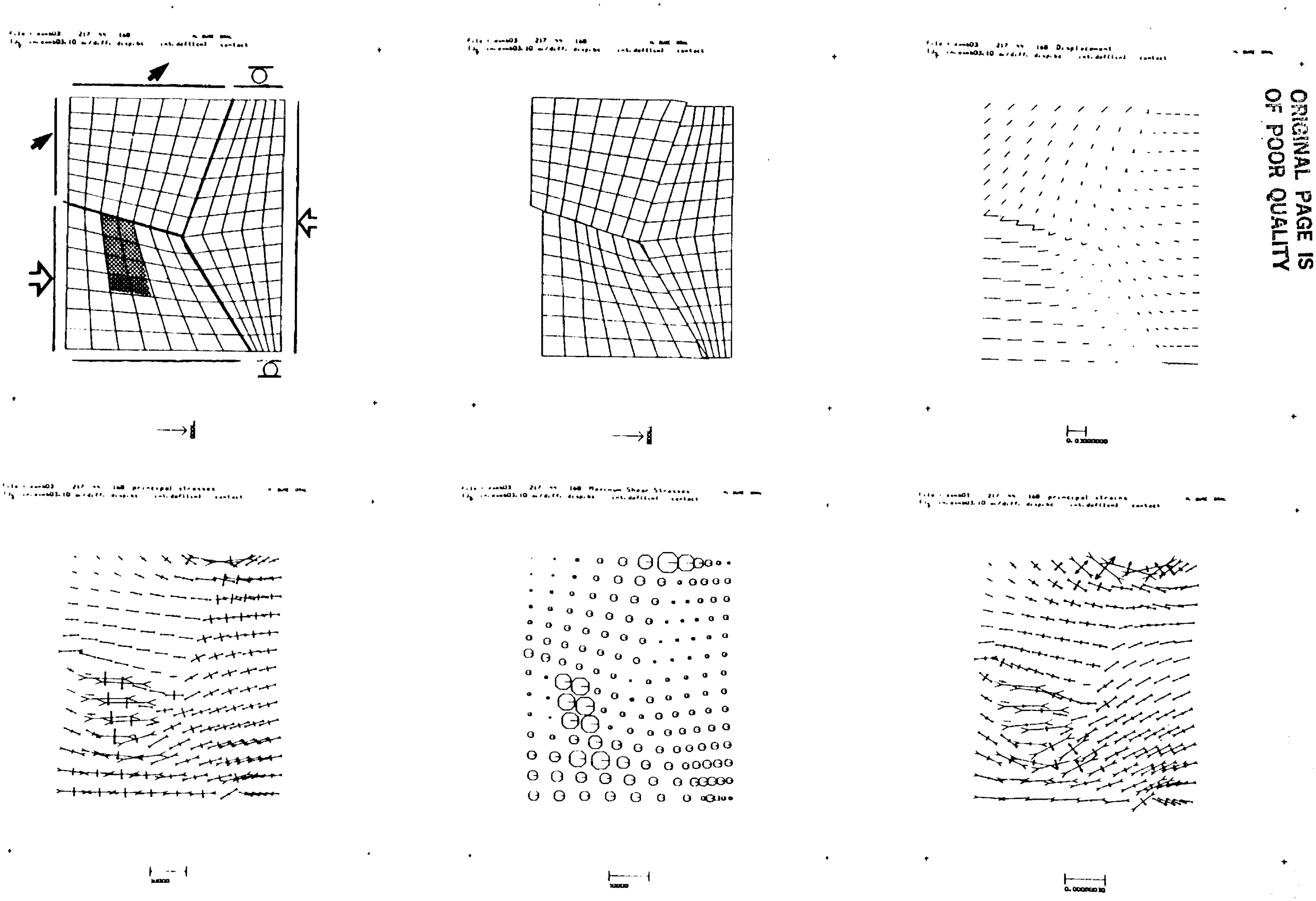

Fig.13 : Deformation pattern of fourth type plate boundary: contact problem mode II with internal deformation.

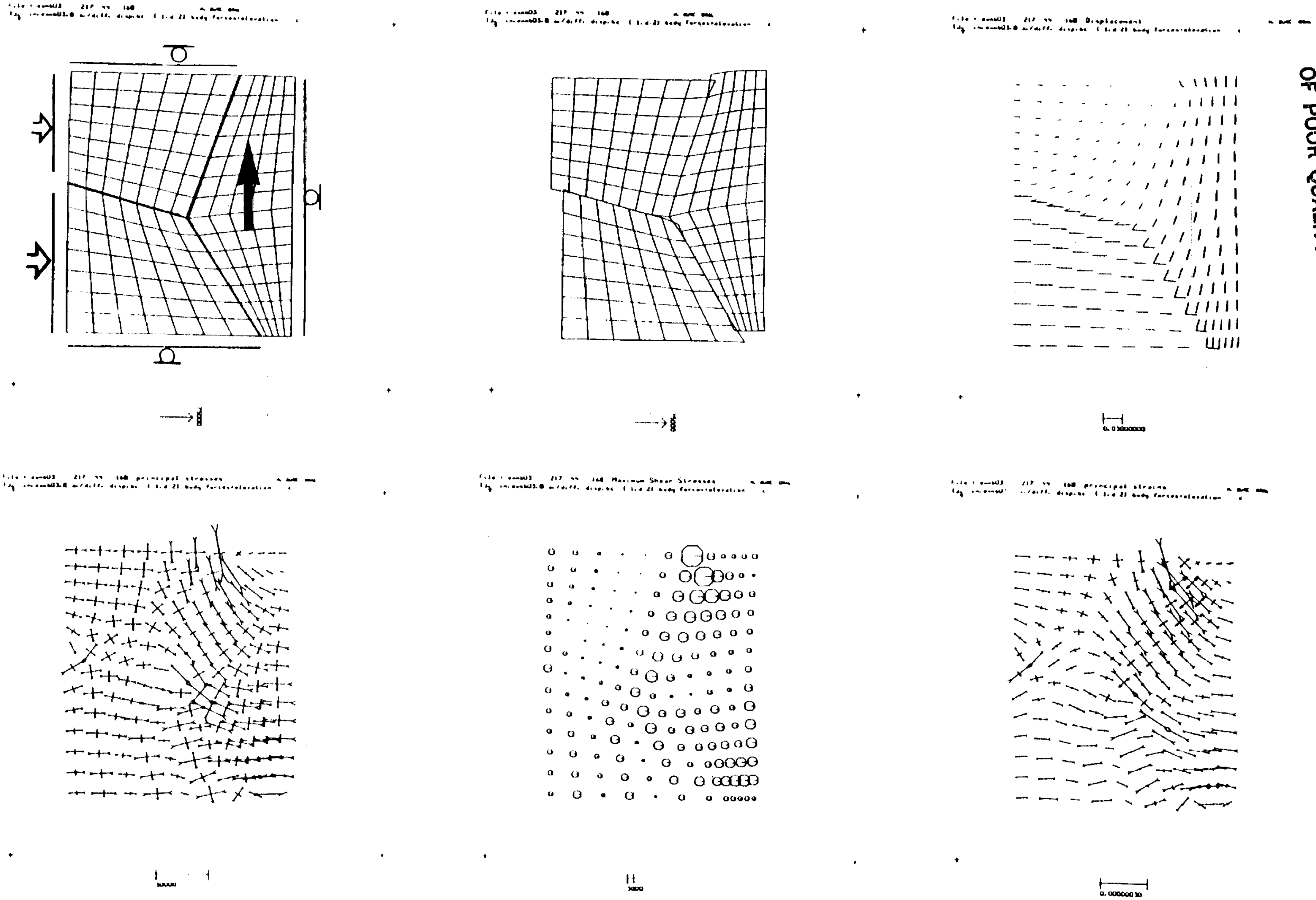

Fig.14 : Deformation pattern of third type plate boundary: contact problem mode II with body forces caused by elevation changes.

ORIGINAL PAGE IS
OF POOR QUALITY

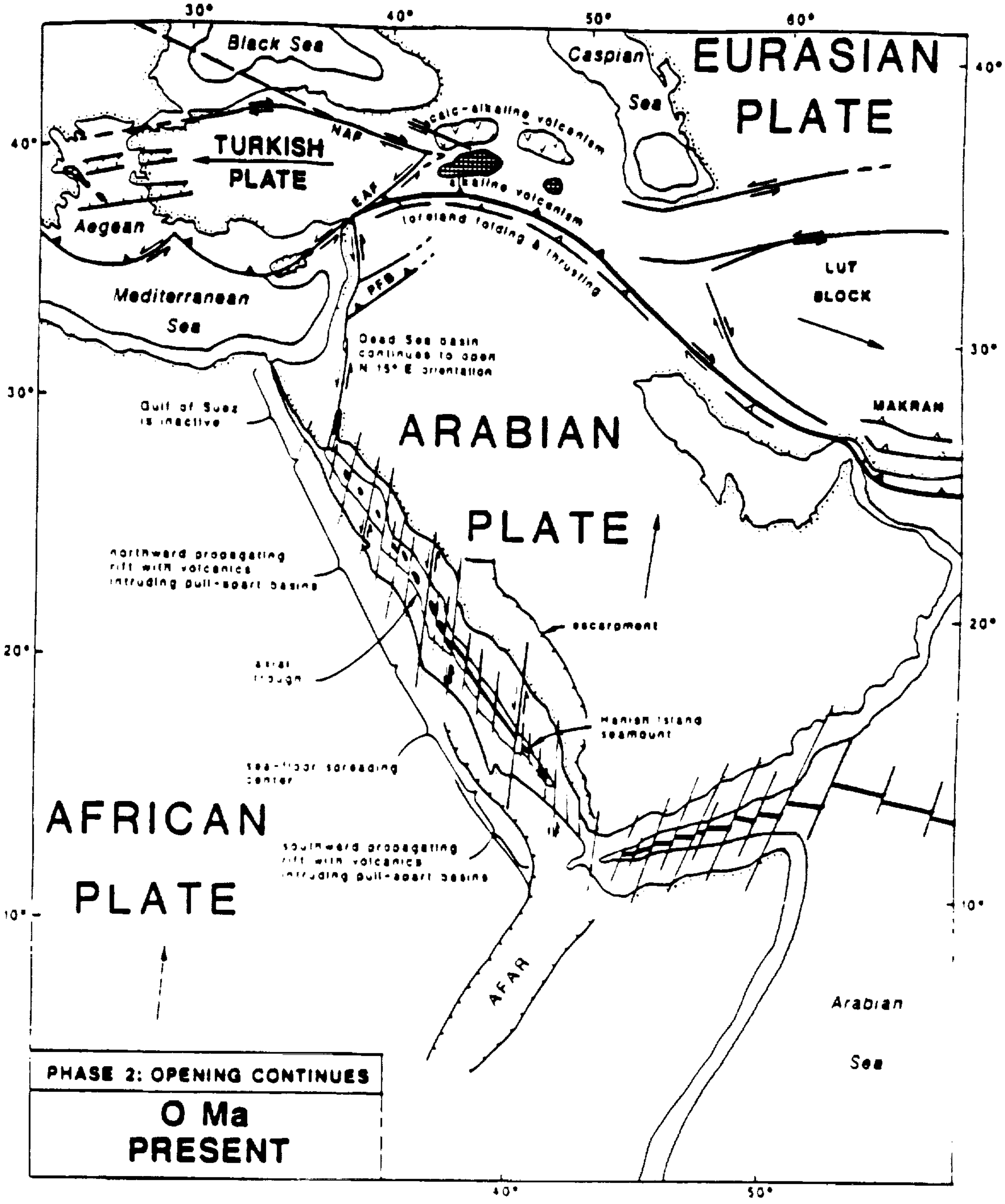

Fig.15 : Present-day tectonics of Eastern Mediterranean. After Hempton, 1985.

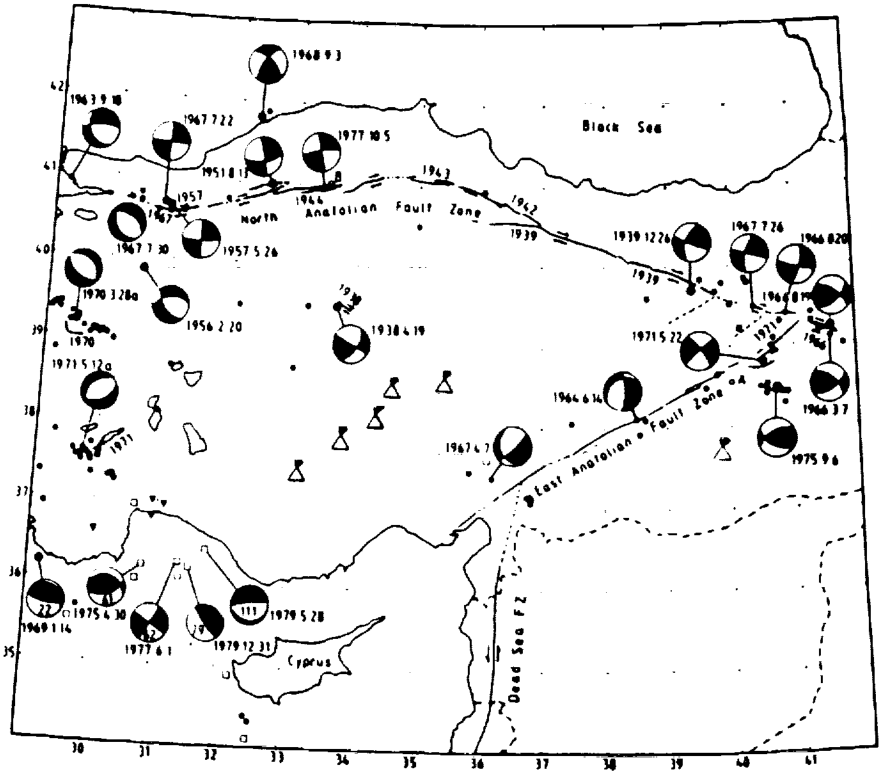

Fig.16 : Focal Mechanism Solutions. After McKenzie(1978)

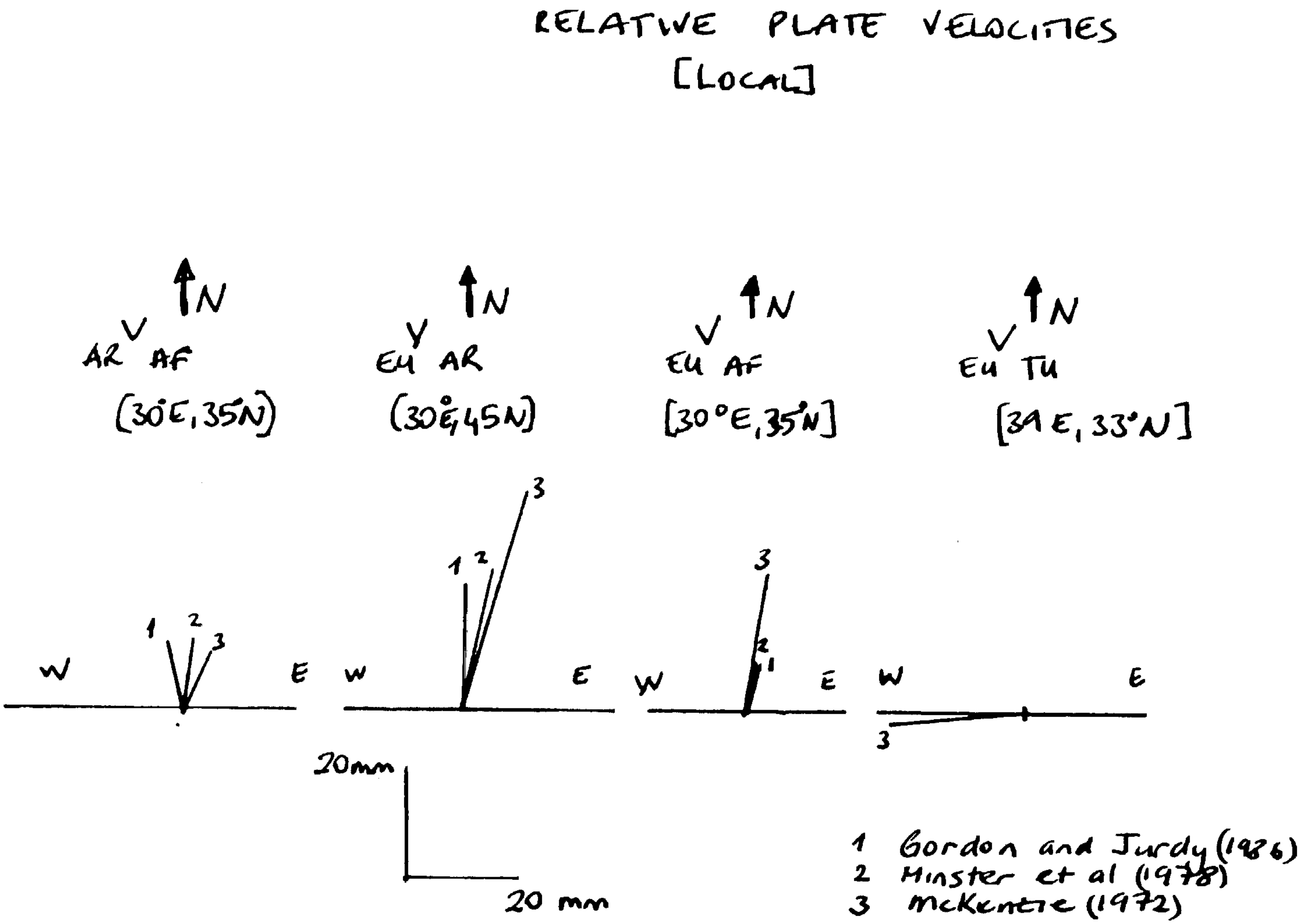

Fig.17 : Local relative plate velocities.

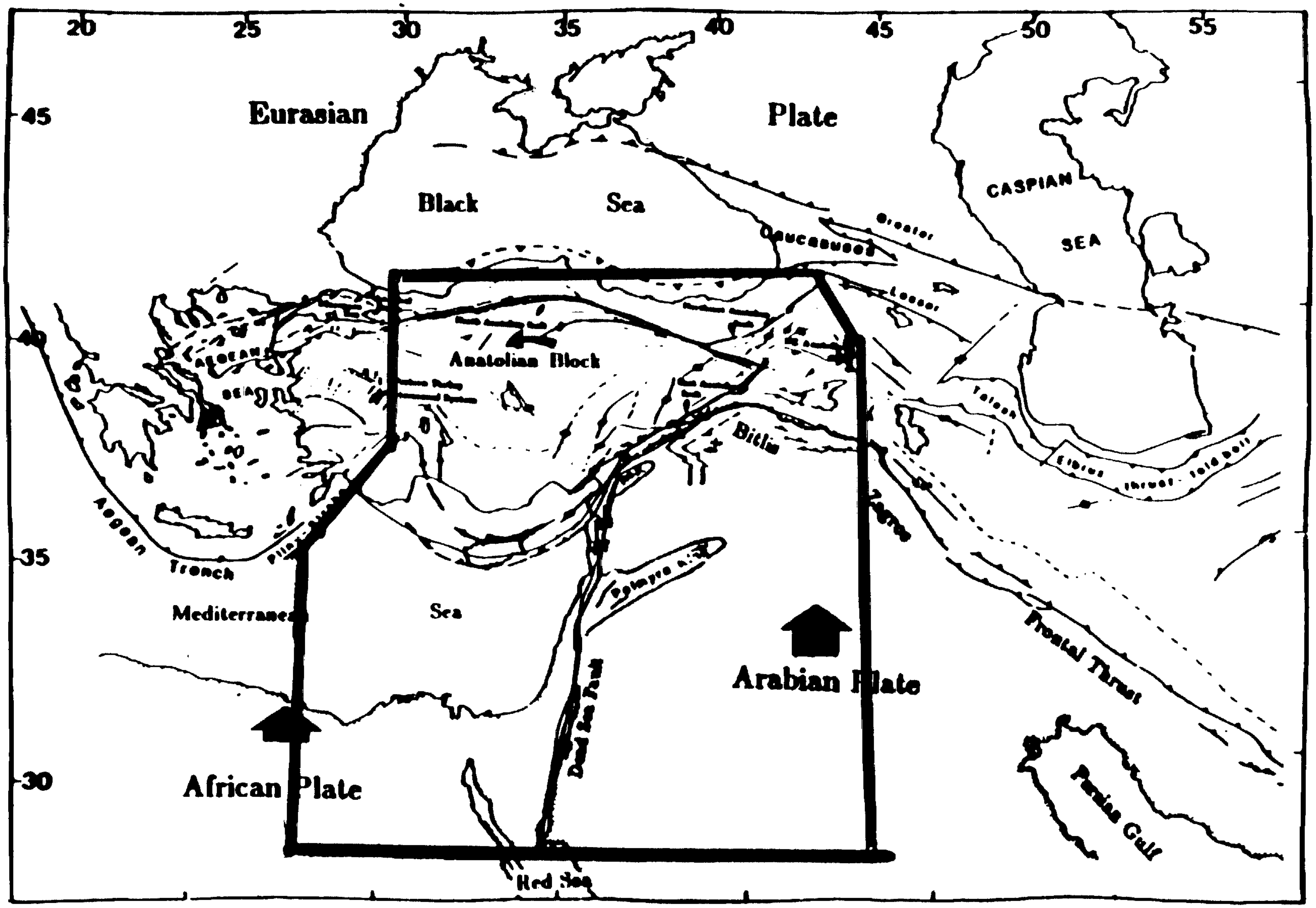

Fig.18 : Index map of the region where the finite element contact problem is applied.

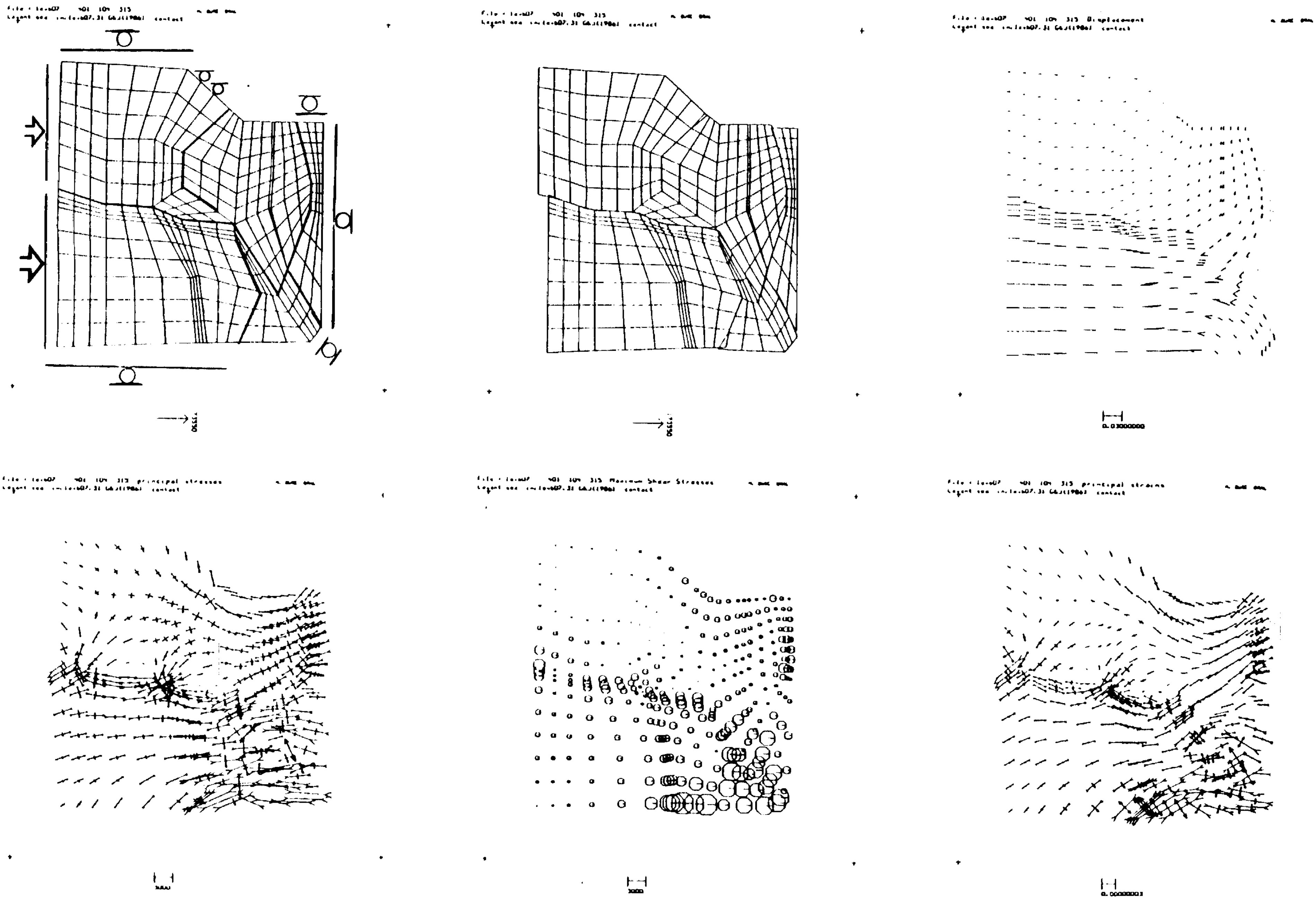

Fig.19 : Deformation pattern of the eastern Mediterranean[Model 1]: Contact. Driving force: boundary displacements.

ORIGINAL PAGE IS
OF POOR QUALITY

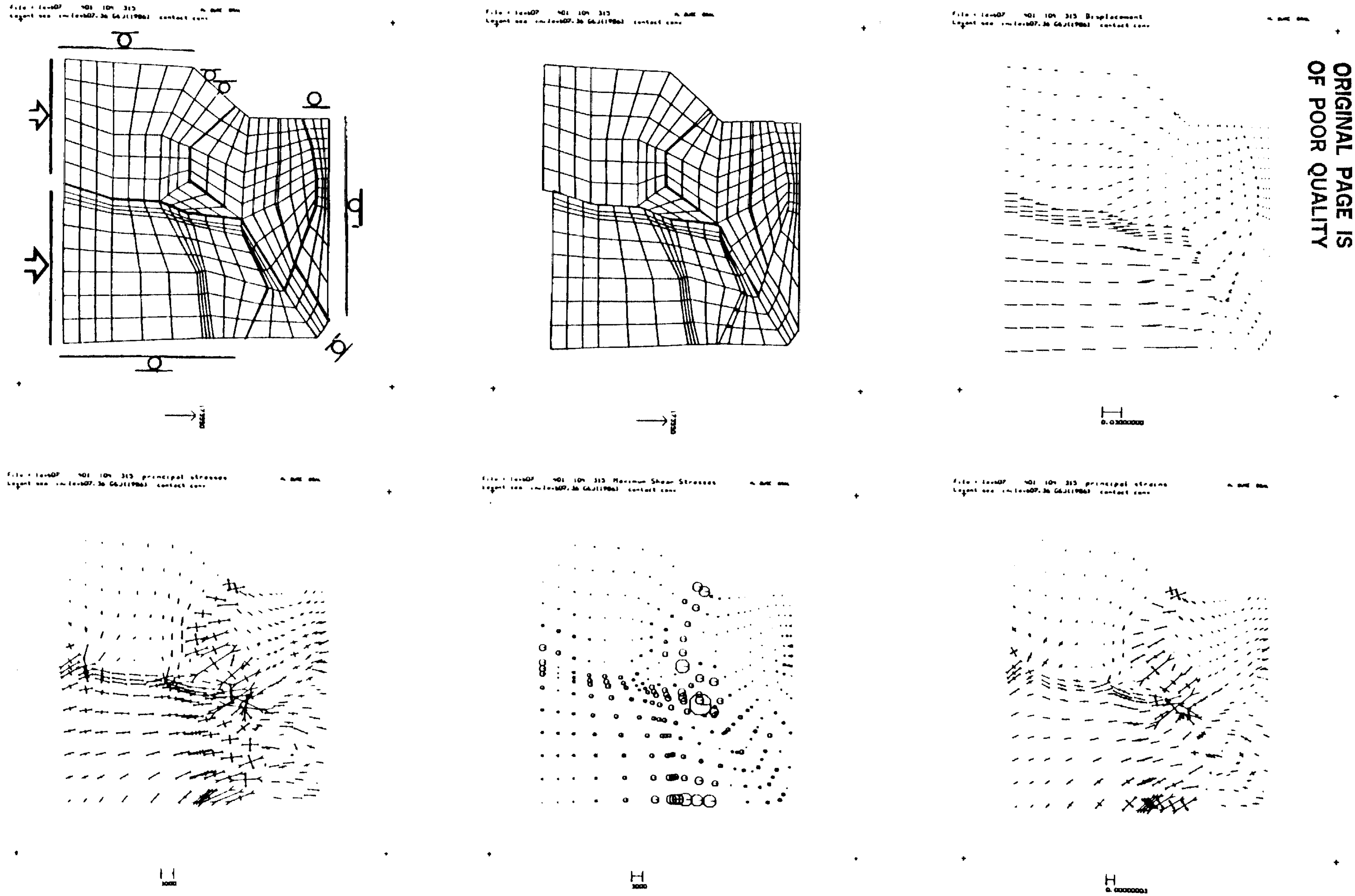

Fig.20 : Deformation pattern of the eastern Mediterranean[Model 2]: Contact. Driving force: boundary displacements. The convergence at the Cyprean arc and shortening at the Bitlis Suture are included.

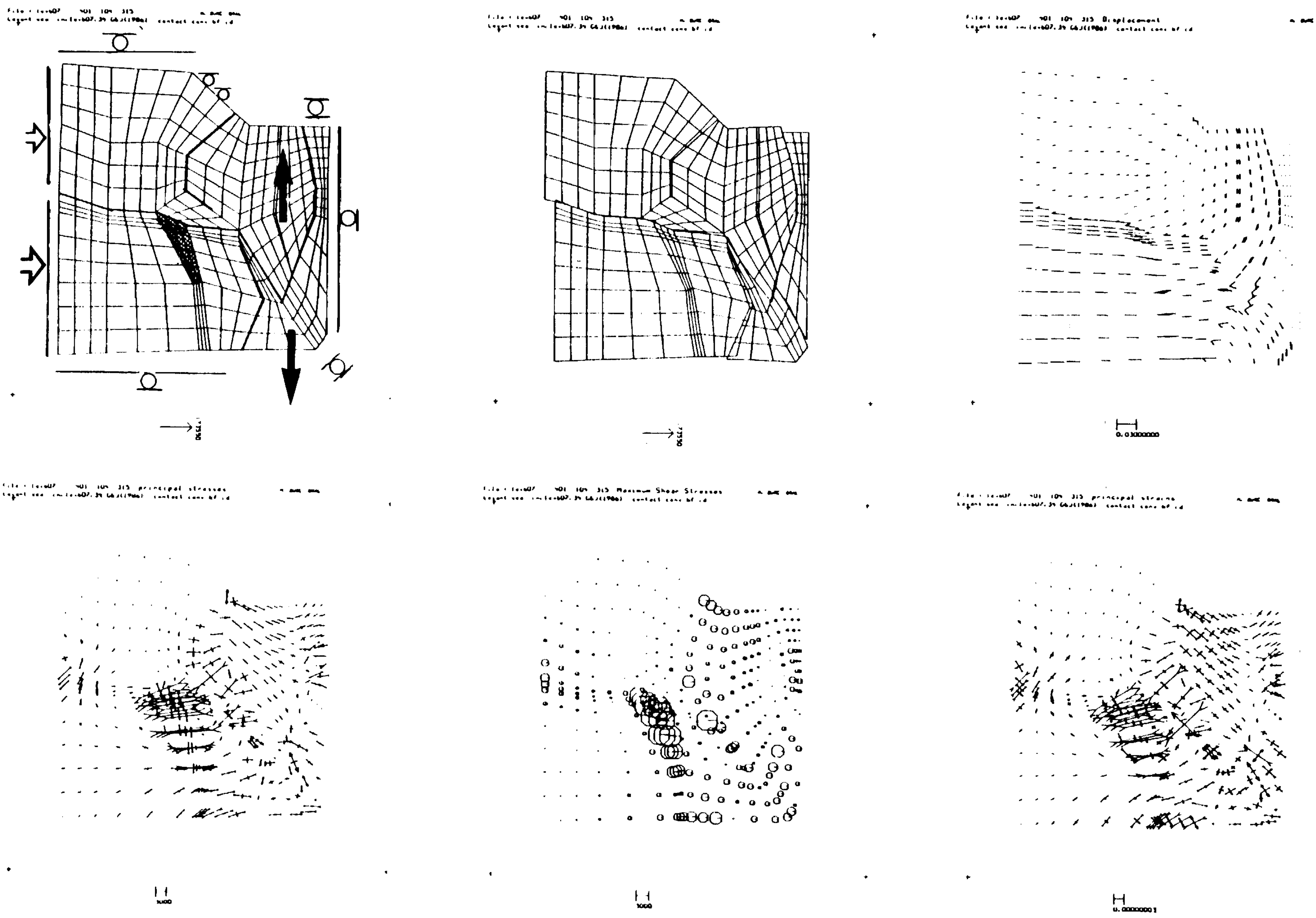

Fig.21 : Deformation pattern of the eastern Mediterranean[Model 3]: Contact. Driving forces: boundary displacements and gravitational forces. The convergence at the Cyprean arc and shortening at the Bitlis Suture, internal deformation at the Palmyra Kink are included.

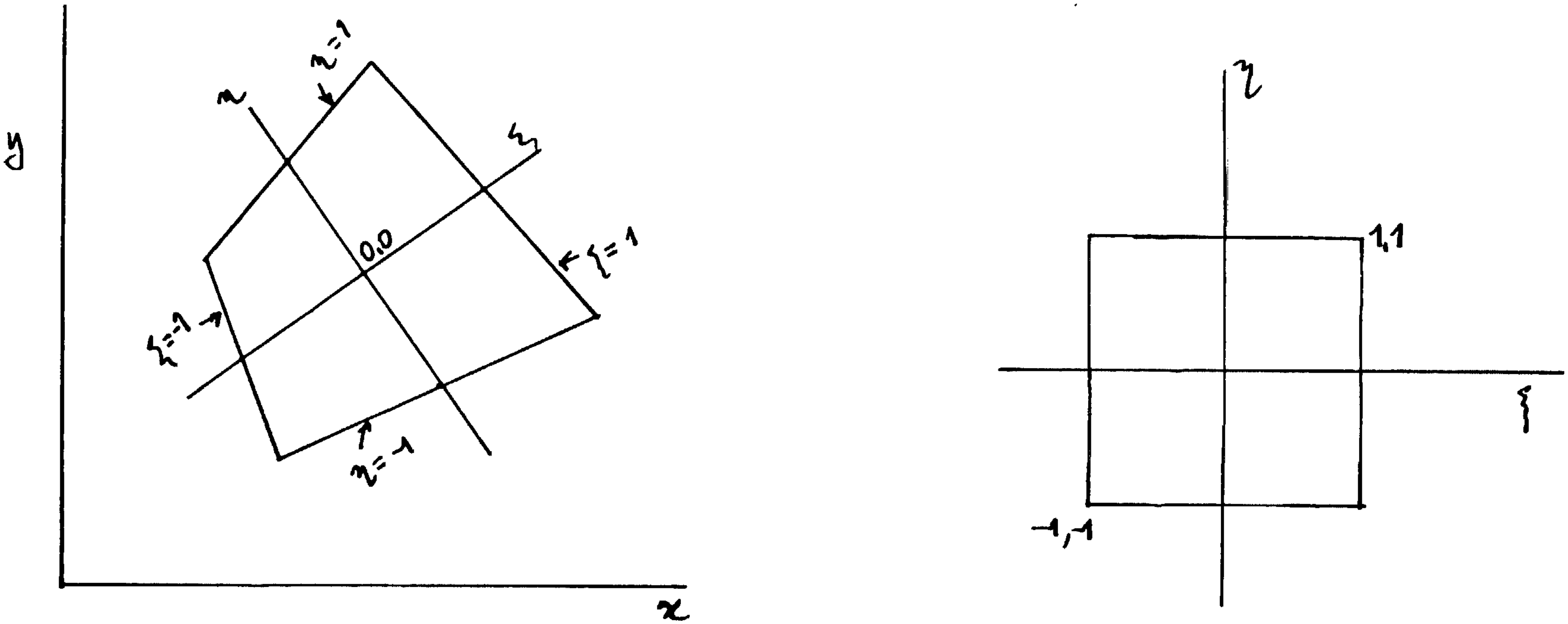

GLOBAL COORDINATE
SYSTEM

Isoparametric
NATURAL COORDINATE
SYSTEM

Fig.A1: Global and isoparametric(natural) coordinate systems and their mapping.

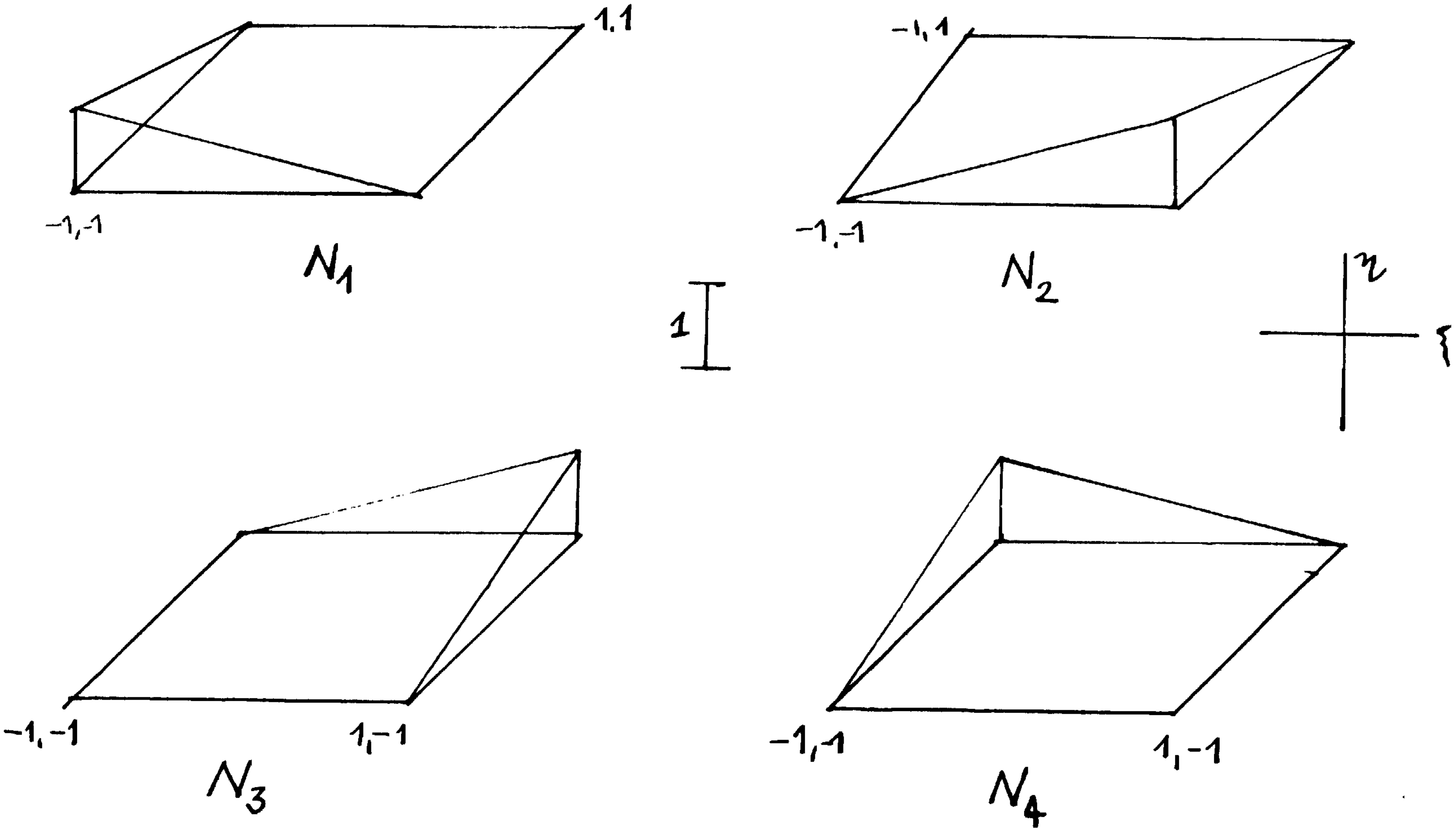

Fig. A2: Bilinear shape functions for 4-node quadrilateral element.

APPENDIX 2

Seismotectonics and Seismic Gaps of the Eastern Part of the North Anatolian Fault Zone

A. Aykut Barka and M. Nafi Toksöz

Earth Resources Laboratory
Department of Earth and Planetary Sciences
Massachusetts Institute of Technology
Cambridge, MA 02142, USA.

Abstract

Historical and instrumental earthquakes in the eastern part of the North Anatolian fault zone between the Erzincan basin and the Karliova triple junction have been examined in relation to fault segmentation and kinematics. The 12/26/1939 Erzincan earthquake (M=8) created a 360 km surface break and it was terminated at the eastern end of the Erzincan pull-apart basin in the east. The 8/17/1949 (M=6.7-7) earthquake was a double bend earthquake which affected the easternmost three fault segments (FS1, FS2 and FS3) of the North Anatolian fault zone. According to the historical data, the 1784 earthquake (I=VIII-IX) occurred between the 1939 and 1949 rupture segments (FS4-FS9, about 75 km long). From this data it appears that the North Anatolian fault zone could have two seperate sequences of westward migrating large earthquakes. One of the two sequences originates from the triple junction between the NAFZ and the Ovacik fault in eastern end of the Erzincan basin, and extends to the west about 900 km, as happened between 1939-1967. The second one extends between the Karliova triple junction and the Erzincan basin and consists of two rupture segments, 1949 and 1784. The main reasons for these two separate

migrations are firstly different recurrence intervals of large earthquakes of the rupture segments which is controlled by the geometry and length of the rupture segment and secondly, the eastern part of the westward escaping Anatolian block divided into two wedge shaped blocks (A1 and A2) each of which moves independently. From historical records it may appear that the recurrence interval of the western migration could be about 900 years while the recurence interval is about 200-300 years for the eastern migration. Furthermore, the eastern migration has not yet completed during the current twenteeth century migration. Thus, within the eastern sequence, the 1784 rupture segment to the east of the Erzincan basin is identified as a potential seismic gap. Recurrence intervals of historical earthquakes and geological data indicate that slip rate in this part of the fault zone is about 0.8-1 cm/yr. This results in an accumulation of about 2 m right-lateral slip along the 1784 rupture segment.

Introduction

It has recently been emphasized that fault geometry plays a critical role in the earthquake rupture process (e.g., Segall and Pollard, 1980, Bakun et al. 1980, Lindh and Boore 1981, Barka and Hancock 1982, King and Nabelek 1985, Sibson 1986, Schwartz and Coppersmith 1986, Barka and Kadinsky-Cade 1988, Wesnousky 1989). The term "fault geometry" includes stepovers, bends, and their many combinations. In this study we focus on strike-slip fault geometry and earthquake activity in the eastern part of the North Anatolian fault zone. We have studied the geometry of active fault segments in detail on the field and aerial pothographs, belonging not only the North Anatolian fault also other major faults in the region. Then, we combined this information with distribution of intrumental and historical earthquakes in the region. We also examined the extents of the surface ruptures of the large earthquakes thorough the litrature and some on the field. As a result our purpose is to understand how the fault moves and examine seismic gaps along the fault zones.

Figure 1 shows major tectonic elements of Turkey in an area where the northward motion of the Arabian plate causes active convergence in eastern Turkey. As a result, the Anatolian block escapes westward and the Northeast Anatolian block eastward (Ketin 1948, McKenzie 1972, Sengor 1979, Kasapoglu & Toksoz 1983, Gulen 1984, Dewey et al. 1986). The wedge shaped Anatolian block is bounded by the right-lateral North Anatolian fault to the north, and by its conjugate, the East Anatolian fault, to the south. These two fault zones intersect at the Karliova Triple junction (Ketin 1969, Allen 1969, 1975, McKenzie 1972, Dewey 1976, Tchalenko 1977, Sengor 1979, Toksoz et al. 1979, Jackson & McKenzie 1984, Sengor et al. 1985, Dewey et al. 1986). The eastern part of the Anatolian block is divided into two smaller blocks (A1 and A2 in Fig. 2) by the left-lateral strike-slip Ovacik fault. This fault intersects the NAF zone at the southeast end of the Erzincan basin which forms an an other triple junction (ETJ1). The eastward escape of the NE Anatolian block is complicated by the extensive internal deformation and by the existence of a number of sub-blocks. The Northeast Anatolian fault zone (NEAFZ), forms the northern boundary of the NE Anatolian block. The dominant tectonic feature in this region is the NAF, which is a joint boundary between the two blocks escaping in opposite directions. The NAFZ intersects the NEAFZ in northwest of Erzincan (ETJ2, Figures 1 and 2). Figure 2 shows the major blocks and boundary faults in the area of concern, between the Erzincan and Karliova triple junctions. Genuinly, both historically and during the modern times, the Erzincan region has been one of the most active seismic regions in Turkey (Sieberg 1932, Ergin et al. 1967, Soysal et al. 1981, and see Table 1) because the area is situated within a most critical tectonic center from where continental blocks escape sideways.

Between 1939 and 1967 most of the North Anatolian Fault west of Erzincan ruptured through a westward migrating series of major earthquakes, as shown in Figure 1. In this series of earthquakes, the largest one was the 1939 Erzincan earthquake (M=8.0). East of Erzincan, earthquakes along the NAF followed a more complicated pattern, as can be seen in Figure 2.

Fault and Rupture Segments

Fault segmentation is defined by the distribution of the geometric discontinuities along straight fault segments. For the definition of minumum sizes of these discontinuities which control the fault segmentation, we used Barka and Kadinsky-Cade (1988) criteria (stepover widths and bend angles larger than 1 km and 5 respectively). Rupture segments are the extents of surface rupture zones produced by characteristic large earthquakes. The North Anatolian fault zone consists of a number of fault and rupture segments in this area, as shown in Figure 2 (Barka and Kadinsky-Cade, 1988). In this section we outline the geologic and seismic details of each fault and rupture segment belonging to the major fault zones.

The North Anatolian Fault Zone

The NAFZ initiates at the Karliova triple junction (Figs. 1 and 2). Although there is extensive seismic activity to the east of this junction (between Karliova and Varto). it is believed that this part is no longer the continuity of the NAFZ, but a rather complex suture zone which has developed by the westward escape of the Anatolian block. In other words, one interprate this as the triple junction was initially in the Varto area and as a result of the westward escape the Anatolian block, the triple junction has moved to the Karliova area. Barka and Gulen (1988) have called this zone as a "zipper zone". The complex suture zone has been formed by a thrust formation extending through the bisector of the angle between the boundary strike-slip faults (Fig. 3) which is the manifastation of closure of the space at the tip of the escaping block. The 1946 and 1966 Varto earthquakes occurred along this zone (Tasman 1946, Ambraseys and Zatopek 1968, Wallace 1968, Ketin 1969 and see Figs 2 and 3). According to McKenzie (1972) and Canitez (1973) the fault plane solution of the 1966 Varto earthquake differed from other solutions of eartquakes which occurred along the NAFZ by having a trust component with right-lateral strike-slip motion (Fig. 4). This is in good agreement with suture zone formation. In the same context, an E-W trending thrust morphology was interprate from aerial photos in the Karliova area extending through the bisector angle between the boundary strike-slip faults, NAFZ and EAFZ, (Fig. 3). This north dipping thrust seems to splay from the segment 1 of NAFZ and indicates that the Karliova basin can not be an extensional basin, instead it is a complex ramp basin formed by the interaction of coeval strike-slip faulting and thrusting. Although the epicenter of 7/07/1957 earthquake, M=5.5, is located 30-50 km west of the Karliova area, its thrust mechanism (Canitez and Ucer 1967), indicates that the internal deformation of the Anatolian block includes an approximately E-W thrusting which can be used as supporting evidence for the thrust formation in the Karliova area (Fig.4).

Fault segments 1, 2 and 3 (FS1, FS2 and FS3) form a restraining doublebend between the Yedisu basin and Karliova triple junction. Double bend angles are 20 in east and 25 in the west (Fig. 3). FS1 extends from the triple junction to the west about 30 km and has very clear physiographic expressions. Along this segment many small streams and ridges which are normal to the fault trace are offset and curved in a right-lateral sense (see also Allen 1969 and 1975). This segment, the fault trace is expressed by a long norrow trough along its entire lenght (Fig. 3). FS2, which is the restraining segment of the double bend, has two small releasing stepovers and runs within the Elmali river. Its physiographic expressions are much less clearer developed. FS3 forms the western part of the double bend and also has a very clear strike-slip morphology like FS1 (Fig. 3). The 8/20/1966 Ms=5.3–6.2 and some other smaller aftershocks of the 1966 Varto earthquake were located on FS1 (Ambrasesy and Zatopek 1968, Dewey 1976). During the 8/20/1966 aftershock most of the villages in the vicinity of this segment were destroyed (Fig. 3). The fault plane solution of this earthquake (Mckenzie 1972, Canitez 1973) indicated a pure strike-slip motion along FS1. The 8/17/1949 Ms=6.7–7 earthquake affected all three segments. According to data collected during our field survey and Ambraseys (1987, personal communications) this earthquake might have created ruptures mostly along FS2, and the eastern part of FS3 and the western part of FS1. Ambraseys (1987, personal communation) also reported that right-lateral displacements might have reached up to 1.5-2 m in places. Most of the damage occurred along FS2 which makes up the restraining area of the doublebend (Fig. 3). The fault plane solution of this event had a slight thrust component (Canitez 1973).

FS3 and FS4 form the 2.5 km wide Yedisu pull-apart basin (Fig. 5). There is a restraining angle about 10 between these two segments. FS4 is about 28 km long and has clear morphological expresions. FS4 has also two small stepovers first of which is a releasing type located in the Yedisu basin and the second one is a restraining type situated in middle of the segment. The 7/26/1967 Pulumur earthquake, M=5.6–6.2, took place west of this second stepover and created 4 km surface breaks and 20 cm right-lateral displacement along this part of FS4 (Ambraseys 1975). Figure 5 shows intensity contours and destroyed villages along the FS4 (Tutuncu and Demirtasli 1967). The fault plane solution of this earthquake (Mckenzie 1972 and Canitez 1973) indicated that the motion was also pure strike-slip and confirms the right-lateral motion of the NAFZ (Fig. 4).

FS4, FS5 and FS6 form a releasing double bend (Fig. 5). In the vicinity of FS6 there are several other faults which trend parallel to FS6. There is a long and narrow small lake along FS5 which is consistent with its extensional nature. FS7, FS8 and FS9 create a combination of releasing bend and restraining stepover. The width of the restraining stepover is about 2 km. FS7, FS8 and FS9 have relatively less clear morpological expressions. This is probably due to fact that they all run within the Ephratus valley where fluvial activity is quite high. Fault expressions are well developed only between Tanyeri and Caykomu villages along FS9 (Fig. 5). Ambraseys (1975) reported that the 1784 large earthquake occurred to the east of the Erzincan basin and created 90 km long surface rupture. Based on this information it is believed that this rupture segment extended along the entire lenght of FS4-FS9. In other words, 1784 rupture segment took place between the Yedisu and Erzincan releasing stepovers.

FS9 and FS10 form a releasing bend (15) and stepover (4-5 km) combination which is responsible for the opening of the Erzincan basin (Fig. 2). FS10 is 60 km long, and has clear physiographic expressions in its western half. The southeast half of FS10 is characterized by short en-echelon strike-slip faults and contemporaneous volcanics (Barka and Gulen 1989). FS10 is separated from FS11 by a 20 restraining bend. FS11 is about 110 km long, and extends from this bend, situated about 10 km NW of the Erzincan basin, to Susehri - the location of a releasing double bend (Kocyigit 1988). The area of interest in this paper terminates in the eastern part of FS11 (for the details of the other fault segments to the west see Barka and Kadinsky-Cade 1988). FS11 has clear strike-slip morphology especialy in the vicinity of Mihar village. Along all these fault segments the strike-slip motion is associated with a vertical component. According to field observations, the southern block is usually uplifted except that this varies where the fault segments form extensional structures (releasing bend and/or releasing stepover).

The 1939 Erzincan earthquake created surface ruptures along FS10, FS11 and extended further west along the Kelkit valley and terminated south of Amasya where there is a 24 restraining bend between the fault segments (e.g. Pamir and Ketin 1941, Parejas et al. 1941, Ketin 1969 see also Figure 1). The total lenght of surface ruptures was about 360 km. Although, Parejas et al. (1941) reported 3.7 m maximum displacement, according to recent studies (Kocyigit 1988, Barka in prep.) the maximum displacement reached 7.5 m in along FS11. During the same earthquake the southern block was uplifted about 2 m . Pamir and Ketin (1941) reported that two foreshocks were felt within the week preceding the main shock in the Erzincan basin. The epicenter of the earthquake was located near the 20 restraining bend, on FS10 (Dewey 1976). Many of the 1939 earthquake aftershocks caused damage in the Erzincan and Niksar pull-apart basins (Nature 1940a, b, c, d, Ergin et al., 1967; Tabban, 1980; see also Riad and Meyer, 1983). Fault plane solution of this earthquake was pure strike-slip motion and agreed with the motion along the fault zone. An another fault plane solution for a moderate size earthquake (Mb = 4.8, 11/18/1983) near the city of Erzincan is characterized by ENE-WSW extension (International Seismological Centre Bulletin solution 1983), also in agreement with the pull-apart character of the Erzincan basin (Fig. 4).

The East Anatolian fault zone

The left-lateral East Anatolian fault zone is the southern boundary of the westward escaping Anatolian A1 block. The most northeastern fault segment (FS1) is about 60 km long and extends from the Karliova triple junction to Bingol (Figs. 1and 2). The segment is straight and has clear morphological left-lateral strike-slip expressions and it is also accompanied by a normal component (western block down) along the northern half. The southern half of this segment runs within the Goynuk river valley where the expressions are not so clear. The 1971 Bingol earthquake (M=6.7) created surface ruptures mostly along the southern half of the segment (Arpat and Saroglu 1972 and Seymen and Aydin 1972). The fault plane solution of this earthquake indicated pure left-lateral slip along this segment (Fig. 4). At least one other historical earthquake (1789) of a similar size has been documented from Soysal et al.(1981) in the vicinity of the same segment. According to Arpat and Saroglu (1972) and Seymen and Saroglu (1972) the fault zone has 15-27 km left-lateral post-Miocene displacement revealing about 0.5 cm/yr slip rate.

The Ovacik fault

This is another left-lateral fault and is about 120 km long trending NE-SW. According to Barka and Gulen (1989) who studied the tectonic evolution of the Erzincan basin, the Ovacik fault has also been participating in the opening of the Erzincan basin The Ovacik fault splays into several branches before it enters the Erzincan basin. The Ovacik basin is situated on a releasing bend along the segments of the Ovacik fault. In the Ovacik basin the fault cuts Quaternary alluvial fans, and forms very distinct 5–10 m high fault scarps (see also Arpat and Saroglu, 1975). Although the fault, in general, has a left-lateral strike-slip character, these scarps indicate that the motion in the Ovacik basin is also associated with a normal component. However, outside the Ovacik basin the fault has a thrust component that causes the uplift of the Munzur Montains. As far as historical earthquakes are concerned there are no spesific events in the last 1000 years that can be associated with this fault. During the present field survey occurence of one large earthquake 1200 years ago was interpreted from the Legend of the Munzur Springs in the Ovacik area. Barka and Gulen (1989) estimated 5-7 km left-lateral displacement along the Ovacik fault from the geometry of the southeastern part of the Erzincan basin. They also considered that the age of the Ovacik fault is younger than the NAFZ (approximately 3–3.5 Ma). These values may reveal about 0.15–0.25 cm/yr slip rate along the Ovacik fault.

The Northeast Anatolian Fault Zone

This fault zone consists of several segments with a combined length of approximately 350 km. The southwesternmost segment (FSA) is located to the north of the Erzincan region (Figure 2). Approximately 70 km long, it strikes NE-SW. Although very little is known about this fault segment, it is assumed to have an oblique movement, consisting mostly of left-lateral slip with a subordinate thrust component (Tatar, 1978). The study of earthquake records (Soysal et al., 1981; Sipahioglu, 1983; Riad and Meyers, 1985) indicates that it is less active than the segments of the North Anatolian Fault zone. Pamir and Ketin (1941) showed ESE-WNW trending isoseismals parallel to the NAFZ, covering the area between Tercan and Baskoy for the 11/21/1939 Tercan earthquake (M=5.9). And because of this, this earthquake was always considered to be the foreshock of the 1939 Erzincan earthquake. However, after locating the damaged villages and the main trace of the NEAFZ, we believed that this earthquake may have occurred on FS-A of the NEAFZ and has no relation with the NAFZ (for example, 130 buildings collapsed in Karakulak which is situated next to the fault zone; Pamir and Ketin, 1941; Ergin et al., 1967; Tabban, 1980, see also Figure 2 where the locations of other destroyed villages are shown). This is also confirmed by the relocation of the earthquake (Dewey 1976, Fig. 7). Apart from the 1939 Tercan earthquake and several aftershocks of the 1939 great Erzincan earthquake, the only known historical event associated with this segment is the 1254 earthquake (I=IX). This event caused surface breaks to occur over a 50 km length on FS-A (Ambraseys, 1975).

Seismicity

Historical Earthquake Records

The history of damaging earthquakes in the Erzincan region was recognized and fairly well documented even before the great earthquake of 1939 (Ali Kemal, 1932). Sieberg (1932) listed some of the Erzincan earthquakes and stated that between 1045 and 1784, at least 17 damaging earthquakes had occurred in the Erzincan region. In Table 1 we have tabulated the significant earthquakes affecting the Erzincan region since 1000 A.D., based on sources referenced in the table. Figure 6 is an intensity-time plot of known earthquakes which have affected the Erzincan region. From this figure. earthquakes can be categorized according to two large sizes: (a) great earthquakes for which I X (Modified Mercalli intensity),and (b) large earthquakes with VIII I IX According to Figure 6, at least 3 great earthquakes have occurred during the last 1000 years, including the one in 1939. Ambraseys (1970) reported that the 1045 earthquake produced a surface break of length comparable to the one which occurred in 1939: and that the 1458 earthquake caused the death of about 32,000 people, however, although this figure is comparable to the casualties of the 1939 earthquake, in most catologs the affected area is described as taking place between Erzincan and Erzurum.

At least 10 large earthquakes (VIII I IX) have occurred in the Erzincan region.

since 1000 A.D., causing considerable damage and large numbers of casualties. Among the earthquakes of this size only 1254 and 1784 earthquakes can be associated with specific segments; 1254 was on FS-A of the NEAFZ and 1784 was on FS4-FS9 of the NAFZ (Ambraseys 1975). The other two large earthquakes similar 1784 were 1578 and 1422 which were separeted by about 156 years. Furthermore, there is the possibility of only one large earthquake along the Ovacik fault occuring about 1200 years ago which is interpreted from the Legend of Munzur Springs. In other words, none of the listed earthquakes in Table 1 is specifically associated with the Ovacik fault.

The recurrence interval (900 year) combined with displacement created during the great earthquakes (7.5 m), give a slip-rate of approximately 0.8 cm/yr. This slip-rate is similar to that obtained from geological data which reveals about 0.8–1 cm/yr for this part of the fault zone (Barka and Gulen 1988). Note also that FS1-FS10 form a joint boundary between opposite-moving blocks (the Anatolian and Northeast Anatolian blocks). Thus the slip rate is expected to be higher in this area than along the main section of the NAF to the west. However, some amount of the slip should be taken up by the internal deformation of A1 block as expressed by extensive internal faulting and related seismic activity at tip of the wedge shape block. From Figure 6 the recurrence interval for large earthquakes (VIII I IX) is approximately 100-150 years.

Instrumental Earthquake Records

Figure 7 shows the distribution of earthquakes M 4.9 in the region between 1900 and 1985. Epicenters for the interval 1900–1930 are taken from Tabban (1980) and Riad and Meyers (1985). Epicenters of those earthquakes which occurred between 1930 and 1971 are taken from Dewey (1976) who relocated the events M 5. Moreover, epicenters of all earthquakes for the period of 1964-1984 belonging to ISC, are also shown in Figure 8. From both maps two significant points can be made; a) many moderate-large earthquakes are mostly concentrated along the NAFZ, and b) there is also concentrations of the small-moderate earthquakes at the tips of the wedge shaped blocks. The tip of A1 block has the most clear activity out of the escaping blocks.

Seismic Gaps

Both historical data and the 1939 earthquake have shown that great earthquakes in this region appear to be consistent with the 1939 rupture segment which includes FS10, FS11 and fault segments (FS11–FS14) to the west along the NAFZ (see Barka and Kadinsky-Cade 1988). If we consider the recurrence interval of 1939 earthquake (M=8) to be about 900 years (Fig. 6) this rupture segment is safe for long time for a similar size of earthquake. On the other hand there is no historical data obtained before the 1949 earthquake which took place at the eastern end of the fault zone (Fig. 9). This is propably due to that the area is sparsly populated because of its raged morphology. However, if we take the estimated slip rate as about 1 cm/yr and similar amount of slip (1.5-2 m) on the fault, one can simply calculate 150–200 years recurence interval for the 1949 size of earthquakes. Along the 1784 rupture segment, before 1784 earthquake, there are two other comparable earthquakes which affected the Erzincan region within last 500 years(1578, I=VIII and 1422, I=VIII, Fig. 9), but their locations are not known. The recurrence interval of these earthquakes are 156 and 206 years. Since it has been 205 years since 1784 earthquake, this rupture segment (FS4–FS9), stands out as a clear seismic gap. The geometry of the fault segments also indicate that the restraining features along the rupture segment are not large enough to restore so much stresses. Thus, one can conclude that the geometry and historical earthquake records and long term slip rate along the rupture segment indicate that this gap should have a large earthquake near future. The estimated 1 cm/yr slip rate results in over 2 m slip accumulation along this rupture segment. An other important point with this gap is that during the 20th century this rupture segment is the only segment along the NAF zone which has not experienced a large earthquake between

Varto and the western end of the Mudurnu valley (900 km). Moreover, this gap along the NAFZ is different from the gap mentioned by Toksoz et al., (1979), and was first briefly mentioned by Ambraseys and Zatopek (1969).

There is no any significant earthquake that can be specifically associated with the Ovacik fault since 1900 during the instrumental period and/or last 1000 years. Thus, it has been 1200 years since the last known large earthquake along this fault. With the given rate (0.15–0.25 cm/yr), about 1.5–2.5 m left slip might have accumulated along this fault. Therefore, the Ovacik fault may well be another candidate for future large earthquakes.

The amount of total displacement along the FS-A of the NEAF zone is similar to the Ovacik fault (about 5 km). The 11/21/1939 Tercan earthquake and 02/03/1949 aftershock of the 1939 Erzincan earthquake might have occurred on this segment. From the historical earthquake records, we are only aware of the 1254 large earthquake, which created 50 km of surface faulting along segment A, trending 60 with 5 m (?) maximum vertical displacement (Ambraseys, 1975). The slip rate with the historical data indicates that about 1 m left-lateral slip may have been accumulated along this rupture segment.

Migration of Large Earthquakes

The historical data is not long enough to clearly understand the migration patterns of the North Anatolian fault zone. However, from available data, two separate westward migration of large earthquakes along the North Anatolian fault can be interprated. One starts from the triple junction of the North Anatolian and the Ovacik fault (ETJ1) and to the westward as it happened between 1939 and 1967. The second sequence takes place between the Karliova and Erzincan triple juction (ETJ1) which consists of two rupture segments 1949 and 1784. The western migration might occur approximately every 900 years while the eastern migration may repeat every 200-300 years. The longer recurrence interval of 1939 rupture segment is related to the 20 restraining bend which is the largest restraining feature along the North Anatolian. Furthermore, two separate Anatolian blocks (A1,A2) move to west thus two separate sets of migration earthquakes would be expected when each block moves. As far as most recent sequences concerned as has mentioned the eastern migration has not yet completed.

Fault Geometry and Earthquake Rupture Processes

Some of the details of the fault geometry and rupture processes have been already discussed by Barka and Hancock 1982, Barka and Kadinsky-Cade 1988 and Kadinsky-Cade and Barka 1989. Some of these can be sammurized as follows,

a) It is apparent that two ends of the 1784 rupture segment is controled by the Erzincan and Yedisu pull-aparts.

b) Each rupture segment has restraining feature in itself, the size of which proportional to the size of earthquake, length of rupture segment and the amount of slip. For example, as has mentioned the above, the characteristic great Erzincan earthquakes (1045 and 1939) are closely related to the 20 restraining bend (110 km long) northwest of the Erzincan basin and the restraining bend of the 1939 is larger than those observed along the 1949 (20 and 15 km long) and 1784 rupture segments so as the size of earthquakes, the rupture lengths and the displacements. More details of these issues have been discussed by Barka and Kadinsky-Cade (1988), Kadinsky-Cade and Barka (1988) and Wesnousky (1988).

c) As it has been also poited out that location of epicenters, in other words, rupture initiation take place mostly nearby the locked segments (e.g. Barka and Hancock 1982, King and Nabalek 1985, Barka and Kadinsky-Cade 1988). For example, the epicenter of the 1939 earthquake is located near the restraining bend (Barka and Hancock, 1982; Barka and Kadinsky-Cade, 1988). Similarly, the epicenter of 1949 double bend earthquake is located on FS3, near the the western bend where angle is higher relative to the eastern bend. Thus, from these examples one can assume that for the case of the 1784 seismic gap the epicenter of the large earthquakes may take place in western part of FS4 and/or FS5 (Fig. 9).

d) Furthermore, as mentioned earlier, in the easternmost part of the fault zone FS1, FS3 and FS4 have clear morphological expressions. Many stream beds and ridges normal to the segments are curved in a right-lateral sense. These three segments have a linear geometry and also are parallel to the slip direction. It should be noted that most of the area of interest including the Ovacik fault and segment A of the NEAF zone, is located within the serpentinite-rich ophiolites and ophiolitic melange associated with the Anatolide/Tauride - Pontide suture zone. These three aspects, morphological expressions, linearity in geometry and plasticity of the rocks indicate high potential of creep phenomena along these segments. In other words the motion along the straight segments is considered to be easy. The seismicity indicate that this assumed creep is accompanied with continuous small and moderate earthquake activity, if we consider that those moderate earthquakes (such as the 1966, M=6.3 along the FS1 and the 1967 Pulumur earthquake, M=5.6-6.2, along the FS4, Figure 9) are characteristic earthquakes of these straight segments . Note that for any case these activities (creep and small-moderate earthquakes) do not exclude the potential for future large earthquakes along the FS1-FS9 as it was experienced in the 1949 and 1784 events. However, we believe that the amount of slip during those large earthquakes should be less along the those segments that have creep and small-moderate earthquake activity.

In summary, one can postulate that straight segments which are parallel to the slip direction has interseismic activity of small-moderate earthquakes and creep, and they continuously transfer the slip (or stresses) to the locked areas (Fig. 9). Locked segments who has restraining geometries move coseismicly by large events (Fig 9). During the large earthquake those straight segments which have already transfer the slip to the locked areas would have obviously less slip. For example, if the above mention gap along the North Anatolian fault creates a large earthquake, we would expect maximum slip to the west of FS4 and much less slip along the FS4.

Finally, we can conclude that releasing stepovers or releasing double bends appear to be site of preseismic and post seismic activity such as foreshocks and aftershocks (Fig. 9). If this is so, the 1784 seismic gap could have a high potential of foreshock activity and most of the aftershock could also take place in the Erzincan and Yedisu pull-aparts.

Conclusion

From this study it is clear that examination of earthquakes and fault geometry provide many useful information in understanding not only the tectonics of the sideway escapes of the continental blocks but also to in defining seismic gaps along the major fault zones which form the boundaries of blocks and earthquake rupture processes.

This study also indicates that there is a clear 75 km long seismic gap along the North Anatolian fault immidiately to the east of the Erzincan basin. This segment last ruptured in 1784 and since the estimated slip rate is about 1 cm/yr, about 2 m slip has accumulated. The recurence interval of large earthquakes along this rupture segment is an average of 180 years. Although the damage and casualties were less severe than 1939, the 1784 earthquake was also very destructive for the Erzincan region killing at least 5 000 people. The other significant seismic gap appears to be associated with the Ovacik fault along which 1.5-2.5 m slip might have accumulated over last 1200 years.

There could be two separate westward migration of large earthquakes along the North Anatolian fault zone, first one is from the Erzincan basin to the west and second one is from Karliova triple junction to the Erzincan basin. This is caused by primarily different recurrence intervals of large earthquakes along the rupture segments and two separate block motion to the west.

Slips along the straight segments which are also parallel to the general slip direction seem to be easy and expressed by clear morphological expressions, frequent small-moderate earthquakes and possible creep activity trnsfering the stresses to the locked segments. Finally, a high potential of foreshock activity is associated with the pull-apart structures and a releasing double bend along the the gap segment.

Acknowledgement

This work was supported by Mineral Research and Exploration Institute of Turkey, U.S. Geological Survey contract no. 14-08-0001-61151 and NASA grant no. NAG5-753. We would like to thank to Prof. N.N. Ambraseys and K. Kadinsky-Cade for many constructive comments.

Figure Captions

Figure 1. Tectonic map of Turkey showing the surface ruptures due to major earthquakes since 1900. The Anatolian and Northeast Anatolian Blocks are wedged out to the west and east respectively by the convergense of Arabia and Eurasia as shown in the inset map (lower left). The rectanle in the Figure delinates the area of study and is enlarged in Figure 2 (compiled from Arpat and Saroglu 1972, 1975, Arpat et al. 1977, Barka and Hancock 1984, Sengor et al. 1985).

Figure 2. Simplified geometry of major blocks and distribution of fault and rupture segments between Erzincan and Karliova. Thick and dashed lines and dates indicate rupture segments and dates of related earthquakes, respectively. Doted areas are Plio-Quaternary basins being formed mostly by strike-slip faulting. A1 and A2 are sub-blocks within the Anatolian block. Stars near the rs 1939b show the destroyed villages by the 11/21/1939 earthquake (taken from Ergin et al. 1967).

Figure 3. Simplified tectonic map of the Karliova-Varto area. rs 1949, fs2 are rupture segments of major earthquakes and fault segments, respectively (see also Tutkun 1986 and Saroglu et al.1987). The observed extents of surface ruptures of the 08/19/1966 Varto earthquake is indicated by dashed lines (from Wallace 1968). The triangles are the villages destroyed by the largest aftershock of the 1966 Varto earthquake. Closed squares within the squares are the villages knocked down by the 08/17/1949 earthquake (information collected during the present survey and Ambraseys 1987 written communication).

Figure 4. Fault plane solution of major earthquakes of the region (compiled from Mckenzie 1972 and Canitez 1973).

Figure 5. Characteristic features of the North Anatolian fault between Yedisu and Erzincan basins. Doted contours are isoseismals of the 07/26/1967 Pulumur earthquake and stars are the destroyed villages both taken from Tutuncu and Demirtasli (1967). Squares are the destroyed villages by the 08/17/1949 earthquake.

Figure 6. Time (T)/intensity (I) distribution of earthquakes in the Erzincan area

Numbers above the dotes are the number of casualties resulting from each particular event. a and b are the categories of earthquakes. For explanation and references see the text and Table 1.

Figure 7. Distribution of earthquake epicenters ($M \geq 4.9$) in the easternmost part of the North Anatolian fault zone for the interval 1900-1987. Solid circles indicate the epicenters taken from Dewey (1976) and the open circles indicate epicenters taken from mostly Riad and Meyers (1985) and Tabban (1980).

Figure 8. Distribution of ISC epicenters of all earthquakes between 1964-1984 in the region.

Figure 9. Summary of the relationship between geometry of the fault segments and seismicity along the eastern part of the North Anatolian fault zone. Horizontal axis represents the extent of the fault and vertical axes are time and slip. The continuous vertical lines indicates each rupture segments and dashed vertical lines separate the straight segments and locked segments. Stars with dates ilustrate locations relocated epicenter of the 1939 and 1949 earthquakes (Dewey 1976). The star with exclamation mark is the location of epicenter of the expected large earthquake within the gap area. The horizontal arrows indicate the direction of the slip by moderate earthquakes. The dates, size and the amount of slip of the large earthquakes are also indicated.

REFERENCES

Allen, C.R.,(1969), Active faulting in northern Turkey: Contr. No. 1577. Div. Geol. Sci., Calif. Inst. Tech., 32 p.

Allen, C.R.,(1975). Geological criteria for evaluating seismicity. Geol. Soc. Amer. Bull. 66, 1041-1057.

Ambraseys, N.N. (1970). Some characteristic features of the North Anatolian fault zone. Tectonophysics 9, 143-165.

Ambraseys, N. N. (1975). Studies in historical seismicity and tectonics. In: Geodynamics of Today. The Royal Soc. London, 7-16.

Ambraseys, N. N. and Finkel, C.F. (1987a). The Anatolian earthquake of the 17 August 1668. Proceedings of the Symposium on Historical Seismograms and Earthquakes. Ed., W. H. K. Lee, 400-407.

Ambraseys, A. A. and Finkel, C. F. (1987b). The seismicity of the northeast Mediterranean region during the early twentieth century. Ann. Geophys., 5B(6), 701-726

Ambraseys, N. N. and Zatopek, A. (1968). The Varto-Ustukiran (Anatolia) Earthquake of 19 August 1966; Summary of a Field Report. Bull. Seis. Soc. Amer. 58, 47-102.

Ambraseys, N. N. and Zatopek, A. (1969). The Mudurnu valley, West Anatolia, Turkey, earthquake of 22 July 1967. Bull. Seis. Soc. Amer. 59, 521-589.

Arpat, E. and Saroglu, F. (1972). The East Anatolian fault system: thoughts on its development. Bull. Mineral Res. Explor. Inst. Ankara, Turkey, 78, 33-39.

Arpat ve Saroglu, F., (1975). Some recent tectonic events in Turkey. Bull. Geol. Soc Turkey, 18, 91-101.

Arpat, E., Saroglu, F. and Iz, H. B. (1977). 1976 Caldiran earthquake. Yeruvari ve Insan, 2, 1, 29-41.

Bakun, W. H., Stewart, R. M., Bufe, C. G. and Marks, S. J. (1980). Implication of seismicity for failure of a section of San Andreas Fault. Bull. Seism. Soc. Amer 70, 185-202.

Barka, A. A., and Hancock, P. L., (1982). Relationship between fault geometry and some earthquake epicenters within the North Anatolian fault zone. Progress in Earthquake Prediction, edited by A.M. Isikara and A. Vogel, Friedr. Vieweg and John, F.R.G., 2, 137-142.

Barka, A. and Hancock, P.L. (1984). Neotectonic deformation patterns in the convex-northwards arc of the North Anatolian fault, in The Geological Evolution of the Eastern Mediterranean (edited by Dixon, J.G. and Roberston, AHF). Spec. Publ. Geol. Soc. London. 763-773.

Barka, A. A. and Gulen, L. (1988). New constraints on age and total offset of the North Anatolian fault zone: Implications for tectonics of the Eastern Mediterranean region. In, 1987 Melih Tokay Symposium. Spec. Publ.Middle-east Techn. Univer. Ankara, Turkey. In press.

Barka, A.A. and Gulen, L., (1989). Complex evolution of the Erzincan basin (Eastern Turkey) and its Pull-apart and continental escape origin. J. Struct. Geol., 11, 3, 275-283.

Barka, A.A. and Kadinsky-Cade, K. (1988). Strike-slip fault geometry in Turkey and its influence on earthquake activity. Tectonics, 7, 3, 663-684.

Can, R. (1974). Seismo-tectonics of the North-Anatolian fault zone. M. Phil. Thesis University of London, 255 pp.

Canitez, N. (1973). Studies on the recent crustal movements and the North Anatolian fault problem. In, Symposium on the North Anatolian Fault and Earthquake Belt. Spec. Publ. Mineral Res. Explor. Inst. Turkey. 35-55.

Canitez, N. and Ucer, B. (1967). A catalogue of focal mechanisms for Turkey and adjoining areas. Uni.Istanbul, Inst. Earth Phys., 25.

Dewey, J.W. (1976). Seismicity of Northern Anatolia. Bull. Seism. Soc. Am., 66. 843-868.

Dewey, J. F., Hempton, M. R., Kidd, W. S. F., Sarolgu, F., Sengor, A. M. C. (1986). Shortening of Continental lithosphere: the tectonics of Eastern Anatolia - young collision zone. From Coward, M.P. and Ries, A.C. (Eds.) Collision Tectonics, Geological Society Spec. Pub. 19. 3-36.

Ergin, K. Guclu, U., Uz, Z., (1967). A catalogue of earthquakes for Turkey and surrounding area. Publ. Ist. Techn. Univer. Mining Fac. 24.189 pp.

Gulen, L. (1984). Sr, Nd, Tb isotope trace elemtns, geochemistry of calcaline and alcaline volcanics, Eastern Turkey. Ph.D. Thesis, Massachusetts Institute of Technology, 232pp.

Hempton, T. P. and Dunne, L. A. (1984). Sedimantation in pull-apart basins : Active examples in eastern Turkey. J. Geol., 92, 513-530.

Jackson, J. and McKenzie, D., (1984). Active tectonics of the Alpine-Himalayan Belt between western Turkey and Pakistan. Geophys. J. R. Astr. Soc. 77, 1, 185-265.

Kadinsky-Cade, K. and Barka, A. A. 1988. Relationship between restraining bends and earthquake magnitude: Large earthquakes in strike-slip zones. USGS Workshop on Fault Segmentation and Controls of Rupture Initiation and Termination (in press)

Karnik, V., (1971). Seismicity of the European area. D. Reidel Pub. Com., Dordreet. Holland, Part II, 218 pp.

Kasapoglu, E. and Toksoz, M. N., (1983). Tectonic consequences of the collision of the Arabian and Eurasian plates: finite element models, Tectonophysics, 100, 71-96

Kemal, A., (1932). Erzincan earthquakes. Annual book of the Erzincan province. 225 pp.

Ketin, I., (1948). Uber die tektonisch-mechanischen Folgerungen aus den grossen anatolischen Erdbeben des letzten Dezenniums. Geol. Rdsch., 36, 77-83.

Ketin, I., (1969), Uber die nordanatolische Horizontalverschiebung: Bull. Mineral Res Explor. Inst., Ankara, 72, 1-28.

King, G. and Nabelek, J., (1985). Role of fault bends in the initiation and termination of earthquake rupture, Scinece, 228, 984-987.

Lahn, E., (1952). Seismic activity in Turkey from 1947- 1949. Bull. Seism. Soc. Amer

42, 111-114.

Lindh, A.G. and Boore, D. M. (1981). Control of rupture by fault geometry during the 1966 parkfield earthquake. Bull. Seism. Soc. Amer. 71, 95-118.

McKenzie, D., (1972). Active tectonics of the Mediterranean Region. Geophys. J.R. Astr. Soc., 30, 109-185.

Nature, (1940a). The earthquake in Turkey. 145, 62.

Nature, (1940b). The earthquake in Turkey, 145. 96.

Nature, (1940c). Aftershocks of the Earthquake in Turkey, 145, 259.

Nature, (1940d). Earthquakes in Turkey, 145, 346.

Pamir, H.N. and Ketin, I., (1941). Das Anatolische Erdbeben Ende 1939. Geolog. Rundsch., 32, 278-287.

Parajes, E., Akyol, I. H. and Altinli, E., (1941). Le tremblement de terre d'Erzincan du 17 Decembre 1939. Revue Fac. Sci. Univ. Istanbul, NVI, 177-222.

Pinar, N. and Lahn, E., (1952). Earthquake catalog of Turkey. Bayin. Bakan. Yapi Imar Isle. Reis yayin. 6. 36. Ankara.

Riad, S. and Meyers, H., (1985). Earthquake catalog for the Middle East countries 1900-1983. World Data Center A., Report, SE-40. 133.

Salomon-Calvi,l W., (1940). Study of earthquakes in Turkey, Publ. Mineral Res. Explor. Inst. Turkey. B. 5, L-121.

Saroglu, F., Boray, A. and Emre, O. (1987). Active faults of Turkey. Mineral Res Explor. Inst. Turkey. Unpubl. Report 8643, 394 pp.

Schwartz, D. P. and Coppersmith, K. J. (1986). Seismic hazards: New trends in analysis using geologic data. In Active Tectonics, National Acad. Press.Washington. D.C. 215-230.

Segall, P. and Pollard, D.D., (1980). Mechanics of discontinuous faults. J. Geophys Res., 85, 4337-4350.

Sengor, A. M. C. (1979). The North Anatolian transform fault: its age, offset and tectonic significance. J. Geol. Soc., 136, 269-282, 1979.

Sengor, A. M. C., Gorur, N. and Saroglu, F., (1985). Strike-slip faulting and related basin formation in zones of tectonic escape: Turkey as a case study. I: Biddke, K.T. and Christie-Blick, N. (eds.). Strike-slip Faulting and Basin Formation, Society of Econ. Paleont. Min., Sp. Publ., 227-264.

Seymen, I. and Aydin, A. (1972). The Bingol earthquake fault and its relations to the North Anatolian fault zone. Bull. Mineral Res. Explor. Inst. Turkey. 79, 1-8.

Sibson, R.H. (1986). Earthquakes and lineament infrastructures. Phil. Trans. R. Soc. London. 317, 63-79.

Sieberg, A., (1932). Untersuchungen uber Erdbeben und Bruchscholenbau im ostlichen Mittelmeergebiet.Denk. d. Mediz. Natw. Ges. zu Jena, Bd. 18. Jena, 159-273.

Sipahioglu, S., (1982). Seismo-tectonic features of the North Anatolian fault zone. Ph. D. Thesis, Ist. Univ. Science Fac. Geophys. Dept. 169 pp.

Tabban, A., 1980. Geology and earthquake activity of the cities of Turkey. T.C. Imar Iskan Bahanligi. Afet Isleri Genel. Mud. Ankara, 343 pp.

Tasman, C. E. (1946). Varto and Van earthquakes. Bull. Mineral Res. Explor. Inst. Turkey.

Tatar, Y., (1978). Tectonic investigations on the North Anatolian fault zone between Erzincan and Refahiye. Publ. Inst. Earth. Sci., Hacettepe Univ. 4, 201-136.

Tchalenko, J. S., (1977). A reconnaissance of the seismicity and tectonics at the northern border of the Arabian Plate (Lake Van region): Revue de ge'ographie physique et de ge'ologie dynamique, v. XIX, p. 189-208.

Toksoz, M.N., Shakal, A.F. and Michael, A. J. (1979). Space-time migration of earthquakes along the N. Anatolian fault zone and seismic gaps. Pure Appl. Geophys. 117, 1258-1269.

Tutkun, S. Z. (1986). The systematics of the North Anatolian fault zone between Esil (Erzincan) and Karilova (Bingol). Bull. Fac. Engin. Cumhuriyet Uni. Sivas-Turkey. A, 3, 1, 15-26.

Wallace, R. E. (1968). Earthquake of August 19, 1966, Varto area, Eastern Turkey

Table 1. List of historical earthquakes[*] in the Erzincan Region.

Number	Date	Intensity (I)	Number of casualties
(1)	1045	X-XI	
(2)	1161	VI	
(3)	1165	VII	
(4)	1166	VI	
(5)	1168	VIII	12,000
(6)	1170	VIII-IX	
(7)	1236	VI	
(8)	1251	VIII	
(9)	1254-55	VIII	16,000
(10)	1268	IX	15,000
(11)	1287	VIII	
(12)	1289	VIII	
(13)	1308	VI	
(14)	1356	V	
(15)	1366	VI	
(16)	1374	VII	
(17)	1422	VIII	
(18)	1433	VI	
(19)	1458	X	32,000
(20)	1543	VII	
(21)	1578	VIII	1,500-15,000
(22)	1605	?	
(23)	1667-8	VIII-X	Half of the town was destroyed
(24)	1784	VIII-IX	5,000-15,000
(25)	1887	VI	

---

[*] Documented from Sieberg 1932 A, Ketin 1932, Solomon-Calvi 1936-1940, Parejas *et al.*, 1941, Pinar and Lahn 1952, Ergin *et al.* 1967, Ambraseys 1970, 1975, Karnik 1972, Can 1974, Soysal *et al.*, 1981, 1982, [illegible] 1982, 1983

ORIGINAL PAGE IS
OF POOR QUALITY

Bull. Seis. Soc. Amer. 58, 11-46.

Wesnousky, S. G.(1988). Seismological and Structural Evolution of Strike-Slip faults. USGS Workshop on Fault Segmentation and Controls of Rupture Initiation and Termination.(in press)

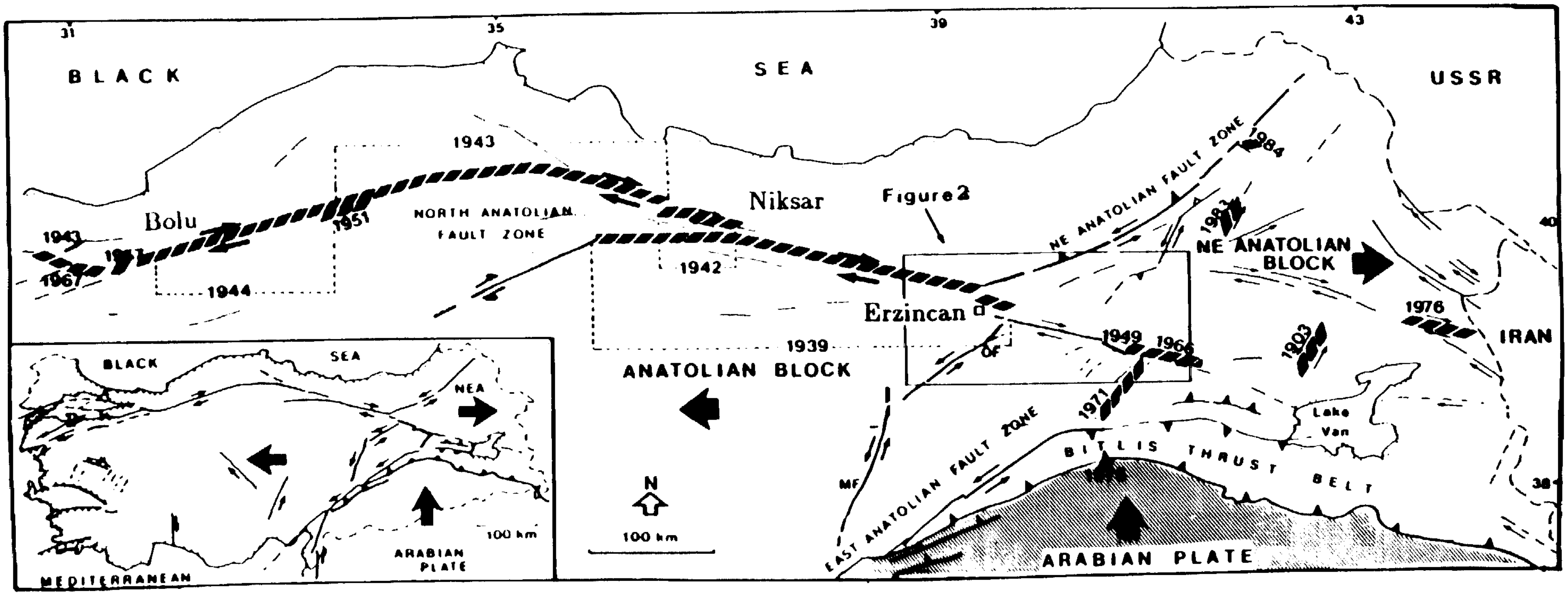
31
35
39
43
BLACK
SEA
USSR
1943
Bolu
1951
NORTH ANATOLIAN
FAULT ZONE
Niksar
Figure 2
1943
1957
1967
1944
1942
NE ANATOLIAN FAULT ZONE
1984
1983
NE ANATOLIAN
BLOCK
40
Erzincan
OF
1939
1949
1966
1976
1903
IRAN
ANATOLIAN BLOCK
1971
Lake
Van
BITLIS THRUST BELT
EAST ANATOLIAN FAULT ZONE
MF
N
100 km
ARABIAN PLATE
38
BLACK
SEA
NEA
MEDITERRANEAN
ARABIAN
PLATE
100 km

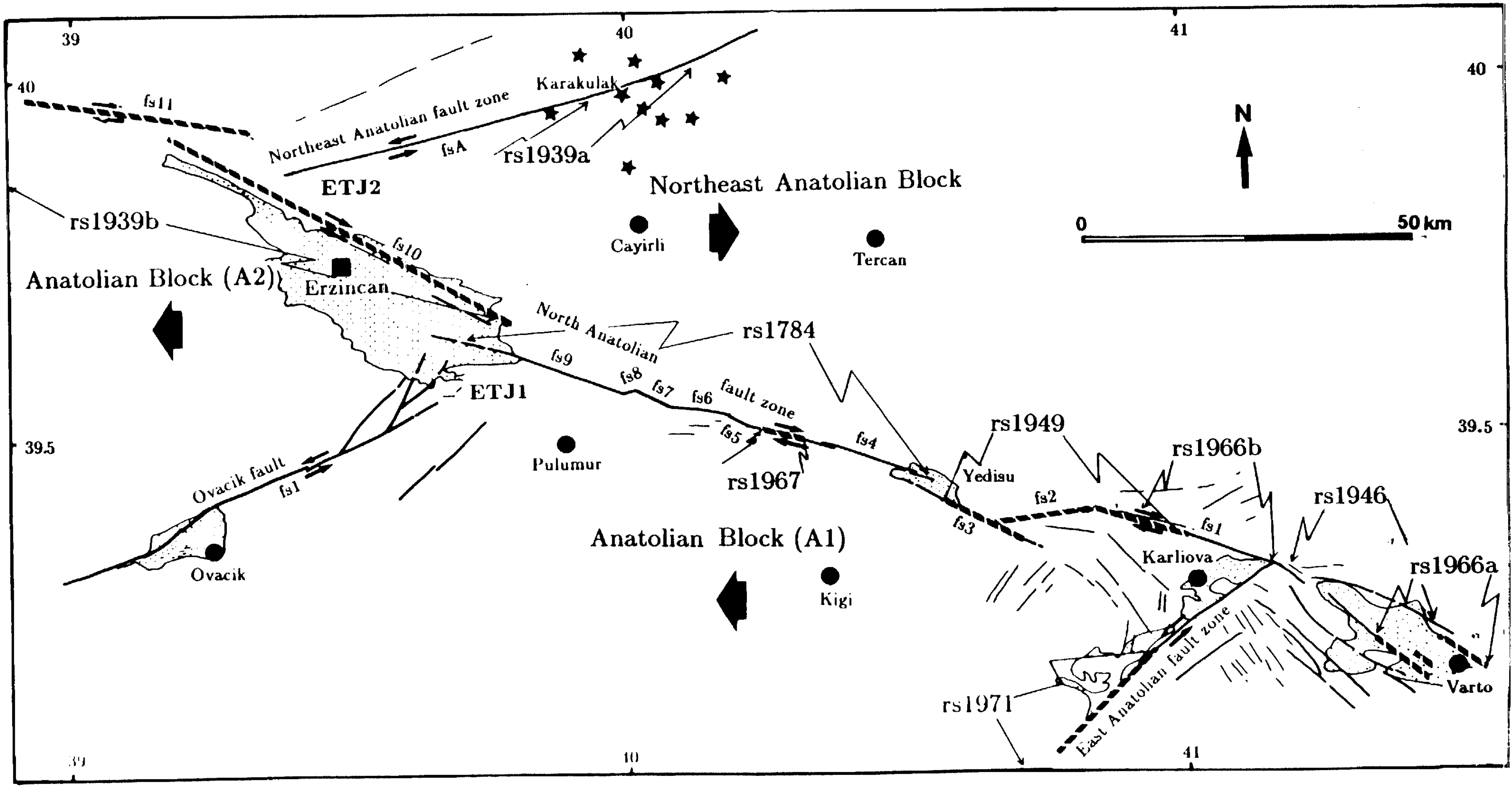
39
40
41
40
39.5
39.5
40
fs11
Northeast Anatolian fault zone
fsA
Karakulak
rs1939a
ETJ2
Northeast Anatolian Block
N
0
50 km
rs1939b
fs10
Cayirli
Tercan
Anatolian Block (A2)
Erzincan
North Anatolian
rs1784
fs9
fs8
fs7
fs6
fault zone
ETJ1
fs5
rs1967
fs4
rs1949
Yedisu
rs1966b
Ovacik fault
fs1
Pulumur
fs2
fs1
rs1946
fs3
Anatolian Block (A1)
Karliova
rs1966a
Ovacik
Kigi
East Anatolian fault zone
Varto
rs1971
39
40
41

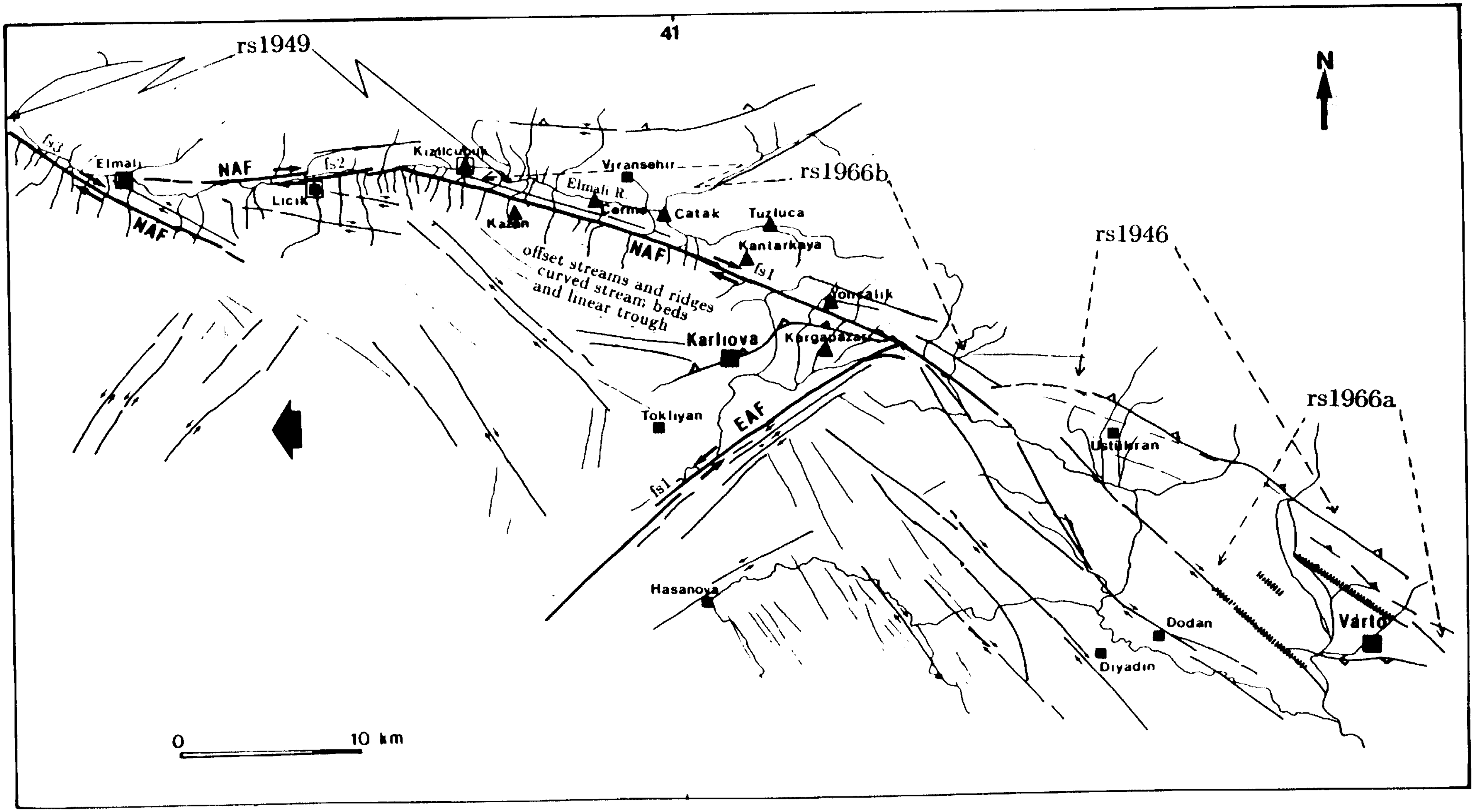
41
rs1949
N
fs3
Elmalı
NAF
fs2
Licik
Kızılcubuk
Viranşehir
rs1966b
Elmalı R.
Cerme
Catak
Tuzluca
Kazan
NAF
NAF
Kantarkaya
fs1
rs1946
offset streams and ridges
curved stream beds
and linear trough
Yoncalık
Karlıova
Kargapazarı
Toklıyan
EAF
fs1
rs1966a
Ustukran
Hasanova
Dodan
Diyadın
Varto
0
10 km

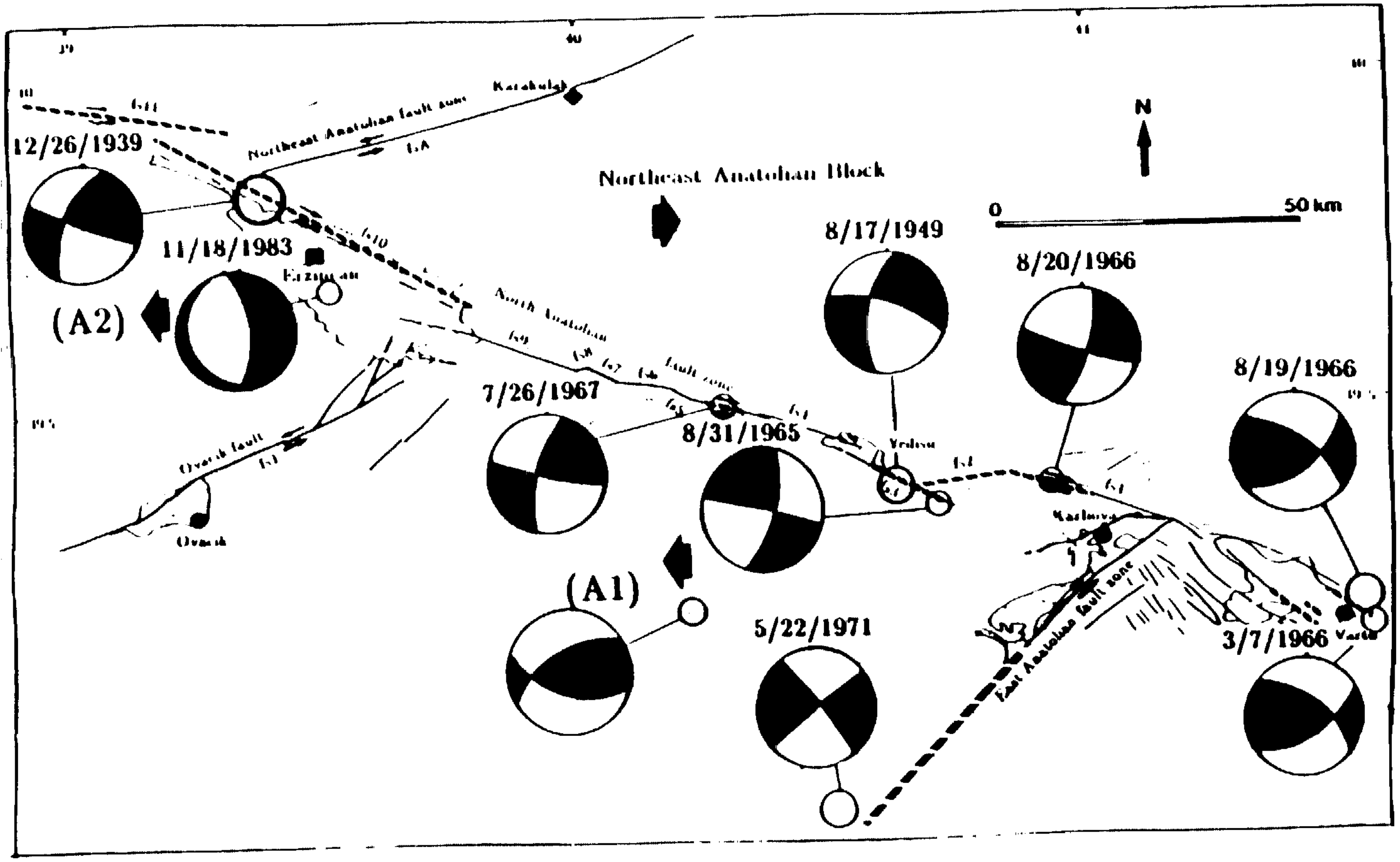
39
40
41
N
0
50 km
Karakulak
Northeast Anatolian fault zone
Northeast Anatolian Block
12/26/1939
11/18/1983
Erzincan
(A2)
North Anatolian fault zone
Ovacık fault
Ovacık
7/26/1967
8/31/1965
(A1)
8/17/1949
Yedisu
8/20/1966
Karlıova
8/19/1966
5/22/1971
East Anatolian fault zone
3/7/1966
Varto

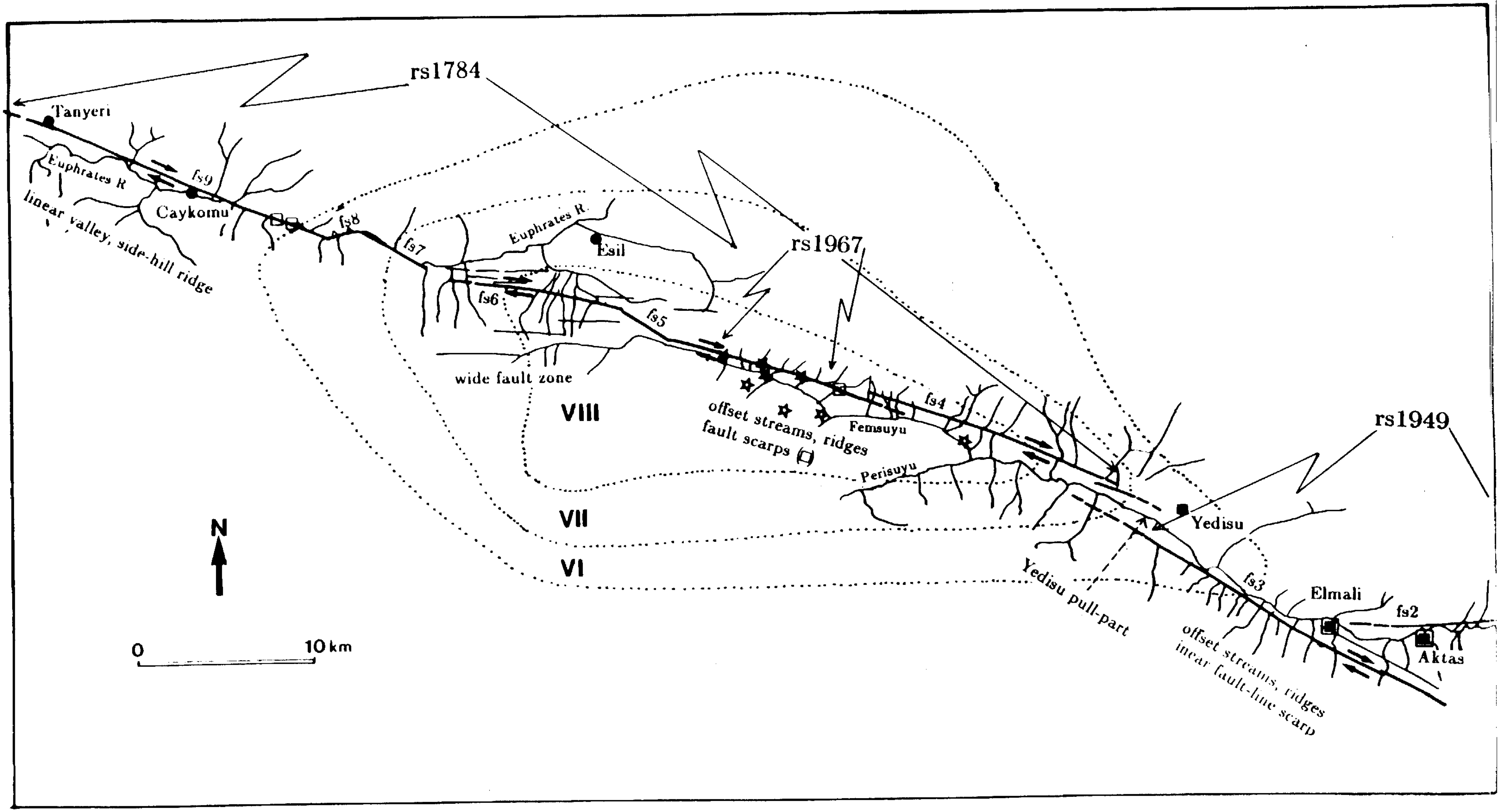
rs1784
Tanyeri
Euphrates R
fs9
Caykomu
linear valley, side-hill ridge
fs8
fs7
Euphrates R.
Esil
rs1967
fs6
fs5
wide fault zone
VIII
offset streams, ridges
fault scarps (□)
Femsuyu
fs4
Perisuyu
VII
VI
rs1949
Yedisu
Yedisu pull-part
fs3
Elmali
fs2
Aktas
offset streams, ridges
inear fault-line scarp
N
0
10 km

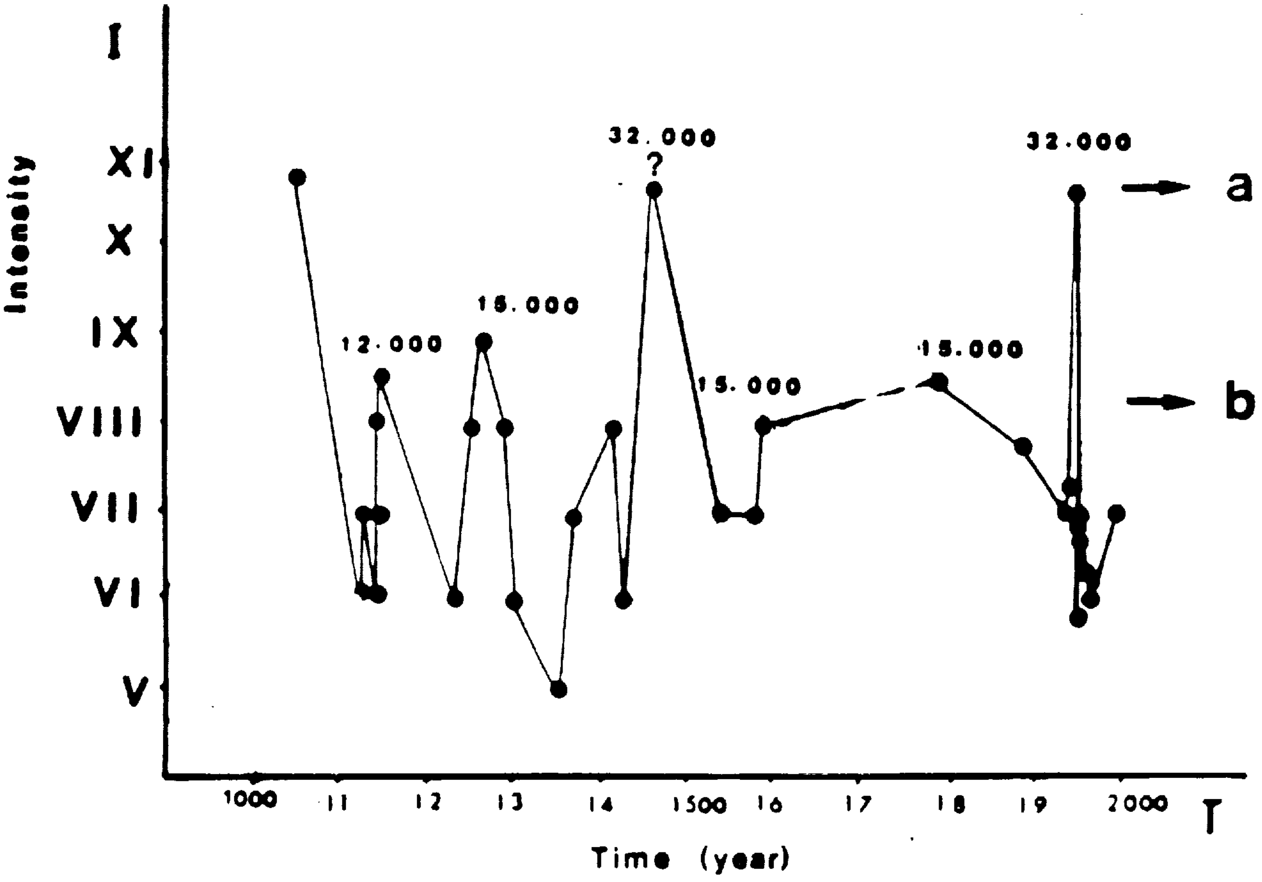
Intensity
I
XI
X
IX
VIII
VII
VI
V
12.000
15.000
32.000
?
15.000
15.000
32.000
a
b
1000
11
12
13
14
1500
16
17
18
19
2000
T
Time (year)

C-2

ORIGINAL PAGE IS
OF POOR QUALITY

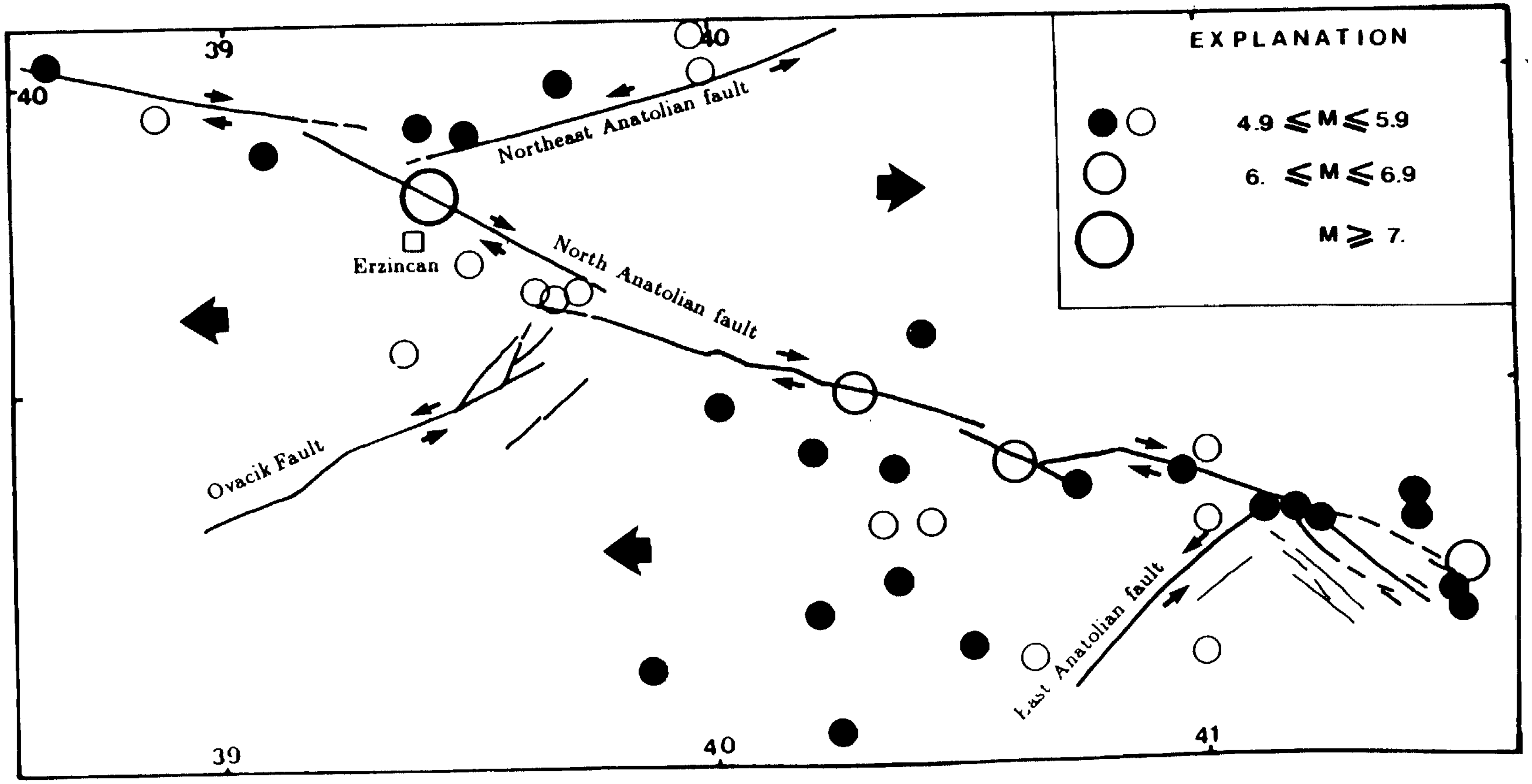

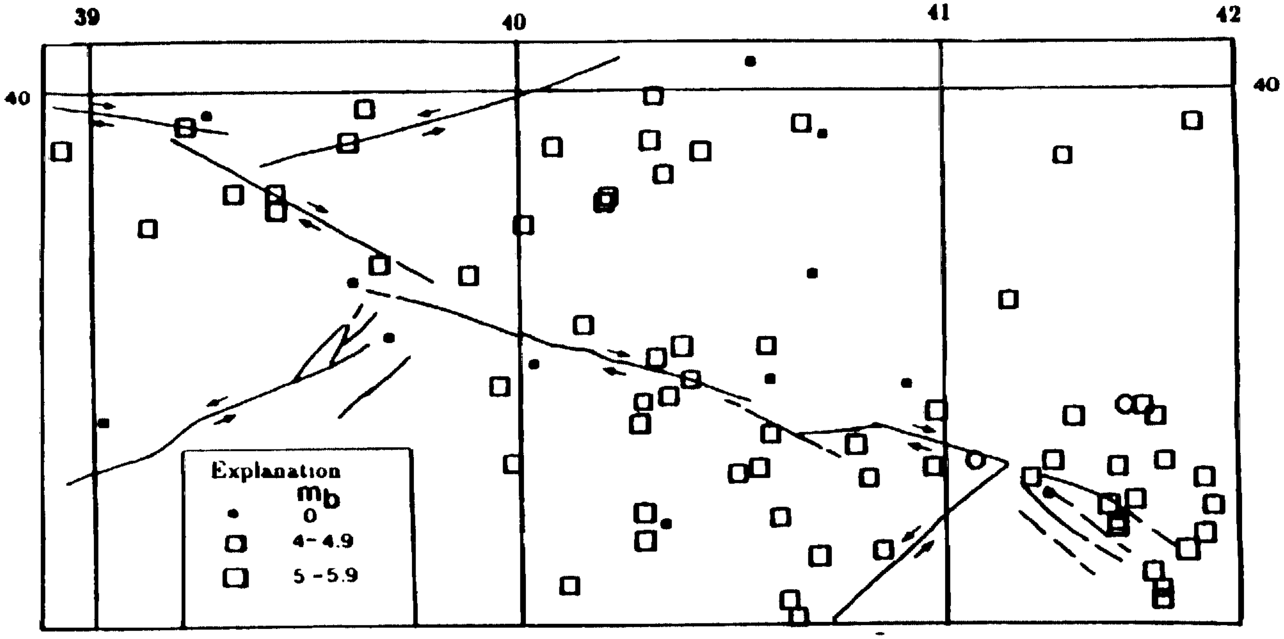
39
40
41
42
40
40
Explanation
m_b
● 0
□ 4-4.9
□ 5-5.9

Explanation

▨ Straight segments → Interseismic → small-moderate eathquakes/creep

▩ Locked segments → Coseismic → Large earthquakes

⁙ Releasing stepover/bend → Preseismic/postseismic → Foreshocks/aftershocks swarms

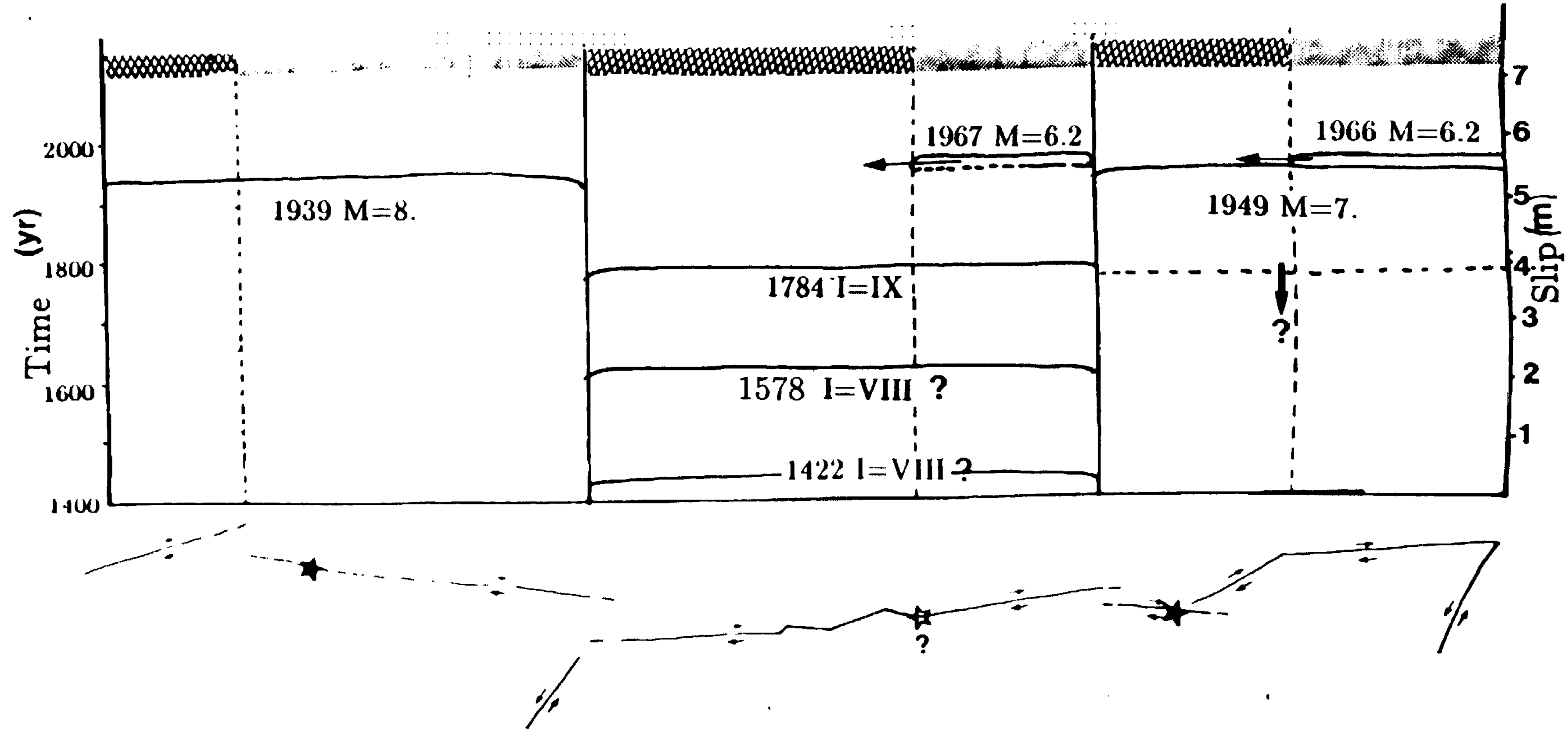

APPENDIX 3

Slip Distribution of the Great 1939 Erzincan Earthquake, Eastern Turkey

A. Aykut Barka, Katharine Kadinsky-Cade and M. Nafi Toksöz

Earth Resources Laboratory
Department of Earth, Atmospheric and Planetary Sciences
Massachusetts Institute of Technology
Cambridge, MA 02142

The December 26, 1939 Erzincan earthquake (M=8) is the first and largest of a remarkable westward migrating series of six M=7-8 earthquakes that occurred along the North Anatolian fault zone between 1939 and 1967 (Ketin, 1948, 1969; Ambraseys 1970). The 1939 earthquake created a 360 km long surface break, which is shown in Figure 1 (Ketin, 1969; Barka et al., 1987). The epicenter was located approximately 10 km northwest of Erzincan, as indicated by the star in Figure 1c (Dewey, 1976). The distribution of aftershocks is not known completely, although a number of moderate size aftershocks can be associated with the Erzincan, Suşehri and Niksar basins, which are major releasing features along the rupture zone (Dewey, 1976; Tabban, 1980; Riad and Meyers, 1985). Several small earthquakes were felt by local residents in the Erzincan basin two weeks before the main shock (Pamir and Ketin, 1941). Only one measurement of fault slip was made soon after the earthquake: a 3.7 m right-lateral offset of a side wall along the main road in Reşadiye (Parejas et al., 1942). In this short note we present results from recent field measurements of fault offset along the 1939 earthquake surface breaks. These data are very important, not only because they help constrain the rupture characteristics of the 1939 earthquake, but also because they allow us to compare the 1939 earthquake with other great strike-slip events such as the 1857 and 1906 San Andreas fault earthquakes in California.

The rupture zone can be divided into five major fault segments (Barka and Kadinsky-Cade, 1988). This division is illustrated in Figure 1c. From east to west the lengths and strikes (measured from north) of these segments are: (1) Erzincan - length 60 km, strike 125°, (2) Mihar - length 65 km, strike 105°, (3) Ortakoy - length 45 km, strike 117°, (4) Kelkit - length 100 km, strike 107°, and (5) Niksar - length 90 km. strike 90°. These five segments are related geometrically in the following fashion: (a) segments 1 and 2 are separated by a 20° restraining bend (Barka and Hancock, 1982), (b) segments 2, 3 and 4 form a releasing double bend along which 3 is the releasing segment, and (c) segments 4 and 5 are separated by a 17° smooth restraining bend.

During the field survey we measured offsets of man-made features such as field boundaries, fences, roads, canals and lines of trees defining field boundaries. We also measured offsets of natural features such as streams and the side walls of valleys or ridges. The survey focused on villages that were situated right on the surface breaks. Thus local residents who had witnessed the earthquake were able to confirm our identification of surface breaks as well as some of the offset features.

The 1939 earthquake slip distribution determined from the new measurements is summarized in Figure 1b. Both man-made and geomorphological offset features are included in the figure. An independent set of measurements of surface slip associated with the 1939 earthquake is provided by Kocyiğit (1988). These data points are included in Figure 1b as well. They are in close agreement with our measurements. From the combined data set shown in Figure 1b, the surface slip distribution can be described in the following simplified fashion: 4 - 6 m slip along the western half of segment 1, increasing to 6.5 - 7.5 m along segments 1 and 2, then decreasing to 4 - 4.5 m along segment 4, followed by a further decrease to 2 - 2.5 m along segment 5 (possibly less at the western end of segment 5).

Figure 1a shows a reversed seismogram from the 1939 earthquake (time shown increasing from right to left for purposes of discussion). The seismogram was recorded in Pasadena, California. The epicentral distance for this record is 104°, so that the phase shown in the figure is a diffracted P wave. The semi-major axis of the 90% confidence ellipse for Dewey's (1976) relocated epicenter coordinates (39.80°N, 39.38°E) was only 10-20 km, so we are quite certain that the epicenter can be tied to the 20° restraining bend just northwest of Erzincan (Figure 1c). The Pasadena record starts with an approximately 20 second long low-amplitude wavetrain (emergent phase starting at the "1" label in Figure 1a and lasting until "2"). Most of the moment release, however, occurs during the next 100 seconds (starting shortly after "2" and lasting until "3"), with the largest amplitudes occurring in the first 60 seconds of that 100 second wavetrain. The simplest way to interpret this seismogram is to associate the 20 second long low-ampltude phase with rupture of the 60 km segment (1) located near Erzincan, and the 100 second long phase with rupture of the remainder of the fault zone (west of the epicenter). This interpretation is based on (1) a reasonable rupture velocity of 3 km/sec (60 km in 20 seconds for the low-amplitude phase and 300 km in 100 seconds for the higher-amplitude phase), and (2) a good correlation between the distribution of amplitudes in the seismogram and the distribution of surface slip (Figures 1a and 1b). Clearly, however, a more thorough study of historical seismograms produced by this earthquake needs to be done.

The slip distribution along the fault segments suggests that maximum slip is associated with the restraining (west) side of the 20° restraining bend. That side of the bend is uplifted, and folding and thrusting are common features in the late Cenozoic sediments of that area (Tatar, 1978; Barka and Gülen, 1989). The relocated epicenter near the bend supports a model of bilateral rupture propagation. The fault plane solution of the earthquake determined by McKenzie (1972) is characterized by predominantly right-lateral strike-slip motion with a small component of reverse faulting. The strike of the main fault plane in his solution is 108°, similar to the strike of segment 2 in Figure 1c.

The distribution of slip shown in Figure 1b can be utilised to estimate a static moment for the 1939 earthquake, using the formula Mo=μuA, where μ is the rigidity of the medium, u is the average dislocation and A is the area of faulting. We assume a rigidity of 3.3×10^{11} dyne/cm^2 and a crustal thickness of 15 km, and add the moments from each of the 5 fault segments. Here average slips of 5 m, 7 m, 7 m, 4.25 m and 2.25 m are assumed for segments 1 through 5 based on Figure 1b because a more complicated calculation is not warranted by the data.

$$Mo = (3.3 \times 10^{11} dyne/cm^2)(15km)[(60km \times 5m) + ((65+45)km \times 7m) + (100km \times 4.25m) + (90km \times 2.25m)] = 8.4 \times 10^{27} dyne.cm$$

The corresponding moment magnitude based on the formula

$$logMo = 1.5Mw + 16.1$$

of Hanks and Kanamori (1979) is Mw=7.9.

The slip deficit to the west along segment 4 and 5 can be interpreted in one or both of the following ways. (a) It is possible that another significant earthquake has occurred along this section of the fault in the past, or could occur in the future, to make up the deficit. (b) Internal deformation of the Anatolian Block may be taking place, and the slip deficit may correspond to deformation occurring at the nearby Tokat kink. As supporting evidence for the latter posibility Barka and Gülen (1988) have pointed out that total displacement along the fault zone decreases from 35-40 km in the Erzincan region to 25-30 km in the central section of the North Anatolian fault. However it should be noted that the region of slip deficit along segment 4 coincides with the eastern portion of the surface break produced during the 1668 earthquake (Ambraseys and Finkel 1988).

There is a fundamental difference between the slip distribution of the 1939 earthquake and those of the 1857 and 1906 earthquakes along the San Andreas fault. In the case of the California earthquakes it is possible to compare the fault geometry with slip distributions reported by Thatcher (1975) and Sieh (1978). In the case of the 1857 earthquake the section of the fault between Hwy. 166 and Tejon Pass can be described as the restraining section of a double restraining bend. Here slip was only about 6 m, compared with 9 m in the Carrizo plain to the north. In the case of the 1906 earthquake a similar situation occurred in the southern section of the rupture zone, just north of San Juan Bautista. Reduced slip in the restraining sections suggests that these areas acted as barriers to rupture propagation. In the 1939 Erzincan earthquake case the restraining section just west of the epicenter was the area of maximum slip. That section of the fault may have been acting as an asperity in 1939 and as a barrier in 1668.

REFERENCES

Ambraseys, N. N. (1970). Some characteristic features of the North Anatolian fault zone. Tectonophysics, 9, 143-165.

Ambraseys, N. N. and Finkel, C. F. (1987). The Anatolian earthquake of 17 August 1668. Preceedings of the Symposium on Historical Seismograms and Earthquakes. Ed., W. H. K. Lee, Academic Press, pp. 400-407.

Barka, A. A. and Gülen, L. (1989). New constraints on age and total offset of the North Anatolian fault zone: implications for tectonics of the Eastern Mediterranean region. Spec. Publ. Middle East Tech. University. Ankara, Turkey. In press.

Barka, A. A. and Hancock, P. L. (1982). Relationship between fault geometry and some earthquake epicenters within the North Anatolian fault zone. In Multidisciplinary Approach to Earthquake Prediction, edited by A. M. Işikara and A. Vogel, Friedr. Vieweg and Sohn, F. R. G., 137-142.

Barka, A. A. and Kadinsky-Cade, K. (1988). Strike-slip geometry in Turkey and its influence on earthquake activity. Tectonics, 7, 663-684.

Barka, A. A., Toksöz, M. N., Gülen, L. and Kadinsky-Cade, K. (1987). Segmentation, seismicity and earthquake potential of the eastern part of the North Anatolian fault zone. Yerbilimleri, 14, 337-352.

Dewey, J. W. (1976). Seismicity of Northern Anatolia. Bull. Seism. Soc. Amer., 66, 843-868.

Hanks, T. and H. Kanamori (1979). A Moment Magnitude Scale. Jour. Geophys. Res., 84, 2348-2350.

Ketin, I. (1948). Über die tektonisch-mechanischen Folgerungen aus den grossen anatolischen Erdbeben des letzten Dezenniums. Geol. Rundsch., 36, 77-83.

Ketin, I. (1969). Über die nordanatolische Horizontalverschiebung. Bull. Miner. Res. Explor. Inst. Turk., 72, 1-28.

Kocyiğit, A. (1988). Basic geological characteristics and total offsets of the North Anatolian fault zone in the Suşehri area, NE Turkey. Middle East Tech. Univ. Journal of Pure and Applied Sciences., 228, 984-997.

McKenzie, D.P. (1972). Active tectonics of the Mediterranean region. Geophys. J. R. Astr. Soc., 30, 109-185.

Pamir, H. N. and Ketin, I. (1941). Das Anatolische Erdbeben Ende 1939. Geol. Rundsch., 32, 279-287.

Parejas, E., Akyol, I. H. and Altinli, E. (1942). Le tremblement de terre d'Erzincan du 27 Decembre 1939. Rev. Fac. Sci. Univ. Istanbul. Ser. B, 6, 177-222.

Riad, S. and Meyers, H (1985). Earthquake catalog for the Middle East countries 1900-1983. World Data Center A. for Solid-Earth Geophysics, Report SE-40, Boulder, Col., 133 pp.

Sieh, K. (1978). Slip along the San Andreas fault associated with the great 1857 earthquake, Bull. Seis. Soc. Am., 68, 1421-1448.

Tatar, Y., (1978). Tectonic investigations on the North Anatolian fault zone between Erzincan and Refahiye (in Turkish). Yerbilimleri, 4, 201-236.

Tabban, A. (1980). Geology and earthquakes of cities. Ministry of Construction and Housing, Natural Disasters Division. Ankara, Turkey. 343 pp.

Thatcher, W. (1975). Strain accumulation and release mechanism of the 1906 San Francisco earthquake. J. Geophys. Res., 80, 4862-4875.

Figure Caption

Figure 1. Rupture characteristics of the 1939 Erzincan earthquake. (a) Reversed (time increasing right to left) version of Pasadena (PAS) record of diffracted P from the 1939 earthquake (Z component, To= 1 sec, Tg=0.23 sec, time correction= -20 sec). The origin time of the earthquake was December 26, 23:57:16.0 (GMT). For explanation of numbers above seismogram see text. (b) Slip distribution of the 1939 M=8 Erzincan earthquake. Solid circles correspond to slip measured during this survey. Open squares are measurements of Kocyiğit (1988). The open triangle is the only measurement obtained soon after the earthquake (Parejas et al., 1942). (c) Major fault segments of the 1939 rupture. The inset map shows the location of the 1939 rupture zone relative to the trace of the North Anatolian fault.

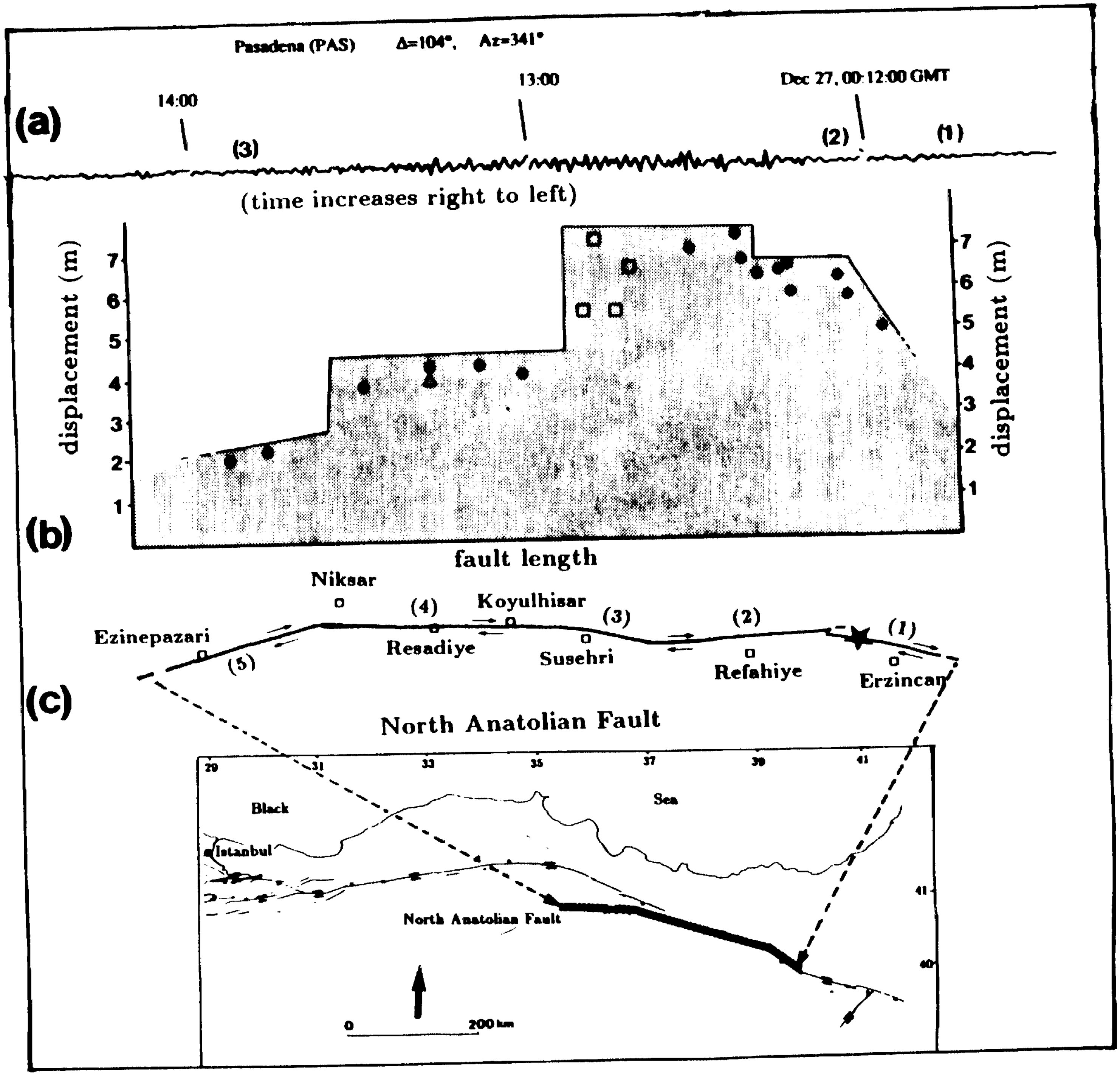

DECEMBER 26, 1939 Ms = 8

APPENDIX 4

PRELIMINARY REPORT ON 1989 TURKEY GPS CAMPAIGN

This is a very brief, preliminary report on the results of the MIT 1989 Turkey GPS field campaign. In short, due to the exceptional effort of UNAVCO personnel, the excellent cooperation and logistical support provided by the Turkish Union of Geodesy and Geophysics (TUJJB), and the dedicated effort of the individual field parties, the measurement campaign was extremely successful. In spite of the failure of one of the Trimble receivers, we were able to observe all 18 stations planned for this year's campaign. This was accomplished by extending the survey by 4 days - a possibility which arose when the Greek/Aegean experiment was postponed.

The accompanying Table lists sites observed this year by MIT/TUJJB. Continuous observations were made at ANKARA (ANKA) and DIYARBAKIR (DIYA) using TI-4100 receivers, while the other sites in Eastern Turkey were observed for 3 days each using Trimble 4000ST receivers. A total of 4 station-days of data were lost, out of 86, due to instrument and logistical problems. As these losses occurred on 3 separate days and on 4 different stations, they will not significantly reduce the strength of the network.

Our GPS measurements were closely coordinated with those made by IFAG and their collaborators at and around SLR sites in Turkey, as well as with the measurements in Western Turkey made by the Durham University group. The accompanying Figure shows the locations of stations observed by our group in 1988 and 1989, those observed by IFAG and 5 of the approximately 30 sites observed by Durham (these 5 sites were established and observed with GPS by MIT/Hacettepe Univ. in 1988). As indicated in the Figure, the 1989 sites established by MIT/TUJJB in Eastern Turkey are well located to monitor regional deformation associated with on-going continental collision in this area. This includes:

1. The distribution of crustal shortening between the Arabian plate and the Eurasian plate along a transect running from the Turkish/Syrian border to the Black Sea,
2. "Extrusion" and rotation of the Anatolian plate with concentrated deformation along the North and East Anatolian faults,
3. "Extrusion" rotation and internal deformation of the East Anatolian block, and
4. Relative movement between the African and Arabian plates along the Dead Sea fault.

In addition, strong ties were established to our 1988 GPS observations in Western Turkey through overlapping observations at 5 sites in central and Eastern Turkey (4 SLR sites and Ankara) and the 5 1988 GPS stations observed this year by Durham. Furthermore, continuous observations at the SLR stations in Askites (ASKI) and Rhodes (RHOD) made by IFAG will provide ties to the Aegean network.

Besides completing a very successful measurement campaign, we established a close working relationship with the Turkish geodetic community. The 1989 campaign was done in close cooperation with the TUJJB. This is an important development for the project both for assuring the long term viability of our measurement program in Turkey and for receiving increased logistical support for future surveys. We feel strongly that the success of this project, as well as all international projects, requires more of the field effort be taken on by local scientists. The relationships developed this year are an important step in this direction.

We will begin processing and analyzing the Turkey GPS measurements using the GAMIT software this month. One Turkish scientist, to be selected by TUJJB and MIT, will visit MIT to participate in data reduction. One of our first efforts will be to compare GPS and SLR baselines, as all 4 SLR sites in Turkey were reobserved by both techniques this year. We are also very interested in comparing 1988 and 1989 GPS observations at SLR sites, the Ankara site, and the 5 GPS sites in Western Turkey observed in 1988 and 1989. We expect that these studies will be undertaken in cooperation with the other groups involved with GPS and SLR measurements in this region.

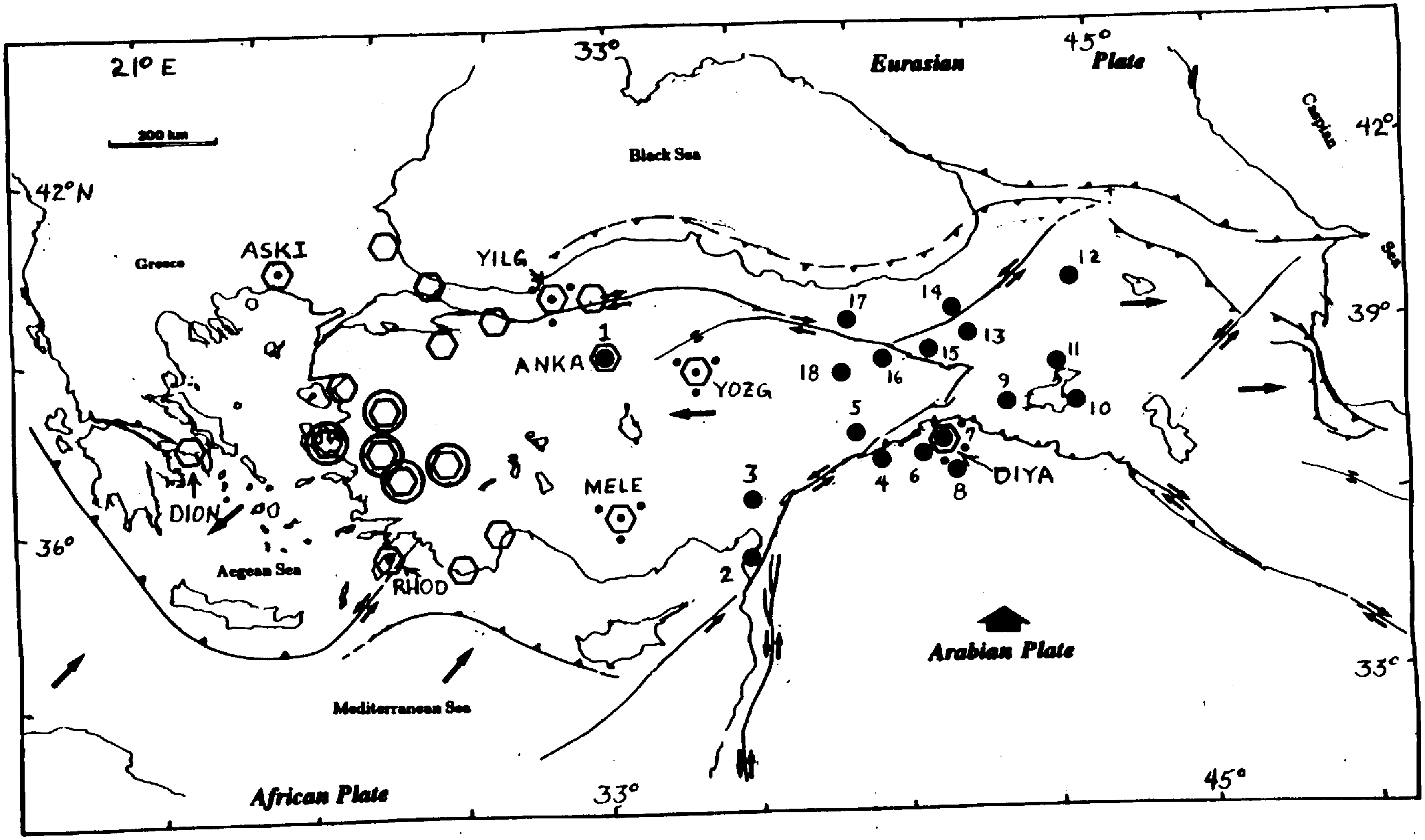

Figure 1. Some of the GPS sites observed in and around Turkey in 1988 and 1989. Key: ● 1989 MIT/TUJJB; ⬡ 1988 MIT/Hacettepe U./IFAG; • 1989 IFAG; ◯ 1989 Durham U.

SLR stations in Rhodes (RHOD) and Askites (ASKI) were observed by IFAG in 1988. Other 1988 sites were observed by MIT/Hacettepe. See Table for details of 1989 MIT/TUJJB sites. Only 5 of approximately 30 Durham sites are shown (these 5 sites were established and observed by MIT/Hacettepe in 1988). IFAG sites close to SLR stations (Footprints) shown schematically. DION, ASKI, RHOD, MELE, YILG, YOZG, and DIYA are SLR sites.